Single and Multiple Frequency Fiber Lasers

Thesis by

Jay W. Dawson

In Partial Fulfillment of the Requirements

for the Degree of

Doctor of Philosophy

California Institute of Technology

Pasadena, California

1993

(Submitted May 11, 1993)

To

Catherine

and to

my parents

Acknowledgments

It is a great pleasure to acknowledge the support and encouragement of my advisor, Professor Kerry J. Vahala. He and his group provided the atmosphere and resources necessary for exciting research and for my growth as an independent scientist.

I would especially like to thank Namkyoo Park, who collaborated with me on much of the work contained in this thesis. I would also like to thank Steve Sanders who collaborated with me on the intensity noise measurements contained in chapter three of the thesis. I have also enjoyed working with Jianhui Zhou, whose experiments in four-wave mixing have helped to provide a test of the fiber laser's usefulness in high resolution spectroscopy.

I would also like to thank the other members of Dr. Vahala's group who have provided support and encouragement during my time at Caltech. These include Dr. John Lebens, Dr. Michael Newkirk, Dr. Michael Hoenk, Dr. Pete Sercel, Dr. Winston Saunders, Charles Tsai, Robert Lee and Dave Geraghty. The help of Rosalie Rowe is truly appreciated.

I am very grateful to the Northrop Corporation whose funding has supported much of this work. I am especially grateful to Dr. Wes Masenten at Northrop, who has been very encouraging of this research. In addition, I would also like to thank Calvin Miller at Micron Optics for use of the narrowband fiber Fabry-Perot used early on in this research. I would especially like to thank the Ortel Corporation for the loan of the high speed photodiode used in the linewidth measurements in chapter four.

The encouragement of my parents and the rest of my family will always be appreciated.

I would especially like to thank my wife Catherine for her love and support.

Abstract

Single frequency, low intensity noise, widely tunable lasers operating in the 1.5 μm region have potential applications in future wavelength division multiplexed optical communications systems, fiber sensor arrays and high resolution spectroscopic measurements. A single frequency fiber laser having these characteristics will be described in detail. The laser cavity contains an erbium doped fiber gain module, fiber isolators to ensure unidirectional travelling wave operation and two fiber Fabry-Perot filters acting in tandem, which provide broadband tunability (1530 nm -1560 nm) combined with stable single frequency operation. Shot noise limited operation of this laser has been observed at frequencies greater than 300 MHz. At lower frequencies (1-300 MHz) the intensity noise has been characterized in terms of sidemode suppression (> 60 dB of minimum sidemode suppression has been realized). Lower still (10 kHz - 1 MHz) the intensity noise is dominated by the laser's relaxation resonance (30 kHz @ 1 mW output, -105 dBc/Hz). The linewidth of this laser has been measured to be less than 4 kHz using a loss compensated recirculating delayed self-heterodyne interferometer (RDSHI). The RDSHI is an improvement over the standard delayed self-heterodyne interferometer in that the effective delay line can be increased by a factor of 30 over the standard method, increasing the resolution by a corresponding amount. The RDSHI also allows measurement of the short term frequency jitter of a laser. In order to reduce laser frequency jitter, the Pound-Drever technique was employed to lock the laser frequency to an external fiber Fabry-Perot. The same technique also permitted the internal mode selection filter to track the laser frequency, completely eliminating residual mode hopping due to thermal length changes of the laser cavity. Finally, fiber laser configurations that allow multiple frequencies to be simultaneously produced in one laser cavity will be described.

Contents

List of Figures

Chapter 1

Introduction

The purpose of this thesis is to describe the development and characterization of single and multiple frequency fiber lasers. Single frequency fiber lasers have several attractive properties which will be useful in a high resolution spectroscopy system or a wavelength division multiplexed communications system. These include narrow linewidth, broadband tunability and inherent compatibility with optical fiber. Fiber lasers are inherently compatible with optical fiber in two ways. First, the light is generated in the fiber making coupling into an optical system a simple matter of a fusion splice. Second, the lasers are based on fiber amplifiers and are by default compatible with the wavelength range at which those amplifiers operate.

This introductory chapter is meant to provide perspective for the discussion of the single-frequency fiber laser. Fiber amplifiers, upon which the fiber laser is based, will be discussed first. Other work in the field of fiber lasers and some applications in which fiber lasers have already made a contribution will then be discussed. Finally, a brief outline of the thesis will be provided.

1.1 Optical Amplifiers for Fiber Optic Systems

There are two types of optical amplifiers commonly considered for use in fiber optic systems: semiconductor based optical amplifiers and rare-earth ion doped optical fiber amplifiers. (Other types of amplifiers such as Raman amplifiers have been demonstrated [1]; however, the broader bandwidths and simpler pumping schemes of rare-earth ion doped fiber amplifiers have virtually eliminated interest in these alternatives.) Although both of these types of amplifiers may now be purchased commercially, they are still the subject of active research.

Semiconductor optical amplifiers are currently being studied as a means of compensating the high loss inherent in integrated photonic devices [2]. Semiconductor amplifiers have a number of impressive qualities including a large gain bandwidth [3] and high saturation output power [4]. However, the fast recovery time of the semiconductor gain media leads to large cross-talk if two or more signals are amplified simultaneously [5]. This makes them unsuitable for use as "in-line" amplifiers in future optical communications systems. Future systems will no doubt utilize multiple wavelengths. There is, however, one "silver lining" to the crosstalk problem and that is that it may be possible to use the cross talk effect to construct an optical frequency shifter [6]. Such a device would be very useful in future wavelength division multiplexed communications systems [7].

Rare-earth ion doped optical fiber amplifiers have, in a very short amount of time, revolutionized the way the telecommunications industry thinks about fiber optic systems. A rare-earth ion doped fiber was first conceived by Snitzer [8] in 1961. However, major interest in fiber amplifiers did not develop until as late as 1985 when Poole et al. [9] demonstrated rare-earth ion doping of single mode optical fibers. Demonstration of a neodymium fiber laser end pumped by a laser diode was published simultaneously [10]. Progress since then has been very rapid in theoretical modelling [11-16], diode laser pump

sources [17,18,19], investigation of dopants [20-24] and in actual amplifier demonstrations [25, 26, 27]. Today, it is rare to see a proposed fiber optic system that does not include a rare-earth doped fiber amplifier as an essential component.

This thesis focuses on fiber lasers based on erbium doped fiber amplifiers (EDFA). EDFAs are currently the most advanced in terms of development of the rare-earth ion doped fiber amplifiers. Several companies now make EDFAs as commercial products. An EDFA for telecommunications applications (Figure 1.1) consists of a length of single mode erbium doped fiber, two wavelength division multiplexers and a laser diode for pumping. A typical fiber core diameter for the erbium doped fiber is 4 μm, with an erbium concentration of 50 ppm. The core is codoped with an index-raising codopant, which forms the single mode waveguide. This codopant has been found to affect the spectral properties of the amplifier gain [28, 29, 30]. Aluminium in combination with germanium has been found to provide the broadest amplifier gain bandwidth and is now most commonly used.

The wavelength division multiplexer (WDM) is a fused fiber coupler that acts as a dichromatic mirror. The WDM combines pump light from a laser diode with signal light to be amplified. The erbium doped fiber is spliced to the WDMs using a thermally expanded core fusion splicing technique [31] to reduce losses due to mismatch between the mode field diameter of telecommunications fiber and the erbium fiber. The second WDM may be employed simply to couple pump light out of the system or to allow bidirectional pumping of the amplifier. If the amplifier is pumped from only one direction, counter-directional pumping is usually preferred because slightly higher gain is attainable [12].

A 980 nm or 1480 nm laser diode is normally used as a pump source. 980 nm pumping is preferred due to a lower amplifier noise figure than that obtained with a 1480 nm pump source [32]. Other pump wavelengths are also possible including, 820 nm [33],

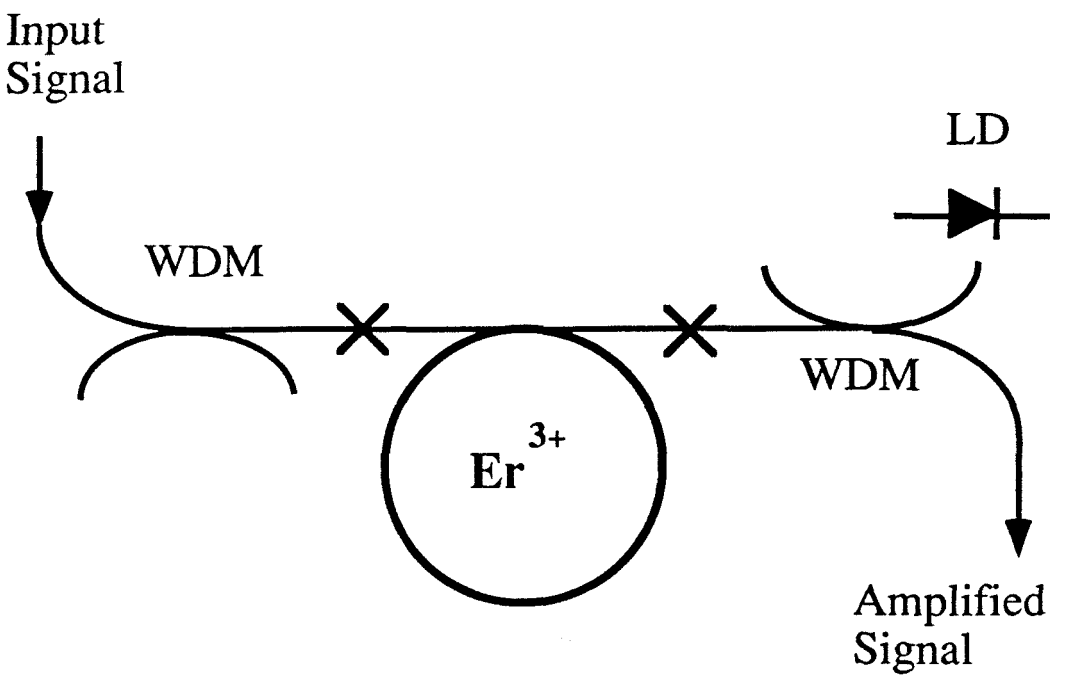

Figure 1.1: Schematic of a typical erbium doped fiber amplifier. WDM: wavelength division multiplexer, LD: pump laser diode, X: thermally diffused core fusion splice, Er^{3+}: erbium doped fiber

514 - 532 nm [34] and 665 nm [35]. Additionally, for erbium doped fiber codoped with ytterbium pumping throughout a broad band from 800 nm to 1100 nm is possible [36]. The ytterbium acts as a broadband absorber and efficiently transfers light into the upper level of the lasing transition.

A typical amplifier consists of a 980 nm pump diode with a maximum output of 30 mW and 25 m of aluminium and germanium codoped erbium doped fiber (50 ppm erbium). Such an amplifier can provide up to 40 dB of small signal gain at the gain peak (1532 nm for aluminum and germanium codoped fiber, 1537 nm for germanium only codoping) and provide a saturation output power of 10 mW. The bandwidth can exceed 50 nm (1520 nm - 1570 nm) [30]. EDFAs made with ytterbium codoped fiber and pumped with a neodymium YAG laser at 1060 nm have been demonstrated with saturation output powers of nearly 1 W [37].

The erbium gain medium is interesting in that the broad gain bandwidth comes from a combination of Stark splitting of the upper and lower laser transition levels and occupation of multiple sites in the glass by the triply ionized erbium atoms. From this, one might expect the amplifier's gain to saturate inhomogeneously; however, it saturates homogeneously [38]. Homogeneous saturation is due to rapid cross relaxation between the closely spaced Stark levels [39]. This cross relaxation occurs at a finite rate leading to very weak (about 1 dB depth, 1 nm width) spectral gain hole burning allowing simultaneous lasing of multiple frequencies [40, 41]. However, for most situations, a simple homogeneous model of the gain is a sufficient description.

For the triply ionized erbium atom in free space, the lasing transition that we are interested in $4I_{13/2}$ --> $4I_{15/2}$ is electric dipole forbidden. However, the ligand field in the glass fiber host mixes the free atom energy states to allow a weak electric dipole transition between these states. The weak electric dipole nature of this transition leads a long upper level lifetime, 12 ms [42]. Thus the EDFA gain responds very slowly in comparison to the

proposed data rate of fiber optic systems, leading to low crosstalk between multiple signals [43].

Current areas of research and development in EDFAs include polarization preserving erbium doped fiber [44], high concentration erbium doped fiber [45] and 980 nm laser sources with output powers greater than one watt in a single transverse mode [18].

1.2 Fiber Lasers

As mentioned previously, the first fiber laser can be attributed to Snitzer [8]. However, current widespread interest in fiber lasers began with Mears, et al., [10] when fiber amplifiers were developed. Presently there are several areas of active research in fiber lasers: mode-locked fiber lasers, upconversion fiber lasers and single frequency fiber lasers.

Both active and passively mode-locked fiber lasers have been demonstrated. Actively mode locked fiber lasers usually employ a ring configuration and an electro-optic modulator [46, 47, 48]. They generate picosecond pulses with repetition rates of up to 30 GHz [49]. Mode locked fiber lasers with cavities constructed from all polarization maintaining fibers have been demonstrated [50]. Stabilized systems that actively control either the drive frequency to the electro-optic modulator or the cavity length, to keep the cavity mode spacing resonant with the modulation, have been demonstrated [51]. In addition a multiple wavelength mode-locked fiber laser has recently been demonstrated [52].

There is great interest in passively mode-locked erbium doped fiber lasers. The most popular scheme for obtaining passive mode-locking of a fiber laser is through the use of a nonlinear amplifying loop mirror (NALM) [53-56]. By splicing together the two output ends of a 3 dB fused fiber coupler, a loop mirror or Sagnac interferometer may be

constructed. All of the light injected into one port of this loop mirror is reflected back out the input port due to the phase shift inherent in the fused fiber coupler, the identical path lengths traversed by the counterpropagating beams and constructive interference. However, if a gain or loss element is placed at an asymmetric location in the loop, the light propagating in one direction will have more power than the light propagating in the opposite direction. For a large enough difference in power, self phase modulation in the fiber will result in light travelling one direction to be phase-shifted with respect to light travelling the opposite direction. For a phase difference of π the reflector becomes a transmitter. Thus the NALM acts as a transmitter for high intensity signals and a reflector for low intensity signals.

The "figure eight" laser or passively mode-locked fiber laser is based on this principle (Figure 1.2). A loop mirror is included in a unidirectional ring. Only high intensity light can propagate completely around the ring. The laser is forced to mode-lock in order to achieve the necessary intensity to oscillate. Both square pulses and solitons have been observed [57] using this configuration. Pulse widths on the order of 300 femtoseconds have been obtained [57]. However, control of the pulse repetition rate is somewhat difficult [58]. In order to get high repetition rates, mode-locking must occur at a high harmonic of the cavity's fundamental repetition rate [55]. More research is needed in this area before the figure eight laser will be a practical device.

Upconversion is a process where an atom absorbs two or more photons then emits a photon of higher energy than any one of the initial photons. Rare earth ions make excellent upconvertors because the large number of closely spaced energy levels translate into an even larger number of available transitions in the infrared. Thus by multiple absorption of infrared photons, an electron can ascend to a high energy level and then fall almost all the way back to the ground state in a single jump emitting a photon of larger

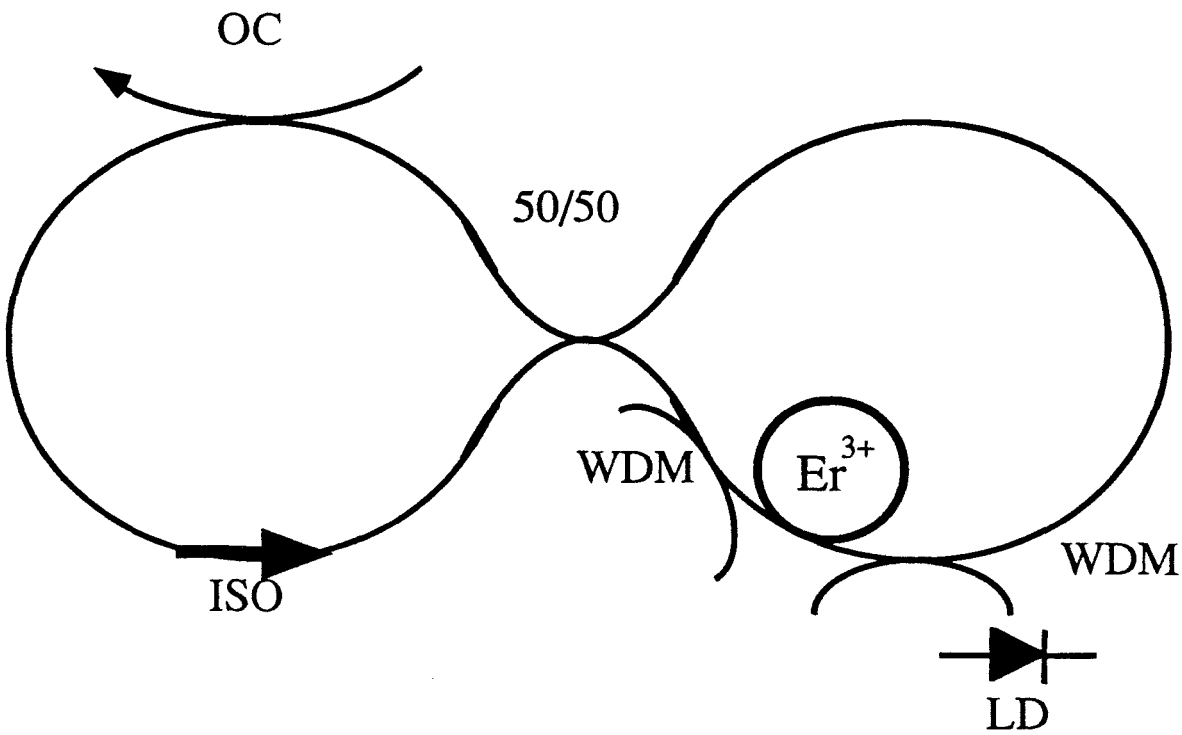

Figure 1.2: Passively mode-locked fiber laser, ISO: isolator, WDM: wavelength division multiplexer, LD: laser diode, 50/50: fused fiber coupler, OC: output coupler

energy than any one of those absorbed. Based on this principle, it is possible to construct lasers that are pumped by efficient semiconductor lasers, but lase at visible wavelengths. A recent review article discusses these processes in more detail [59]. Rare earth ion doped fibers are excellent candidates for upconversion lasers, because the pump light intensity can be kept quite high over a long interaction length. Several such upconversion fiber lasers have been demonstrated [60, 61, 62]. Erbium has been shown to lase in the green 546 nm, when placed in a fluorozirconate fiber and pumped at 801 nm [62]. A praseodymium doped fluoride fiber sensitized with ytterbium was shown to lase in the red at 635 nm when pumped in the 810-860 nm region [60]. Another praseodymium doped flouride fiber was simultaneously pumped at 1010 nm and 835 nm and exhibited lasing in the red (635 nm, 605 nm), green (520 nm) and blue (491 nm) [63]. Holmium and thulium doped fiber lasers that are pumped in the red or infrared and lase in the visible region have also been demonstrated [64, 65]. These upconversion fiber lasers have potential to be compact sources of visible coherent light for applications such as displays and data storage.

Single frequency fiber lasers have been demonstrated based on neodymium and erbium doped fibers [66-76]. Many different cavity configurations have been tested (Figure 1.3). These include ring geometries with some kind of broad band filter such as a fiber Fabry-Perot [74], an acousto-optic tunable filter [69], a liquid crystal filter [68] and a bulk optic filter [71, 75]. So far the laser geometry discussed in this thesis, utilizing two fiber Fabry-Perot filters acting in tandem, has been the only ring geometry fiber laser to achieve stable single frequency operation without rapid mode hopping over a range of several GHz.

Standing wave cavity designs must deal with the effects of spatial hole burning, when attempting to achieve single frequency operation. Three means have been demonstrated to deal with this effect. One design uses a bulk optic grating as a mirror [75]. The very narrow feedback properties of the grating combined with a short cavity allow

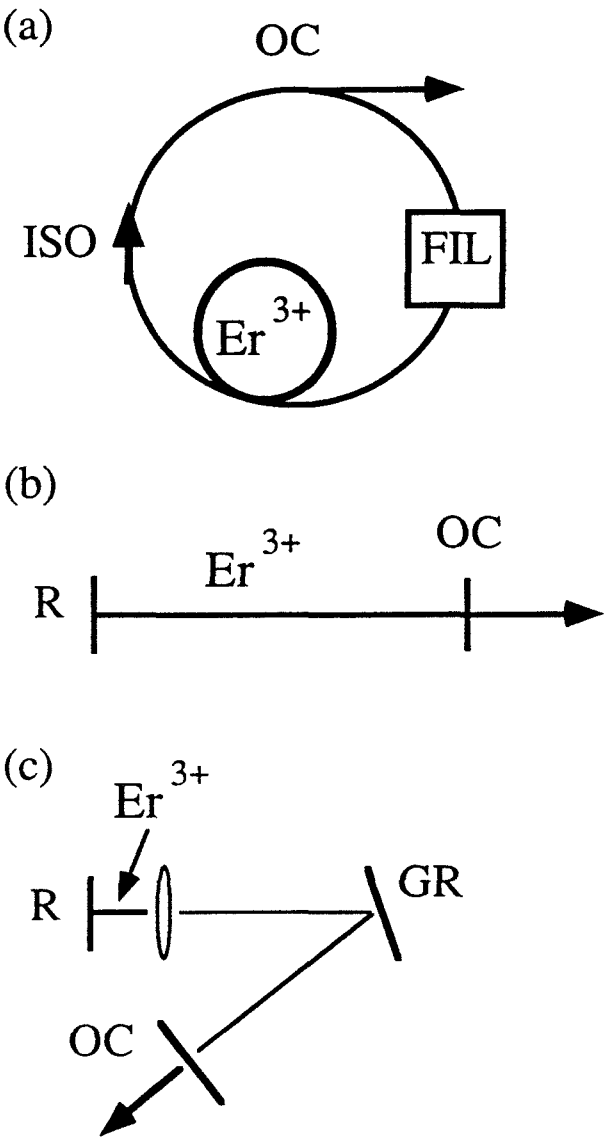

Figure 1.3: Examples of single frequency fiber laser designs, (a) ring geometry, (b) linear geometry, (c) bulk geometry, ISO: isolator, OC: output coupler, Er^{3+}: gain media, FIL: filter, R: reflector, GR: grating reflector.

selection of a single longitudinal mode of the cavity. If no other modes have feedback, spatial hole burning will not be an impediment to single frequency operation. This system allows broad band tuning of the laser combined with stable single frequency operation. However, due to the large losses inherent with this system the lasing threshold is high. Also, its optical alignment must be monitored if the laser is to operate for long periods of time. An all fiber laser does not suffer from this long term alignment problem.

The second method uses a very short (approximately 2 cm) piece of erbium doped fiber combined with intracore Bragg reflectors written with ultraviolet light [66, 76]. This method has several advantages. The system is all fiber, lases stably in a single longitudinal mode, is compact and potentially inexpensive to manufacture. However, the tuning range is limited. These "Bragg reflector" fiber lasers will probably find some applications in sensors [77].

The third method uses a phase modulator at the end of the cavity to sweep the spatial standing wave pattern relative to the fixed gain ions [67]. If the field is swept rapidly relative to the stimulated lifetime of the gain media, the spatial pattern in the gain can be eliminated, eliminating spatial hole burning. However, dithering the cavity length also dithers the laser frequency resulting in a linewidth on the order of the free spectral range of the cavity.

Narrow linewidth is one of the main attractions of the ring cavity configuration. Because unidirectional ring lasers are travelling wave devices, spatial hole burning is eliminated. This allows the construction of longer cavities. The natural or Schawlow-Townes linewidth of a laser is inversely proportional to the square of the resonator length. It is possible to construct single frequency fiber lasers with cavity lengths on the order of 50 m [74]. At the present time, the linewidth of the laser is dominated by fluctuations in the cavity length due to other effects [78]. Frequency stabilization schemes can be employed to eliminate mode hopping and the thermal drift of the cavity length which cause drifts in the lasing frequency [79].

1.3 Applications of Fiber Lasers

It is hoped that fiber lasers may play a role in several areas. These include use of single frequency and mode-locked fiber lasers in fiber optic communications systems; high resolution frequency and time domain spectroscopy; and fiber sensors. Already, single frequency fiber lasers made with the intra-core Bragg grating technique have been demonstrated as temperature and strain sensors [77]. A single frequency fiber laser based on a bulk grating and frequency stabilized to acetylene has been used to as a tool for high resolution spectroscopy in the study of rubidium [80].

Three single-frequency fiber lasers have been employed in an experiment in which two lasers of different frequencies (f1, f2 (f2>f1)) are sent through a multiple quantum well semiconductor travelling wave optical amplifier [81] (figure 1.4). A nonlinear component in the amplifier's gain arising from the effects of interband and intraband dynamics mixes the two optical fields generating new frequencies at f1 - (f2-f1) and f2 + (f2 - f1). The power in these new frequencies is small, so a third fiber laser is employed to allow heterodyne detection of the new frequency.

The advantages of the erbium doped fiber lasers in this spectroscopic application are wide tunability in combination with narrow (< 2 kHz, on time scales < 1 ms) linewidth. The wide tunability allows observation of new frequencies created up to 1 THz away from the pump frequencies. The narrow linewidth of the lasers allow one to narrow the resolution bandwidth of the detection system down to the 10 kHz range, thus lowering the noise floor of the measurement system in comparison to other systems which might employ broader linewidth semiconductor lasers [82].

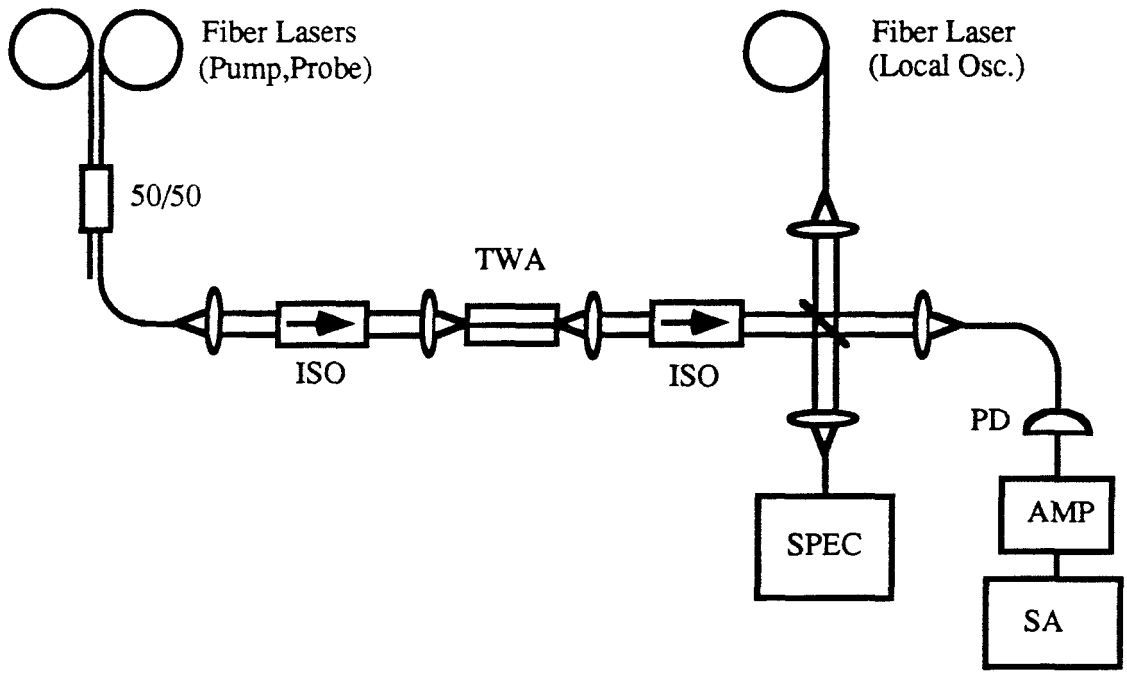

Figure 1.4: Four-wave mixing in a semiconductor optical amplifier, 50/50 fused fiber coupler, ISO: isolator, TWA: travelling wave amplifier, SPEC: spectrometer, AMP: amplifier, PD: photodiode, SA: spectrum analyzer.

1.4 Thesis Outline

This thesis describes the development and characterization of a single-frequency, widely tunable erbium doped fiber ring laser. Chapter 2 discusses in detail the design considerations and basic principles of operation of the single frequency fiber laser. Basics, including the gain media and the selection of the ring configuration, are considered. The tandem fiber Fabry-Perot filters, their interaction with each other and their effect on side mode suppression and tuning are discussed. Experimental verification of single frequency operation, tuning range, threshold pump power, efficiency and output power are described.

Chapter 3 looks at the intensity noise of the laser. The intensity noise is measured in three spectral regimes, noise at frequencies less than the free spectral range of the laser cavity, noise primarily due to nearby ring cavity sidemodes beating with the main lasing mode and noise at frequencies large compared with the narrowband fiber Fabry-Perot filter bandwidth. It is shown that the spectral content of the intensity noise at frequencies greater than twice the narrowband fiber Fabry-Perot filter bandwidth can be reduced to the shot noise limit by proper choice of output coupling and placement of the narrowband fiber Fabry-Perot filter between the gain media and the output coupler. This result is verified experimentally using a balanced homodyne measurement system.

Chapter 4 looks at the fiber laser's phase and frequency noise. Because of the narrow linewidth of the fiber laser, it was not possible to use a standard delayed self-heterodyne interferometer to measure the laser's linewidth as the amount of fiber required for the delay line would be prohibitive (200 km for 1 kHz resolution). A new technique was developed that uses a loss compensated recirculating delay line to measure the laser linewidth to 1 kHz resolution using only 11 km of fiber and to allow measurement of short term (< 2 ms) frequency jitter of the fiber laser. This new technique will be described in

detail. Experimental measurements of the laser's phase and frequency noise using this technique will then be presented.

Chapter 5 discusses frequency stabilization of the fiber laser. The linewidth and frequency jitter measurements described in chapter 4 indicated that the frequency jitter time scale is slow enough so that a frequency control loop of relatively low bandwidth (< 20 kHz) would be sufficient to stabilize the laser frequency. The Pound-Drever technique was used to lock the laser frequency to the transmission peak of an external fiber Fabry-Perot cavity. The Pound-Drever technique for frequency locking of a laser to an external cavity will be reviewed. Implementing frequency stabilization to an external reference required locking the internal mode selector to the external reference as well as locking the cavity mode to the external reference. Changes in design necessary to achieve this result will be discussed. Locking of two lasers to the same external cavity will then be considered. Relative frequency stability of two lasers locked to the same cavity will be investigated using this technique and compared to the measurements from the loss compensated recirculating delayed self-heterodyne interferometer described in chapter 4.

The overall cost of this laser system is quite high (currently around $30,000). However, one of the major cost factors, that of cost per mW of 980 nm pump sources is rapidly falling [19]. Erbium fiber is also becoming more readily available at lower prices. Soon the majority of the cost of a laser such as this one will be contained in the mode selection and frequency stabilization components. Multiple frequency fiber lasers offer the possibility of effectively distributing the cost of these components among several fiber lasers, thus lowering the cost per laser.

Chapter 6 looks at the possibility of multiple frequency fiber lasers. It is possible, using wavelength division multiplexing technology, to generate multiple single longitudinal modes in the same cavity at fixed frequency spacings. There are two ways to achieve this: by giving each wavelength its own gain section or by carefully matching the loss at each wavelength to the gain at that wavelength and employing a single gain module (very weak

spectral hole burning allows simultaneous lasing of more than one wavelength). Two different experiments were conducted that investigated multi-frequency lasing. One involved a tunable dual-frequency laser with one or two gain media. The other involved investigation of wavelength division multiplexing technology and the construction of a six-frequency single gain module device. The weak spectral hole burning effect is investigated using an erbium doped amplifier and two tunable fiber lasers. Finally, an N-frequency fiber laser is proposed based on this work and the work in the preceding chapters.

References

[1] R. H. Stolen, E. P. Ippen, *Appl. Phys. Lett.* **22**, 276 (1973)

[2] T. L. Koch, U. Koren, *IEEE J. Quantum Electron.* **QE-27**, 641 (1991)

[3] M. Bagley, G. Sherlock, D. M. Cooper, L. D. Westbrook, D. J. Elton, H. J. Wickes, P. C. Spurdens, W. J. Devlin, *Electron. Lett.* **26**, 512 (1990)

[4] G. Eisenstein, U. Koren, G. Raybon, T. L. Koch, J. M. Wiesenfeld, M. Wegener, R. S. Tucker, B. I. Miller, *Appl. Phys. Lett.* **56**, 1201, (1990)

[5] G. Eisenstein, R. S. Tucker, J. M. Wiesenfeld, P. B. Hansen, G. Raybon, B. C. Johnson, T. J. Bridges, F. G. Storz, C. A. Burrus, *Appl. Phys. Lett.* **54**, 454 (1989)

[6] K. Inoue, *Electron. Lett.* **23**, 911, (1987)

[7] A. A. M. Saleh, paper ThC1 in *Optical Fiber Communication 1992 Technical Digest Series Volume 5* (Optical Society of America), 199 (1992)

[8] E. Snitzer, *Phys. Rev. Lett.* **7**, 444 (1961)

[9] S. B. Poole, D. N. Payne, M. E. Fermann, *Electron. Lett.* **21**, 737 (1985)

[10] R. J. Mears, L. Reekie, S. B. Poole, D. N. Payne, *Electron. Lett.* **21**, 738 (1985)

[11] J. R. Armitage, *Applied Optics* **27**, 4831 (1988)

[12] P. R. Morkel, R. I. Laming, *Optics Letters* **14**, 1062 (1989)

[13] E. Desurvire, J. R. Simpson, *J. Lightwave Tech.* **7**, 835 (1989)

[14] E. Desurvire, *J. Ligthwave Tech.* **8**, 1517 (1990)

[15] J. R. Armitage, *IEEE J. Quantum Elec.* **QE-26**, 423 (1990)

[16] E. Desurevire, *IEEE Photon. Tech. Lett.* **2**, 208 (1990)

[17] S. Uehara, M. Okayasu, T. Takeshita, O. Korgure, M. Yamada, M. Shimizu, M. Horiguchi, *Optoelctron. Devices Technology* **5**, 71, (1990)

[18] D. Mehuys, D. F. Welch, L. Goldberg, *Electron. Lett.* **28**, 1944 (1992)

[19] T. Moss, *Photonics Spectra* **26**, 28 (1992)

[20] R. J. Mears, L. Reekie, I. M. Jauncey, D. N. Payne, *Proceedings OFC* Reno, Nevada (1987)

[21] E. Desurvire, J. R. Simpson, P. C. Becker, *Optics Letters* **12**, 888 (1987)

[22] I. Sankawa, H. Izumita, S. I. Furukawa, K. Ishihara, *IEEE Photon. Tech. Lett.* **2**, 422 (1990)

[23] Y. Dusteste, M. Monerie, J. Y. Allain, H. Poignant, *Electron. Lett.* **27**, 626 (1991)

[24] S. F. Carter, D. Szebesta, S. T. Davey, R. Wyatt, *Electron. Lett.* **27**, 628 (1991)

[25] R. C. Steele, G. R. Walker, *IEEE Photon. Tech. Lett.* **2**, 753 (1990)

[26] D. A. Fishman, J. A. Nagel, T. W. Cline, R. E. Tench, T. C. Pleiss, et al., *IEEE Photon. Tech. Lett.* **2**, 753 (1990)

[27] G. R. Walker, R. C. Steele, N. G. Walker, *J. Ligthwave Tech.* **8**, 1409 (1990)

[28] M. Nakazawa, Y. Kimura, *Electron. Lett.* **27**, 1065 (1991)

[29] M. Ohashi, K. Shiaki, *Electron. Lett.* **27**, 2143 (1991)

[30] C. G. Atkins, J. F. Massicott, J. R. Armitage, R. Wyatt, B. J. Ainslie, S. P. Craig-Ryan, *Electron. Lett.* **25**, 910 (1989)

[31] C. P. Botha, *Electron. Lett.* **24**, 243 (1988)

[32] M. Yamada, M. Shimizu, M. Okayasu, T. Takeshita, M. Horiguchi, Y. Tachikawa, E. Sugith, *IEEE Photon. Tech. Lett.* **2**, 205 (1990)

[33] M. Nakazawa, Y. Kimura, E. Yoshida, K. Suzuki, *Electron. Lett.* **26**, 1936 (1990)

[34] M. M. Choy, C. Y. Chen, M. Andrejco, M. Saifi, C. Lin, *IEEE Photon. Tech. Lett.* **2**, 38 (1990)

[35] R. I. Laming, M. C. Farries, P. R. Morkel, L. Reekie, D. N. Payne, P. L. Scrivener, F. Fontana, A. Righetti, *Electron. Lett.* **25**, 12 (1989)

[36] J. E. Townsend, W. L. Barnes, K. P. Jedrzejewski, S. G. Grubb, *Electron. Lett.* **27**, 1958 (1991)

[37] S. G. Grubb, W. H. Humer, R. S. Cannon, S. W. Vendetta, K. L. Sweeney, P. A. Leilabady, M. R. Keur, J. G. Kwasegroch, T. C. Munks, D. W. Anthon, *Electron. Lett.* **28**, 1275 (1992)

[38] J. L. Zyskind, E. Desurvire, J. W. Sulhoff, D. J. DiGiovanni, *IEEE Photon. Tech. Lett.* **2**, 869 (1990)

[39] E. Desurvire, J. R. Simpson, *Optics Letters* **15**, 547 (1990)

[40] M. Tachibana, R. I. Laming, P. R. Morkel, D. N. Payne, *Optics Letters* **16**, 1499 (1991)

[41] J. W. Dawson, N. K. Park, K. J. Vahala, *Appl. Phys. Lett.* **60**, 3090 (1992)

[42] J. R. Armitage, "Introduction of Glass Fiber Lasers and Amplifiers" in *Optical Fiber Lasers and Amplifiers* editor P. W. France, CRC Press 1991

[43] R. I. Laming, L. Reekie, P. R. Morkel, D. N. Payne, *Electron. Lett.* **25**, 455 (1989)

[44] K. Tajima, *Electron. Lett.* **26**, 1498 (1990)

[45] Y. Kimura, M. Nakazawa, *Electron. Lett.* **28**, 1420 (1992)

[46] R. P. Davey, K. Smith, A. McGuire, *Electron. Lett.* **28**, 482 (1992)

[47] D. C. Hanna, A. Kazer, M. W. Phillips, D. P. Shepherd, P. J. Suni, *Electron. Lett.* **25**, 95 (1989)

[48] F. Fontana, G. Grasso, N. Manfredina, M. Romagnoli, B. Daino, *Electron. Lett.* **28**, 1291 (1992)

[49] A. Takada, H. Miyazawa, *Electron. Lett.* **26**, 216 (1990)

[50] H. Takara, S. Kawanishi, M. Saruwatari, K. Noguchi, *Electron. Lett.* **28**, 2095 (1992)

[51] X. Shan, D. Cleland, A. Ellis, *Electron. Lett.* **28**, 182 (1992)

[52] H. Takara, S. Kawanishi, M. Saruwatari, J. B. Schlager, *Electron. Lett.* **28**, 2274 (1992)

[53] D. J. Richardson, R. I. Laming, D. N. Payne, V. Matsas, M. W. Phillips, *Electron. Lett.* **27**, 542 (1991)

[54] I. N. Duling, III, *Electron. Lett.* **27**, 544 (1991)

[55] E. Yoshida, Y. Kimura, M. Nakazawa, *Appl. Phys. Lett.* **60**, 932 (1992)

[56] N. J. Doran, D. Wood, *Optics Letters* **13**, 56 (1991)

[57] D. J. Richardson, R. I. Laming, D. N. Payne, M. W. Phillips, V. J. Matsas, *Electron. Lett.* **27**, 730 (1991)

[58] N. Pandit, D. U. Noske, S. M. J. Kelly, J. R. Taylor, *Electron. Lett.* **28**, 455 (1992)

[59] W. Lenth, R. M. MacFarlane, *Optics and Phonics News*, 8 (March 1992)

[60] J. Y. Allain, M. Monerie, H. Poignant, *Electron. Lett.* **27**, 1156 (1991)

[61] J. Y. Allain, M. Monerie, H. Poignant, *Electron. Lett.* **26**, 166 (1990)

[62] J. J. Whitley, C. A. Millar, R. Wyatt, M. C. Brierley, D. Szebestam, *Electron. Lett.* **27**, 1785 (1991)

[63] R. G. Smart, D. C. Hanna, A. C. Tropper, S. T. Davey, S. F. Carter, D. Szebesta, *Electron. Lett.* **27**, 1307 (1991)

[64] A. Saissy, D. B. Ostrowsky, G. Maze, *Applied Optics* **30**, 1933 (1991)

[65] E. W. J. L. Oomen, *J. Luminescence* **50**, 317 (1992)

[66] G. A. Ball, W. W. Morey, W. H. Glenn, *IEEE Photon. Tech. Lett.* **3**, 613 (1991)

[67] H. Sabert, A. Koch, R. Ulrich, *Electron. Lett.* **27**, 2176 (1991)

[68] M. W. Maeda, J. S. Patel, D. A. Smith, C. Lin, M. A. Saifi, A. Von Lehman, *IEEE Photon. Tech. Lett.* **2**, 787 (1990)

[69] D. A. Smith, M. W. Maeda, J. J. Johnson, J. S. Patel, M. A. Saifi, A. Von Lehman, *Optics Letters* **16**, 387 (1991)

[70] P. R. Morkel, G. J. Cowle, D. N. Payne, *Electron. Lett.* **26**, 632 (1990)

[71] K. Iwatsuki, H. Okamura, M. Saruwatarf, *Electron. Lett.* **26**, 2033 (1990)

[72] G. J. Cowle, D. N. Payne, D. Ried, *Electron. Lett.* **27**, 229 (1990)

[73] P. Barnsley, P. Urquhart, C. Millar, M. Brierley, *J. Opt. Soc. Am. A* **5**, 1339 (1988)

[74] N. K. Park, J. W. Dawson, K. J. Vahala, C. M. Miller, *Appl. Phys. Lett.* **16**, 150 (1991)

[75] S. L. Gilbert, *Optics Letters* **16**, 150 (1991)

[76] J. L. Zyskind, V. Mizrahi, D. J. DiGiovanni, J. W. Sulhoff, *Electron. Lett.* **28**, 1385 (1992)

[77] G. A. Ball, W. W. Morey, P. K. Cheo, to be published *IEEE Photon. Tech. Lett.*

[78] N. K. Park, J. W. Dawson, K. J. Vahala, *Optics Letters* **17**, 1274 (1992)

[79] N. K. Park, J. W. Dawson, K. J. Vahala, to be published Optics Letters

[80] S. L. Gilbert, *Proceedings Tenth International Conference on Laser Spectroscopy*, Font-Romeu, France, 17-21 June, 1991, eds. M. Ducloy, E. Giacobino, G. Camy, pp. 359-364

[81] J. Zhou, N. K. Park, J. W. Dawson, K. J. Vahala, M. A. Newkirk, U. Koren, B. I. Miller, submitted to *Appl. Phys. Lett.*

[82] K. J. Vahala, N. K. Park, J. W. Dawson, S. Sanders, in *AGARD Lecture Series 184, Advances in Fiber-Optic Technology in Communications and for Guidance and Control*, 1-1

Chapter 2

A Single-Frequency Fiber Laser

This chapter details the design, construction and testing of a single-frequency fiber laser. The first part of the chapter discusses important design considerations such as the choice of the resonator geometry, the erbium doped fiber amplifier and the constraints on the tandem fiber Fabry-Perot filters which provide single frequency operation in combination with broad band tunability. The second part of the chapter discusses the details of all components in the laser, assembly of the laser and verification of the operating parameters. Finally, the threshold lasing power, slope efficiency, output power, tuning range, single-frequency operation and sidemode suppression are all experimentally verified.

2.1 Design Considerations for Optimal Single-Frequency Operation of an Erbium-Doped Fiber Laser

In order to achieve lasing, the first requirement is to have an optical gain equal to or greater than the optical loss of the system. Erbium doped fiber amplifiers, which provide greater than 40 dB of optical gain, are now commercially available. Amplifiers with gains as high as 54 dB [1] have been demonstrated. With gains this large, improperly isolated amplifiers will lase off their own cleaved end faces. Since oscillation is easy to achieve

using these devices, there exists a great opportunity to make high performance lasers. Many different components can be inserted in the resonant cavity to perform a variety of specialized functions. If a low loss component is not readily available, the amplifier will easily compensate for a higher loss component allowing demonstration of a desired concept. For example, in chapter 5, a phase modulator is inserted into the cavity to aid in frequency stabilization.

The output power of a laser is dependent upon three major factors: the resonator loss, output coupling and the characteristics of the gain medium. In the case of the single frequency fiber laser, the resonator loss can be estimated from the sum of the individual component losses. A variable output coupler was not available at the time of the experiment, so a fixed 50% output coupler was used. The only remaining parameters necessary to estimate the laser output power are the gain characteristics of the erbium fiber amplifier used in the laser.

Data on the gain characteristics are provided with commercial fiber amplifiers (Figure 2.1). For research grade amplifiers this data must be measured in the lab. (While some amplifiers were constructed during the course of this research, optimal EDFA design has been discussed at length elsewhere [1, 2, 3] and that discussion will not be repeated here.) The easiest way to do this is to use a fiber laser as a signal source. This necessitates having two amplifiers. The experimental setup for measuring the gain characteristics is shown in figure 2.2.

First the output of a fiber laser is collimated. The collimated beam is chopped, attenuated and recoupled back into the fiber. The fiber gain responds slowly due to the 12 ms lifetime of the upper level. Chopping speeds above 200 Hz do not significantly modulate the inversion in the amplifier, thus allowing lock-in detection of the amplified signal. For small input signals (< 40 dBm in a commercial amplifier) the amplified spontaneous emission power actually exceeds the amplified signal power. Lock-in

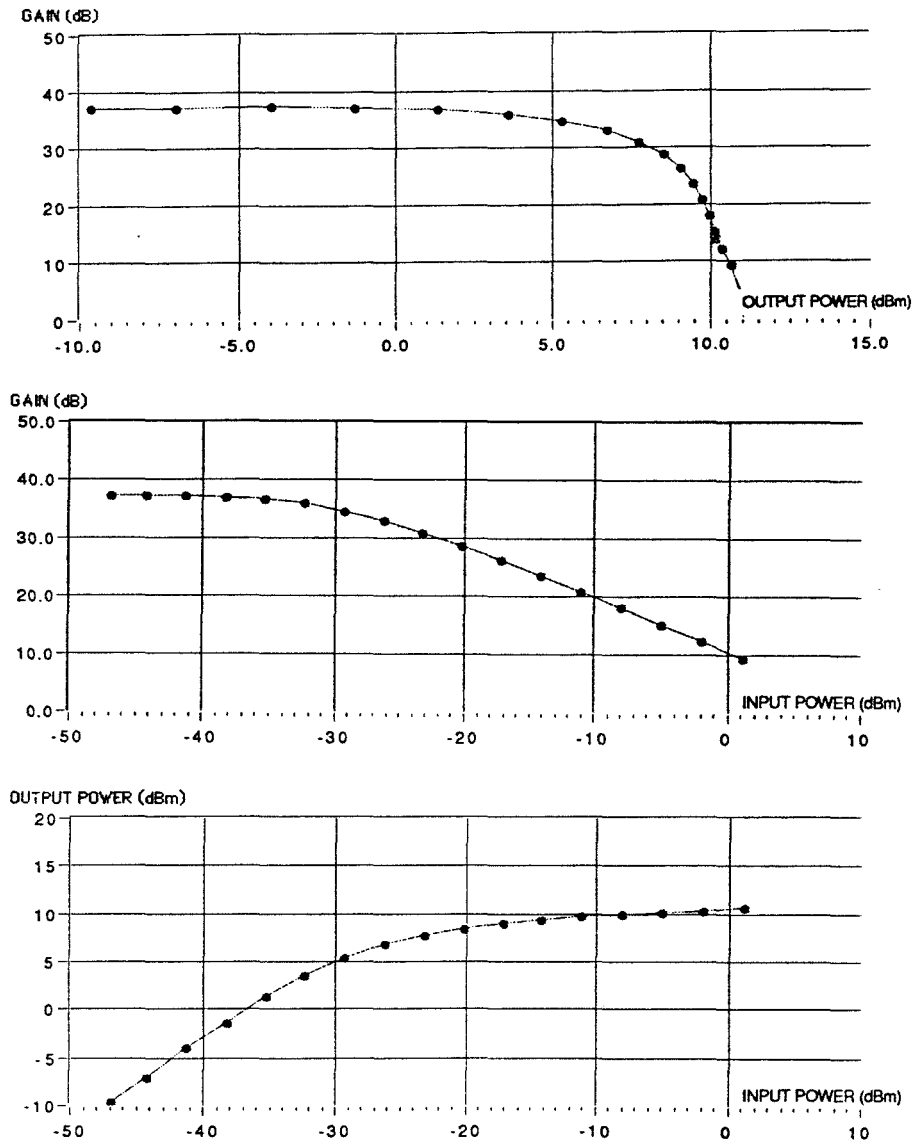

Figure 2.1: Gain characteristics of a commercial EDFA. Corning FiberGain, module P3-21, optical gain at 1532 nm, Al codoped Erbium fiber.

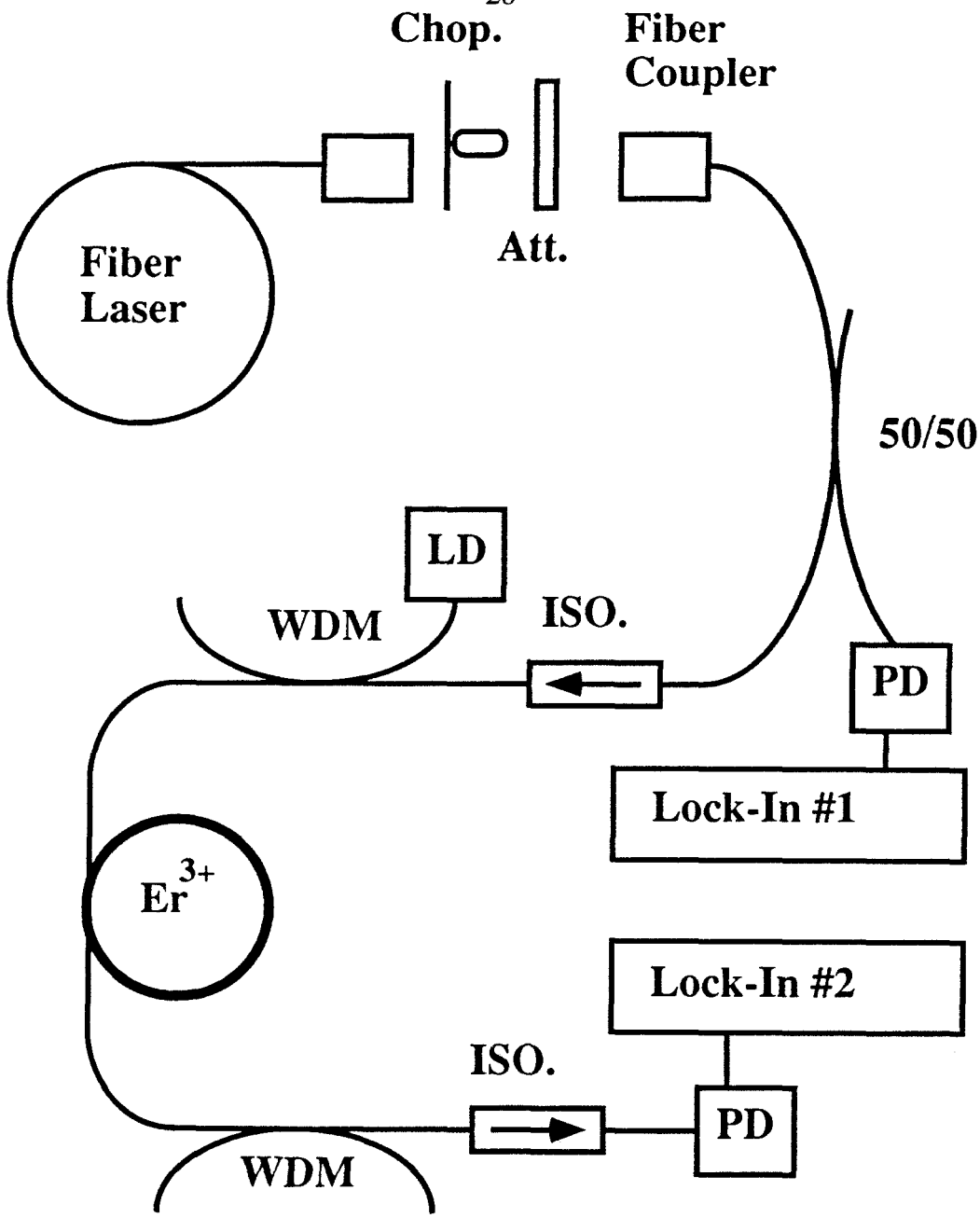

Figure 2.2: Experimental set-up for measuring the gain in an EDFA. WDM: wavelength division multiplexer, ISO: optical isolator, PD: photo-diode, LD: pump laser, Chop: chopper, Att: variable attenuator.

detection of the amplified signal allows it to be separated from the large background noise and minimizes the error due to this noise at larger signal powers.

A fused fiber coupler acts as a beam splitter sending one-half of the signal directly to a photo-detector and the other half through the amplifier to a second photo-detector. Lock-in detection of the input and amplified signals gives an accurate measurement of the gain. Gain may then be measured as a function of input power, output power, pump power and wavelength (provided the fiber laser is tunable). Sample data is shown in figure 2.3.

Measurement of the small signal gain as a function of pump power, combined with knowledge of the laser resonator losses, and the transmission of the output coupler yields the pump power threshold for the laser. Once the gain has been plotted as a function of output power (at maximum pump power), it is a simple matter to determine the amplifier output power at which the gain is equal to the loss. The laser output power is the amplifier output power at that gain reduced by the loss from the components between the amplifier and the output coupler multiplied by the transmission of the output coupler. It should be noted that for small resonator losses, simple formulas may be derived for laser output power as a function of output coupler transmission [4]. However, the loss in a typical fiber laser described in this thesis is greater than 10 dB and in this limit the assumption of small losses does not hold.

Now that threshold and output power have been discussed, the requirements for tuning and single frequency operation are considered. As mentioned earlier, the gain bandwidth of an EDFA is nearly 50 nm; providing an appropriate tuning element can be found, it is not difficult to achieve tuning over this entire range. Stable, single-frequency operation is much more difficult to achieve, however.

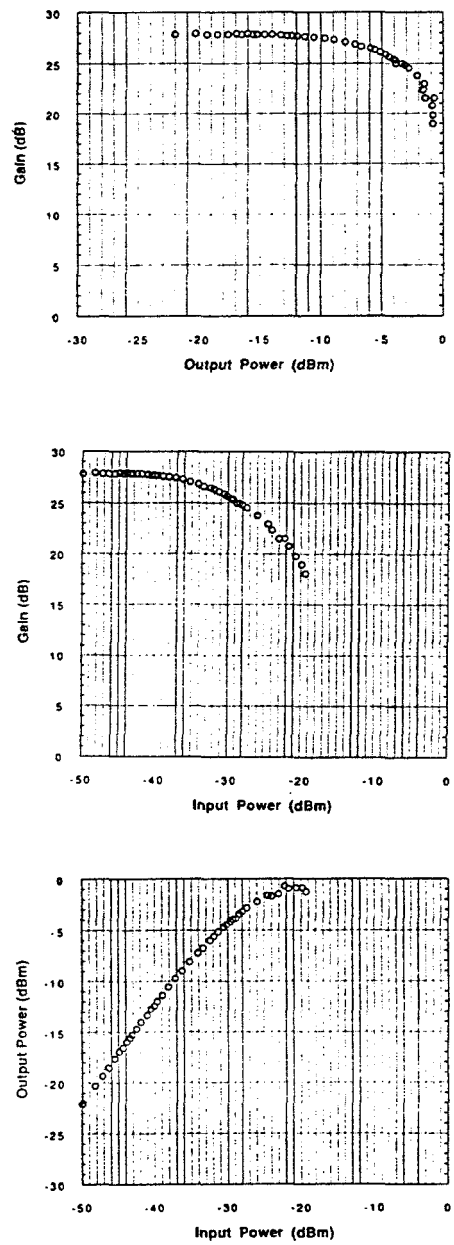

Figure 2.3: Measured gain characteristics of an EDFA. 12 m of York Erbium fiberEr concentration 100 ppm, pump power 30 mW, wavelength 1537 nm, Ge-only codoping.

If the optical field in the resonator is a standing wave, spatial holes will be burned into the gain. The gain will not saturate at the nodes of the optical field, only at the maxima. Other longitudinal modes of the resonator may be able to take advantage of these unsaturated regions to achieve sufficient gain to oscillate. This effect was first observed by Tang [5].

There are two common ways to achieve single frequency operation. One method is to provide feedback to only one resonator mode within the gain bandwidth, by using a short cavity and a very narrow band reflection filter [6]. The second method is to construct a resonator using a ring geometry including optical isolators to ensure unidirectional travelling wave operation. Spatial holes are eliminated in this case because the travelling wave does not have nodes at fixed locations in space. The ring geometry also permits the use of narrow band transmission filters as tuning and wavelength selection elements as opposed to the narrow band reflection filters used in the linear cavity case.

Narrow band transmission filters such as fiber Fabry-Perot filters are commercially available in an electronically tunable form. Furthermore, as more effort is being put into realizing wavelength division multiplexed communications systems, more research addresses electronically tunable narrowband transmission filters [7, 8]. These filters are likely to improve in reliability, tuning range, bandwidth, and availability.

Narrow band reflection filters, by comparison, are not as well developed. There is currently only one device of widespread interest: the intra-core Bragg grating holographically written with an ultraviolet laser [9, 10]. This device is tuned by stretching or heating the grating. The extent of its practical tuning range and speed is unclear. Intracore Bragg gratings are also not yet commercially available.

For these reasons the fiber laser constructed here employs a unidirectional travelling wave ring geometry with fiber Fabry-Perot filters as tuning elements. It is possible to construct fiber Fabry-Perot filters with finesses as high as 2000 [11]. However, currently available commercial devices typically have a finesse of about 120.

It is desirable for the laser's tunability to be limited only by the gain bandwidth and not other components in the system. Therefore, the desirable free spectral range of the fiber Fabry-Perot filter is at least the EDFA bandwidth. This is nominally 30 nm, but it is possible to achieve laser operation over nearly 50 nm [12]. At a wavelength of 1550 nm, 50 nm corresponds to 6.244 THz. Assuming a finesse of 120 this gives a fiber Fabry-Perot filter with a bandwidth of 52 GHz. Fiber lasers with narrowband transmission filters other than a fiber Fabry-Perot but with transmission bandwidths close to this figure [12, 13, 14] have been observed to exhibit rapid mode-hopping over a range of several GHz. To understand why this is so, it is necessary to consider the sidemode suppression of the fiber laser.

The sidemode suppression in a single frequency laser is the ratio of the power in the lasing mode to the power contained in the strongest longitudinal mode of the laser other than the lasing mode. For stable single frequency operation, this ratio needs to be large. In order to better understand the factors that govern the sidemode suppression, a brief derivation of it will be presented at this point.

Consider the rate equations for the cavity modes. Assume the gain, g, is flat in the region of interest. Let P_l denote the power in the lasing mode and P_m denote the power contained in a nearby longitudinal mode. Let θ denote the spontaneous emission into a longitudinal mode at a given gain, g. Finally, let α_l denote the loss in the lasing mode and α_m, the loss in the sidemode of interest. Then the rate equations for the longitudinal modes are

$$\frac{dP_l}{dt} = g P_l - \alpha_l P_l + \theta \qquad (2.1)$$

$$\frac{dP_m}{dt} = g P_m - \alpha_m P_m + \theta \qquad (2.2)$$

The laser is assumed to be operating continuous wave, so the time derivatives in 2.1 and 2.2 may be set equal to zero to solve for the steady state power. Therefore,

$$P_l = \frac{\theta}{\alpha_l - g} \qquad \text{and} \qquad P_m = \frac{\theta}{\alpha_m - g} \tag{2.3}$$

The sidemode suppression is defined to be the ratio of the power in the lasing mode to the power in the sidemode in question. Therefore,

$$\frac{P_l}{P_m} = \frac{\alpha_m - g}{\alpha_l - g} = 1 + \frac{\alpha_m - \alpha_l}{\alpha_l - g} \approx \frac{(\alpha_m - \alpha_l)\, P_l}{\theta} \tag{2.4}$$

where equation 2.3 was used in the last step. The difference between the lasing mode loss and the gain is very small. The loss difference between two modes should be a somewhat larger number if the laser is truly lasing in only one longitudinal mode. This justifies the approximation in the last step of 2.4.

From 2.4 it is clear that the sidemode suppression increases as the loss difference between the lasing mode and the nearest adjacent longitudinal modes increases. The sidemode suppression also increases as the power in the lasing mode increases. The amount of power in the lasing mode will be limited by the output power of the fiber amplifier at the gain necessary to achieve oscillation. Decreasing the overall resonator loss will increase the laser power and lower the amount of spontaneous emission into the mode, thus increasing the sidemode suppression. Dramatic improvement is not possible using this method, however.

This leaves the loss difference between the lasing mode and the adjacent sidemodes to consider. The spacing of the longitudinal modes will greatly affect their loss difference.

The longitudinal mode spacing is inversely proportional to the length of the resonator. The fiber laser's length must be at least as long as the EDFA plus length for optical isolators, an output coupler, a polarization controller and the tuning filter. Using a normal EDFA this puts a lower bound on the length of 25 m. Using an EDFA based on highly doped erbium fiber, it is possible to reduce this length to around 4 m [15]. However, highly doped fiber is neither commercially available or available in the preferred aluminium codoped, wide bandwidth form. If one assumes a fiber laser length on the order of 25 m, the longitudinal mode spacing of the resonator will be 8 MHz. As mentioned above, the tuning filter free spectral range is 6.24 THz and the bandwidth is 52,000 MHz. Assuming a standard Fabry-Perot transmission function, the loss difference between the mode directly under the transmission peak and the mode that is 8 MHz away is $2.6X10^{-8}$. This is a very small number and in practice is insufficient to provide good sidemode suppression.

It is possible to improve the loss difference by choosing a smaller free spectral range and thus a smaller bandwidth. For example, a fiber Fabry-Perot filter with a free spectral range of 10 GHz and a bandwidth of 125 MHz would give a loss difference of $1.6X10^{-2}$. This should result in an increase in sidemode suppression of 58 dB in comparison to above. However, use of this filter alone would reduce the tuning range to 10 GHz.

To prevent the nearest neighbor longitudinal cavity modes from lasing and to restore the wide tuning range, it is possible to combine the best aspects of the two fiber Fabry-Perot filters by using them in tandem. A narrowband fiber Fabry-Perot filter (NB FFP) with a bandwidth of 125 MHz could be employed to ensure a large sidemode suppression and thus high stability. A broadband fiber Fabry-Perot filter (BB FFP) could then be employed to select which NB FFP transmission peak had sufficiently low loss to allow only one of the longitudinal modes of the resonator to lase. Figure 2.4 shows the transfer functions of the two filters, the transfer function of the tandem pair with isolation and the longitudinal mode spacing of the fiber laser.

The last important design consideration is optical isolation. The NB FFP and BB FFP described above are constructed of two fibers with highly reflective dielectric mirrors deposited on the ends. These mirrored fiber ends are brought close together to form an optical cavity. With two FFP filters in the resonator, an optical cavity is also formed by the space between the two filters. In order to ensure the tandem pair of filters is operating correctly (i.e., the transfer function of the tandem pair is the product of the transfer functions of the individual filters), an optical isolator must be placed between the filters.

Finally, isolation around the gain region must be considered. The loss difference between adjacent longitudinal modes of the fiber laser is very small. Small amounts of feedback to the very large gain in the EDFA can cause significant gain ripple. In short this gain ripple can invalidate the assumption of a flat gain over the bandwidth of the NB FFP used in the sidemode suppression calculation. (This is one reason the BB FFP is insufficient to provide stable single frequency operation by itself.) Thus the sidemode suppression can be significantly less than predicted. Furthermore, the gain medium length can drift with temperature and the peaks and valleys of the gain ripple can move with respect to the NP FFP filter peak, actually inducing mode hops.

On the surface one might think that this effect could be easily countered, however, feedback as small as 1 part in 10^3 (30 dB of isolation at both ends of the EDFA) in combination with a gain of 20 dB can lead to gain ripple induced mode hopping. Fortunately, increasing the isolation to 40 dB or shorting the gain medium can eliminate the problem. A general expression for the gain ripple is given in reference 16.

To summarize this section, there are several important points to consider when constructing a single-frequency fiber laser. The first of these is ensuring low loss and appropriate output coupling based on that loss. Determination of the output coupling for high loss lasers requires measurement of the saturation characteristics of the laser amplifier. For wideband tuning combined with single-frequency operation, a narrowband transmission filter in conjunction with a ring cavity configuration is found to give the best

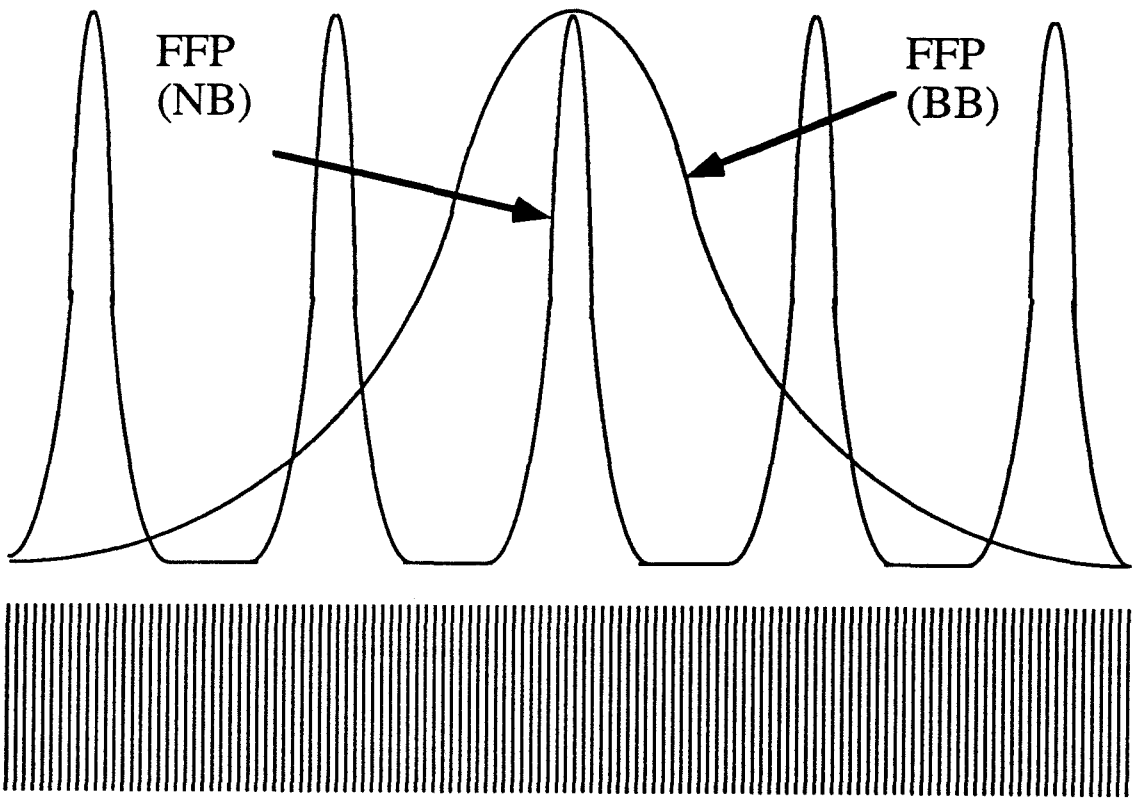

Figure 2.4: Tandem fiber Fabry-Perot filter concept. The BB FFP filter selects the coarse lasing wavelength. The NB FFP provides sufficient loss difference between longitudinal modes so that only one mode lases.

results. For stable operation, an NB FFP and BB FFP are combined in tandem to provide broadband tuning in combination with high sidemode suppression. Finally optical isolation must be considered. Isolation is required between the tandem fiber Fabry-Perot filters and severe restraints are placed on the isolators surrounding the gain media due to the detrimental effects of gain ripple on the sidemode suppression.

2.2 Construction of an All-Fiber, Widely-Tunable, Single-Frequency Erbium-Doped Ring Laser

Figure 2.5 is a schematic of the basic fiber laser design that will be considered throughout the rest of the thesis [17, 18]. The laser is a ring resonator with travelling wave operation to prevent spatial hole burning. The gain element in the laser consists of a commercial EDFA approximately 25 m in length. This EDFA is an aluminium codoped module with a gain peak at 1532 nm and capable of providing 37 dB of optical gain at this wavelength. The gain characteristics are shown in figure 2.1.

There are three isolators pictured in figure 2.5. These isolators are pigtailed with single mode fiber and are designed to operate uniformly independent of the input polarization state. The peak isolation is 40 dB at 1540 nm with a minimum isolation of 30 dB (from 1520-1560 nm) and an insertion loss of 0.6 dB. The isolators are placed as discussed above. One isolator is used to inhibit interaction between the two tandem fiber Fabry-Perot filters and one isolator is placed at each end of the EDFA to minimize the gain ripple.

There are two fiber Fabry-Perot filters in the laser. These two filters act in tandem to provide high sidemode suppression and stable single frequency operation in combination with broadband tunability. The broadband fiber Fabry-Perot filter (BB FFP) has a free spectral range of 4024 GHz or about 32 nm. The BB FFP's finesse is 120 and the corresponding bandwidth is 33 GHz. This filter provides broadband tunability for the

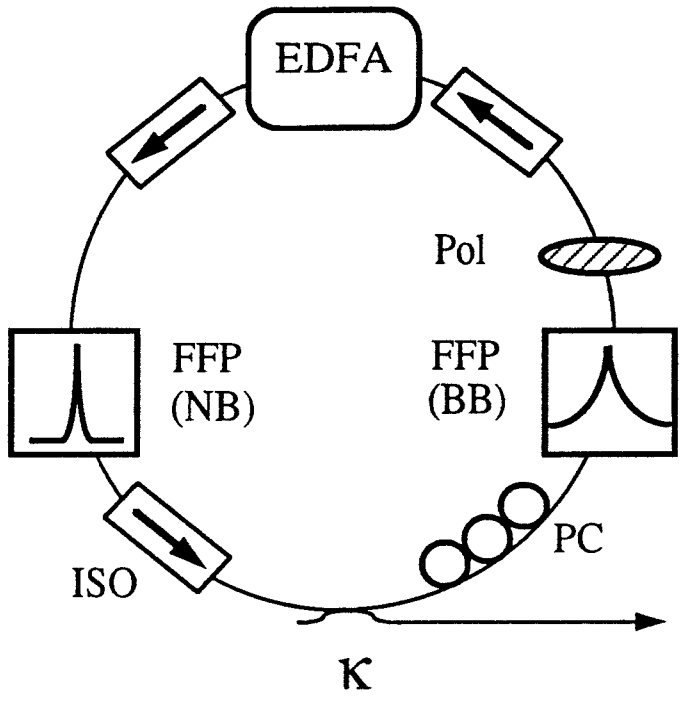

Figure 2.5: Erbium-doped fiber ring laser.FFP: fiber Fabry-Perot filter, Pol: polarizer, PC: polarization controller, κ: output coupler, ISO: isolator, EDFA: Erbium doped fiber amplifier

laser; its insertion loss is 3 dB. The BB FFP can be tuned over its entire free spectral range by applying a voltage of 0-17 V to a piezo-electric stack bonded to the device.

The narrowband fiber Fabry-Perot filter (NB FFP) has a free spectral range of 10.2 GHz or about 0.1 nm. The NB FFP's finesse is 80 and the corresponding bandwidth of the device is 125 MHz. This filter provides high sidemode suppression and stable operation for the laser; its insertion loss is 4 dB. It is not tunable. The cavity for the BB FFP is an air gap between two closely spaced fibers whose facets are coated to form dielectric mirrors. The NB FFP's cavity is longer than the BB FFP's cavity and so a piece of fiber is inserted between the dielectric mirrors to prevent diffraction from lowering or altogether eliminating the FFP finesse.

The intra-cavity fiber in the NB FFP must be fixed in place. The stresses that hold this fiber induce birefringence in the NB FFP. As a result the NB FFP cavity length is a function of the input polarization state and when inserted into the laser ring the laser frequency will be a function of the laser polarization state. To prevent the laser polarization state from fluctuating with temperature and other extrinsic effects, a polarizer and polarization controller have been placed in the resonator.

The polarizer used in the cavity is a plasmon wave type polarizer. It is made from polarization preserving fiber that has been lapped and polished close to the core along one polarization axis. A metal is then deposited onto the fiber. Incoming light polarized perpendicular to the metal coating is essentially unaffected. Incoming light polarized parallel to the metal coating loses energy by exciting surface plasmon waves in the metal coating. The polarization extinction ratio of this device is 27 dB and the insertion loss is less than 0.5 dB (not counting losses in coupling to and from non-polarization maintaining fiber to polarization maintaining fiber).

The polarization controller used in the laser consists of three fiber optic quarter wave plates whose axes of birefringence can be rotated with respect to the others. Each quarter wave plate is a two inch diameter disk about which a single mode optical fiber is

wrapped three times. Bending stresses from the fiber being wrapped around the disk induce birefringence; three wraps provide the correct length for a quarter wave plate.

The output coupler of the laser is a 3 dB fused fiber coupler. These devices are made by twisting two fibers about each other and fusing them together. The twisted section is heated and stretched. During this process the cores of the two fibers are brought close together and as a result there is coupling of light from one core to the other. By monitoring light throughput during the stretching process, the degree of coupling may be controlled. The twisted section is hermetically sealed in a rigid housing to protect it. Wavelength division multiplexers that act as dichromatic mirrors or beamsplitters may be also fabricated by this process.

All of these components are connected together either by fusion splices or by reusable mechanical splices. A fusion splicer brings two cleaved fibers together using xyz translational stages. An electric arc heats the fiber end faces as they are pushed together. This technique can produce low loss (< 0.1 dB) low back-reflection (<60 dB) connections. However, the splices require about 15-20 minutes to make in the lab and may have to be done more than once to achieve good results (newer model fusion splicers can make splices faster and more reliably).

A more convenient way to connect components together is to use mechanical splices. These splices are reusable and can be made in about 2 minutes. They have an insertion loss of 0.2 dB and a back-reflection of < 40 dB. A typical splice consists of a guide to align the two fibers and index matching gel to avoid Fabry-Perot effects that might occur due to the small air gap where the end faces that are brought together. A small piece of plastic can be clamped around the jacketed regions of the two fibers to hold the splice together. Due to convenience, in terms of allowing rapid assembly and interchangability of components, mechanical splices are used for most connections in this research. Only where very low back-reflection was required, such as between the EDFA and the isolators, are fusion splices used.

The total cavity length of the laser for the configuration in figure 2.5 was 50 m corresponding to a longitudinal mode spacing of 4 MHz. This length is somewhat longer than the minimum achievable length. The extra length is primarily due to failure to shorten the fiber pigtails on the components. The components are all relatively new products and as such cost at least $2000 (with the exception of the fused fiber couplers). Shortening the pigtails too much risks destroying the components. If components were to be dedicated to fiber laser use, however, these pigtails could be cut and the components permanently fusion spliced together to form a minimum cavity length device.

The total loss in the laser including the output coupler is 15.3 dB. From figure 2.1 the expected output power of the EDFA at this gain is approximately +10 dBm. This power is attenuated by a 9.0 dB loss between the amplifier output and a photodiode outside the cavity, so that a maximum output power of +1 dBm or 1.25 mW is expected. If the BB FFP were moved to the other side of the output coupler, the output power would increase by 3 dB to approximately 2.5 mW output power.

Looking at figure 2.1 one might be led to believe that a higher output coupling would increase the output power. This is true at the gain peak of 1532 nm; however, a look at gain saturation data at other wavelengths quickly indicates that some other wavelengths would not lase at higher output coupling/higher cavity loss. A 3 dB output coupler gives a relatively flat maximum output power as a function of wavelength, since most wavelengths can readily achieve 15 dB of gain.

2.3 Lasing Characteristics of an All-Fiber, Widely-Tunable, Single-Frequency Erbium-Doped Ring Laser

The laser described above was constructed and fully tested. In order to verify that only one longitudinal mode of the cavity was lasing, the output spectrum was examined with both a spectrometer and a Newport Research Super Cavity Fabry-Perot. The

spectrometer was a SPEX model 340E spectrometer with a resolution of 0.15 nm which corresponds to 18.7 GHz. A spectrometer scan over the full bandwidth of the EDFA (1500-1600 nm, to be absolutely sure) showed only one lasing peak.

The Super Cavity has a free spectral range of 6 GHz and a finesse of greater than 6000. The bandwidth is 1 MHz which is sufficient to resolve the 4 MHz mode spacing of the fiber laser. A scan over one free spectral range of the cavity shows only one lasing mode (see figure 2.6). The smaller peaks in figure 2.6 are transverse modes of the Fabry-Perot analyzer excited by imperfect alignment of the input beam with the fundamental mode of the Super Cavity. These peaks are identifiable by their 800 MHz spacing from the main peak. Figure 2.7 provides a closer look at the lasing mode. The scale in figure 2.7 is 12.5 MHz per division (125 MHz total). This scale is sufficiently narrow so that it may be clearly observed that no other modes are lasing.

Observing the scan from the Super Cavity over a long period of time, the lasing mode can be observed to drift to the left or right, due to thermal expansion/contraction of the laser cavity. As the cavity length expands 1.0 μm (one wavelength in glass), the lasing mode moves out from under the NB FPP transmission peak and one of the nearest longitudinal cavity modes moves under the transmission peak. At this point a mode hop of 4 MHz occurs. This occurs every 30 seconds to a minute. In comparison to previous single frequency fiber ring lasers [12, 13, 14], this is a great improvement since all were observed to mode hop rapidly over several GHz.

To verify the tuning range, the voltage across the BB FFP filter was increased from 0 to 17 VDC in 1 V increments (sufficient voltage to tune the BB FFP one free spectral range). The wavelength was then measured using the spectrometer and single-frequency operation was simultaneously monitored with the Super Cavity. Laser wavelength as a function of voltage applied to the BB FFP is shown in the graph in figure 2.8. (The NB FFP has been moved to the opposite side of the output coupler so the laser is configured for maximum power output.) The laser tunes in 10 GHz jumps from 1528-1558 nm. Two

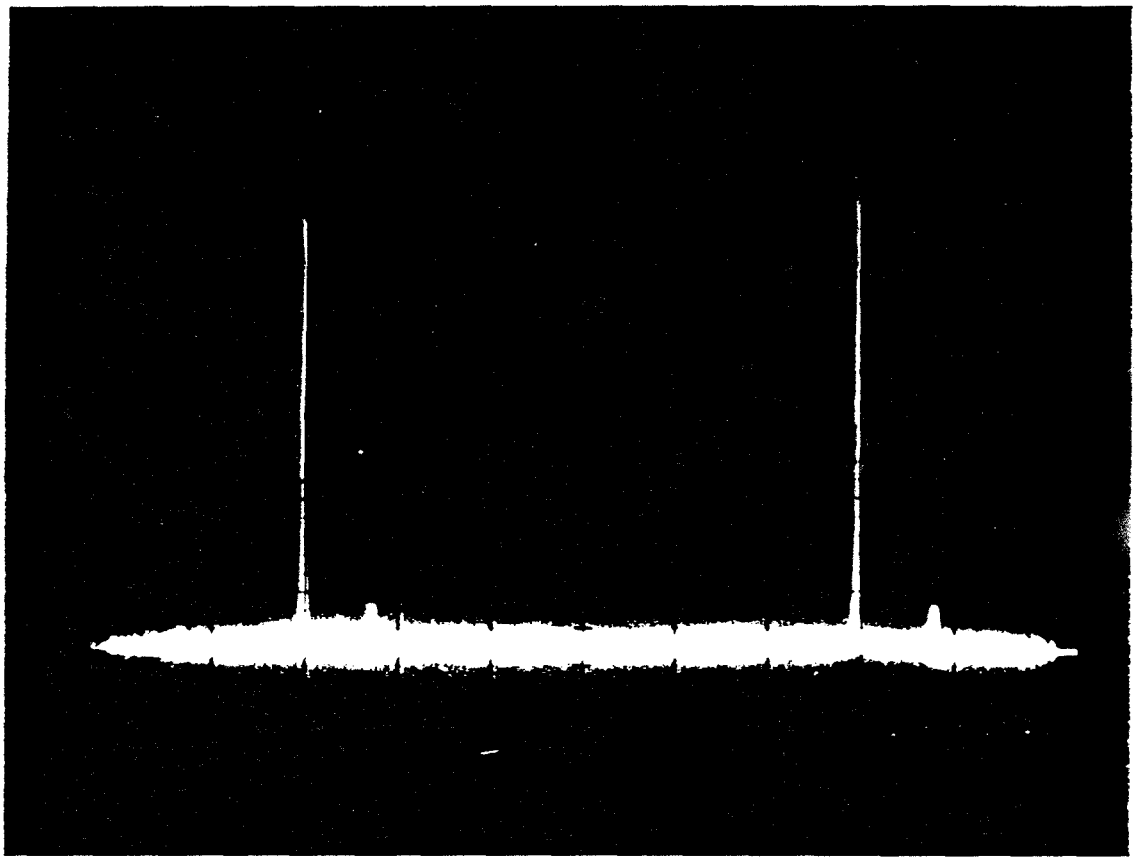

Figure 2.6: Output spectrum of the fiber laser as seen with a Newport Research Super Cavity. The free spectral range is 6 GHz. The smaller peaks are transverse modes of the Super Cavity.

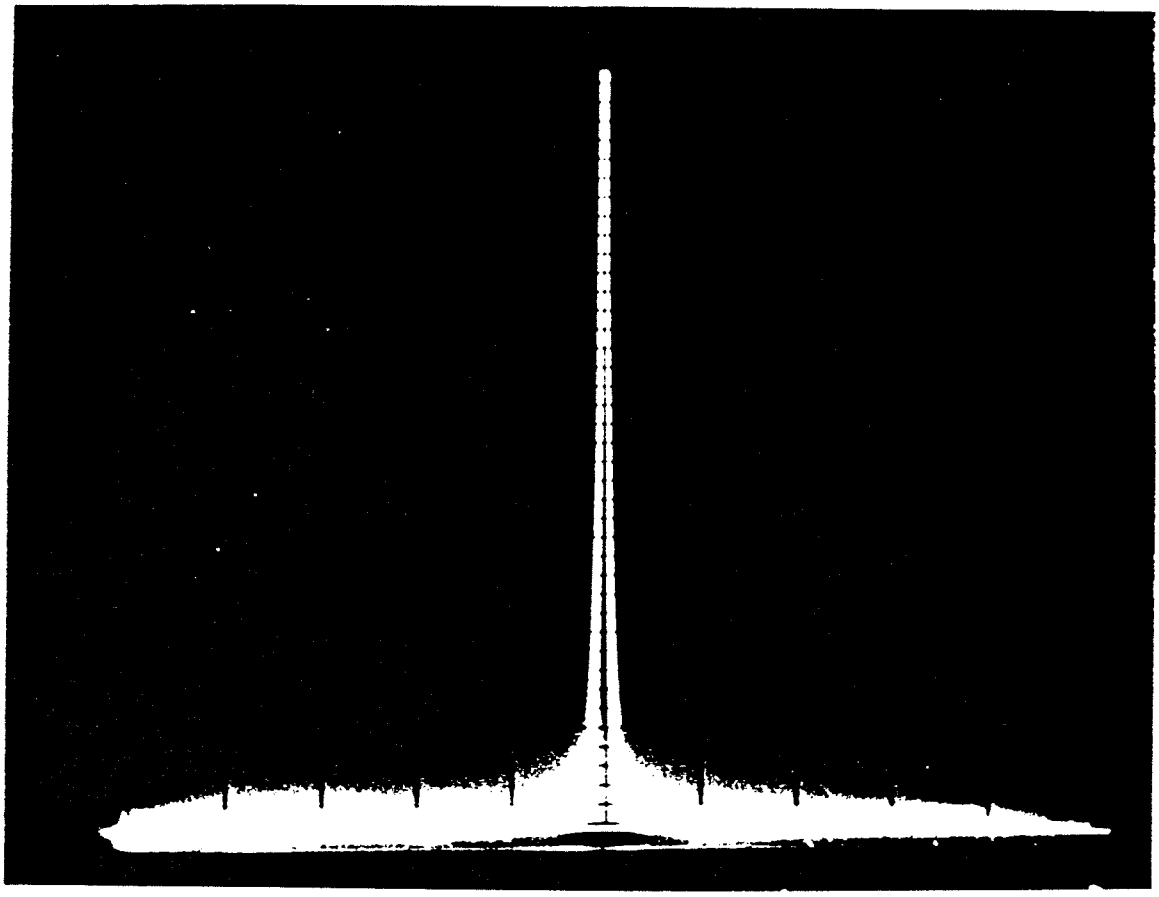

Figure 2.7: Output spectrum of the fiber laser as seen with a Newport Research Super Cavity. The scale is 12.5 MHz/div. The linewidth is limited by the resolution of the supercavity, which is 1 MHz.

modes lase at 11 V, as the gain at 1559 nm approximately equals the gain at 1527 nm (wavelengths that are one BB FFP free spectral range apart).

The laser output power, threshold and slope efficiency were also measured. A typical plot of output power vs. pump power is shown in figure 2.9. The threshold power is around 15 mW. The maximum output power is 1.2 mW as expected and the slope efficiency is approximately 9%. Figure 2.10 shows the output power as a function of wavelength. The output power vs. wavelength is reasonably flat as expected, since for EDFA operation at about 15 dB gain, the output power is approximately + 10 dBm (+/- 1 dB) independent of the operating wavelength.

To complete the initial characterization of the laser properties, the sidemode suppression was also measured. For this measurement the laser output was directed onto a photodiode. A low frequency bias T (10 kHz - 18 GHz) separated the DC component from the AC component of the resulting photo-current. The DC component is measured with an ammeter. The AC component is amplified and sent to an RF spectrum analyzer, where the beating between the sidemodes and the main lasing mode can be observed. The DC photo-current was used to obtain the power in the main mode. The power due to the beating between the main mode and the nearest sidemodes was then read from the spectrum analyzer. From these values the sidemode suppression (ratio of the power in the lasing mode to the power in the largest sidemode) of the laser may be determined. This ratio is as large as 60 dB, which is a good value (for telecommunications systems, 30 dB sidemode suppression is the benchmark for digital communications systems and 60 dB for analog communications systems). The sidemode suppression as a function of laser wavelength is plotted in figure 2.11.

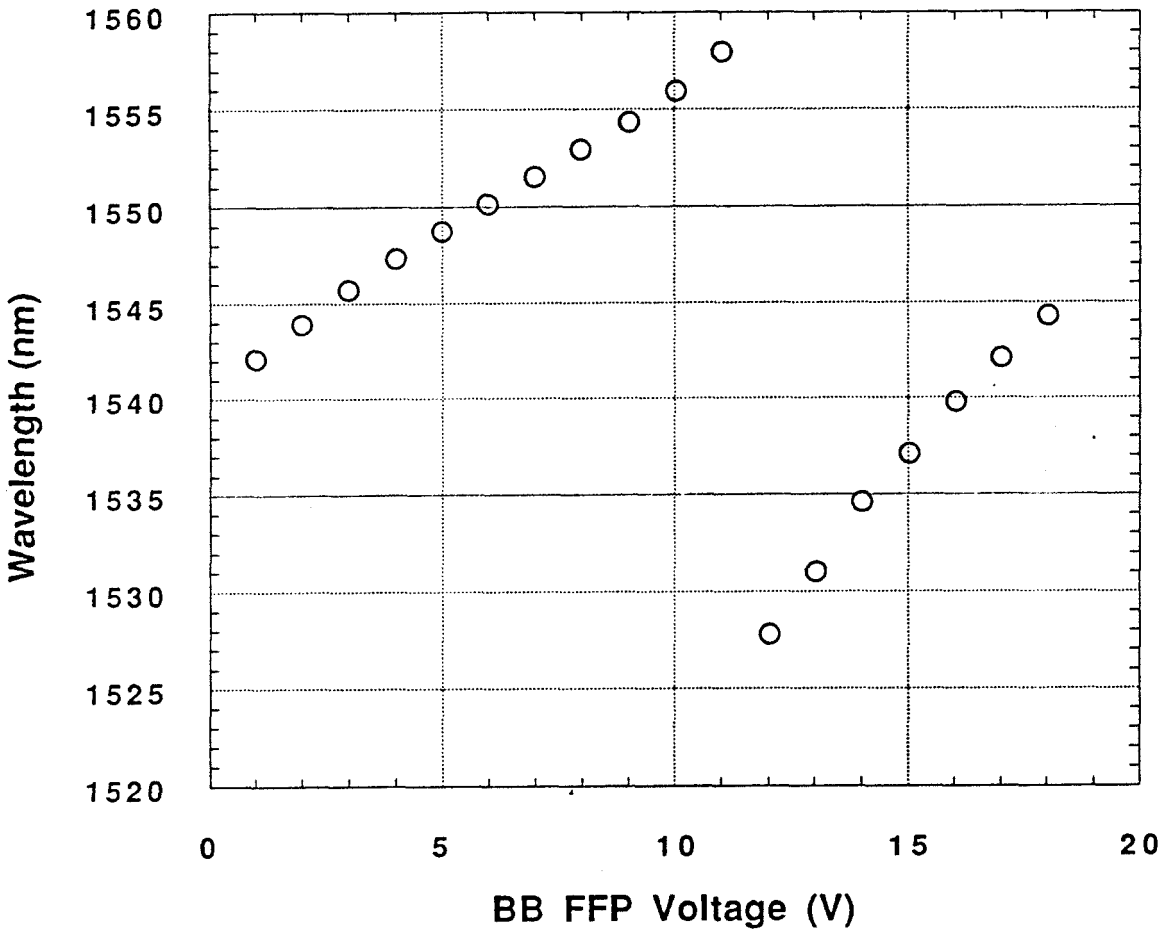

Figure 2.8: Wavelength as a function of voltage applied to the BB FFP. The break at 11 V is the point at which the gain at 1558 nm approximately equals the gain at 1528 nm. The spacing between these wavelengths is one free spectral range of the BB FFP.

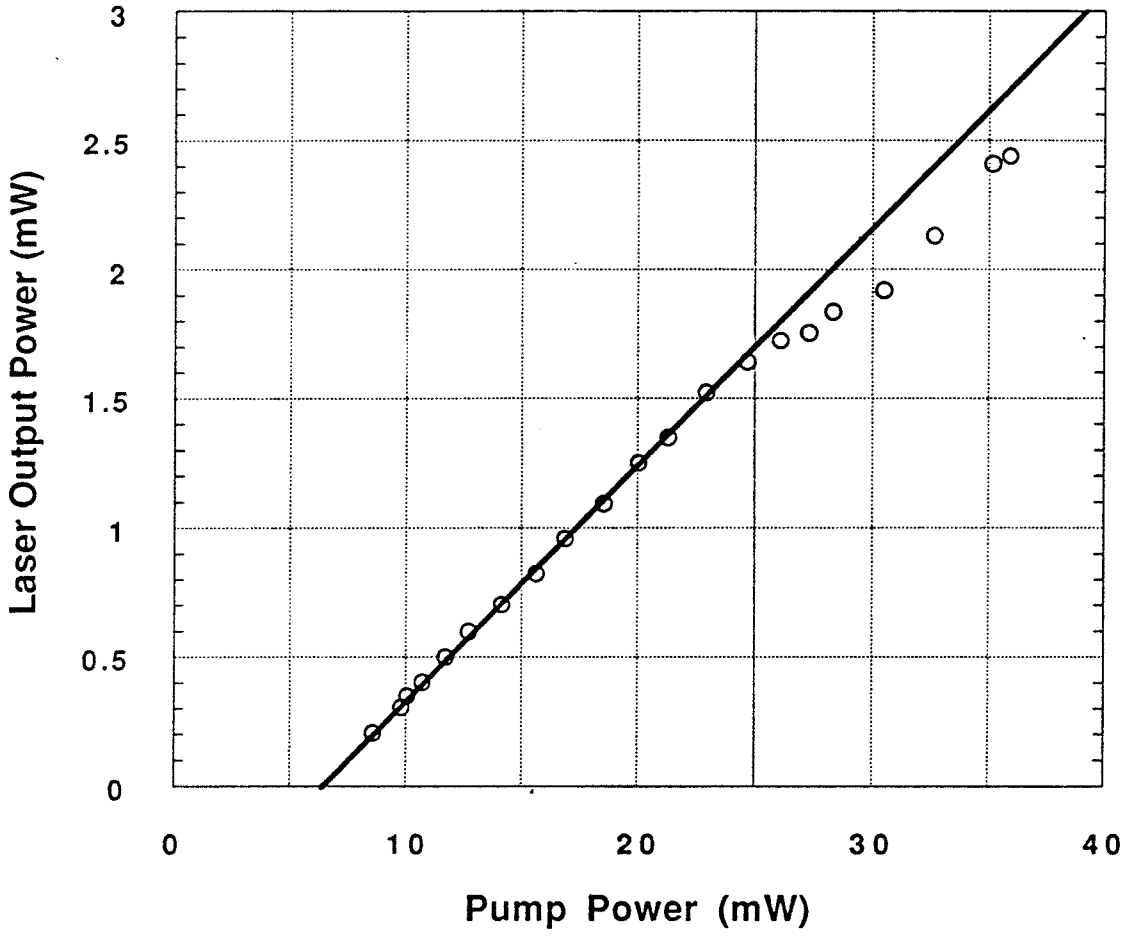

Figure 2.9: Output power vs. pump power. Wavelength: 1550 nm, threshold: 7 mW, slope efficiency: 9%. The roll off at high power is the pump diode lasing spectrum shifting away from 980 nm, changing the pump power absorption.

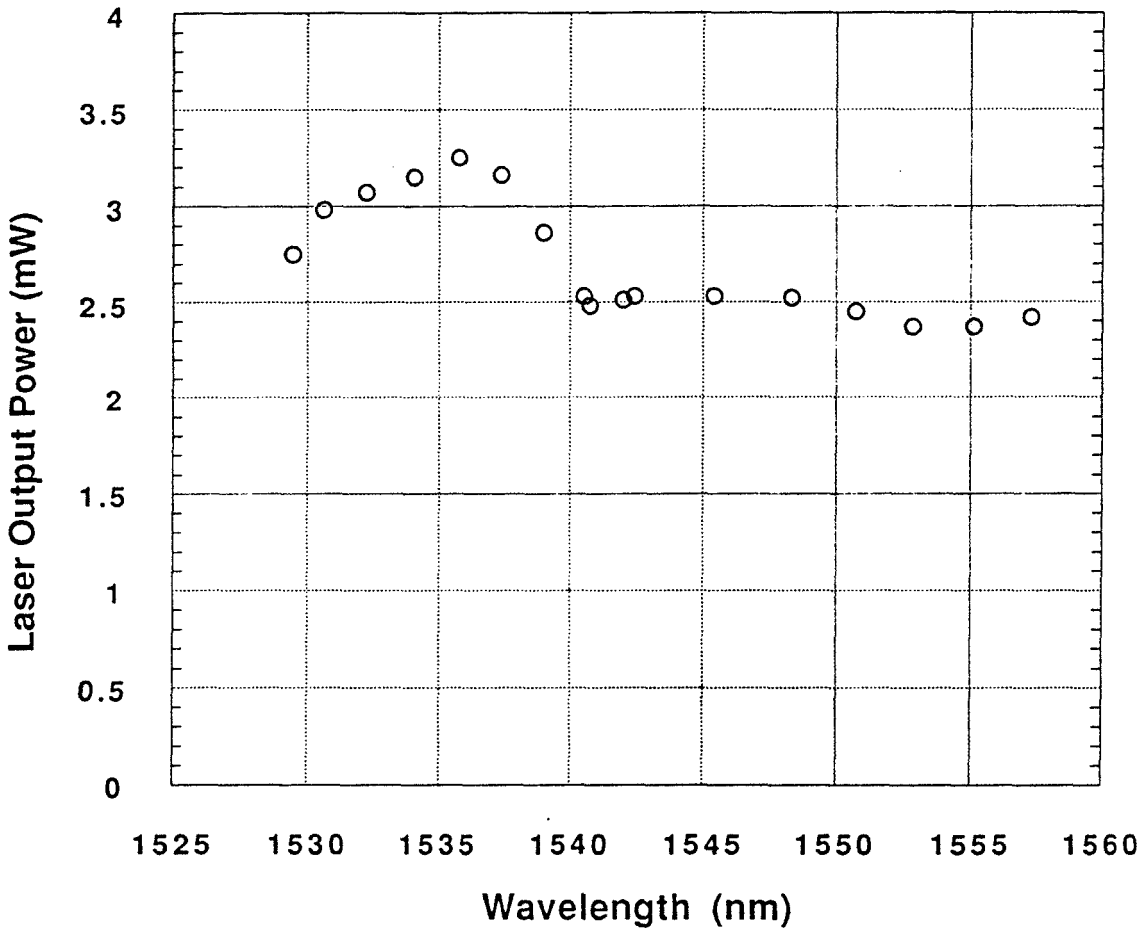

Figure 2.10: Output power vs. wavelength.

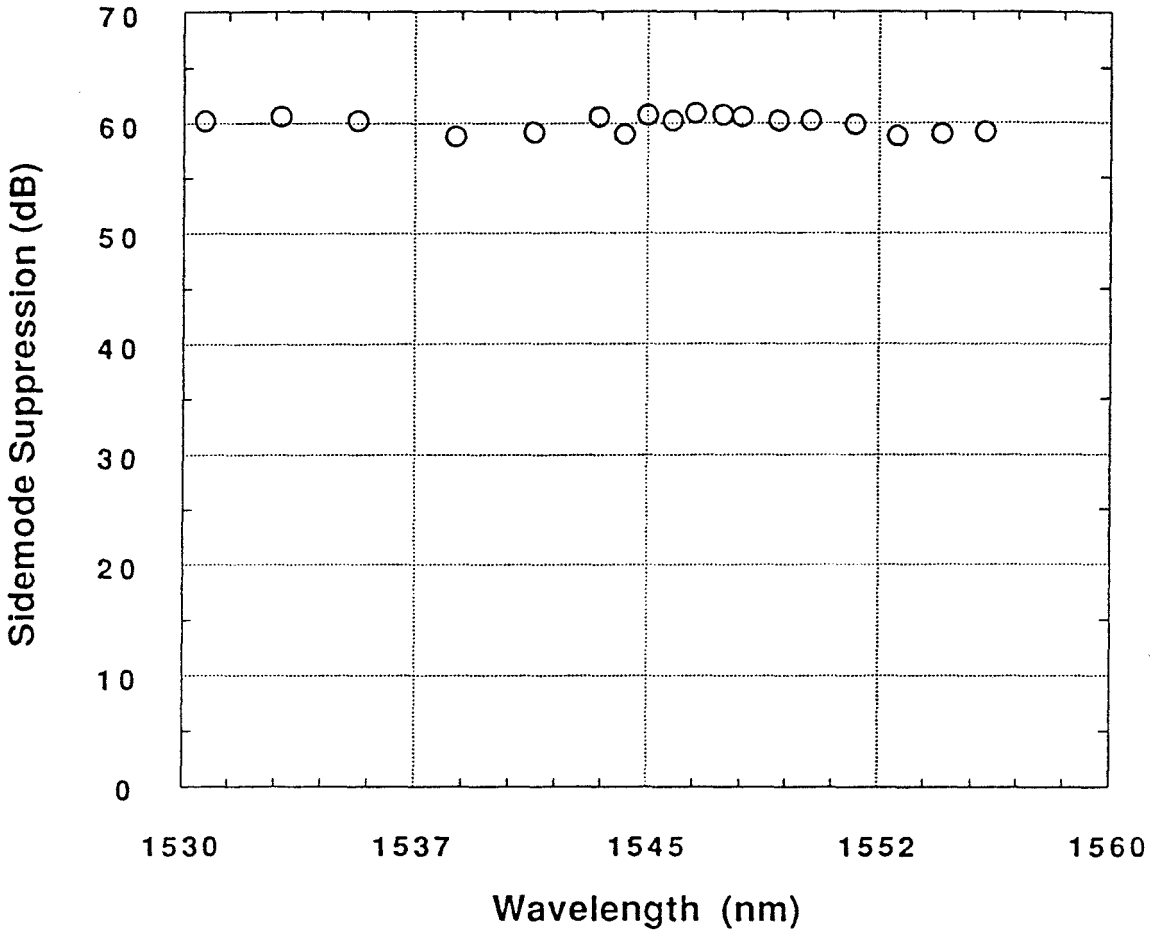

Figure 2.11: Sidemode suppresion vs. wavelength.

Properties of the laser intensity noise including a more detailed discussion of the sidemode suppression will be presented in the next chapter.

References

[1] R. I. Laming, M. N. Zervas, D. N. Payne, *IEEE Photon. Tech. Lett.* **4**, 1345 (1992)

[2] E. Desurvire, J. R. Simpson, *J. Lightwave Tech.* **7**, 835 (1989)

[3] B. Pedersen, A. Bjarkev, J. H. Polvsen, K. Dybdal, C. C. Larsen, *J. Lightwave Tech.* **9**, 1105 (1991)

[4] Amnon Yariv, *Introduction to Optical Electronics, Third Ed.* (Holt, Rinehart and Winston, New York, 1985) p. 160

[5] C. L. Tang, H. Statz, G. de Mars, *J. Appl. Phys.* **34**, 2289 (1963)

[6] G. A. Ball, W. W. Morey, W. H. Glenn, *IEEE Photon. Tech. Lett.* **3**, 613 (1991)

[7] D. A. Smith, paper FB1 in *OFC/IOOC 1993 Technical Digest Series Volume 4* (Optical Society of America), 244 (1993)

[8] Z. Tang, H. F. Taylor, O. Eknoyan, V. P. Swenson, paper FB2 in *OFC/IOOC 1993 Technical Digest Series Volume 4* (Optical Society of America), 245 (1993)

[9] G. Meltz, W. W. Morey, W. H. Glenn, *Optics Letters* **14**, 823 (1989)

[10] R. M. Atkins, V. Mizrahi, *Electron. Lett.* **28**, 1743 (1992)

[11] J. Stone, L. W. Stulz, *Electron. Lett.* **27**, 2239 (1991)

[12] M. W. Maeda, J. S. Patel, D. A. Smith, C. Lin, M. A. Saifi, A. von Lehman, *IEEE Photon. Tech. Lett.* **2**, 787 (1990)

[13] K. Iwatsuki, H. Okamura, M. Sarvwatary, *Electron. Lett.* **26**, 2033 (1990)

[14] D. A. Smith, M. W. Maeda, J. J. Johnson, J. S. Patel, M. A. Saifi, A. von Lehman, *Optics Letters* **16**, 387 (1991)

[15] J. L. Zyskind, J. W. Sulhoff, et al., *Electron. Lett.* **27**, 2148 (1991)

[16] T. Saitoh, T. Mukai, *IEEE J. Quantum Electron.* **23**, 1010 (1987)

[17] N. K. Park, J. W. Dawson, K. J. Vahala, C. Miller, *Appl. Phys. Lett.* **59**, 2369 (1991)

[18] J. W. Dawson, N. K. Park, K. J. Vahala, C. Miller, paper WA5 in in *Optical Fiber Communication 1992 Technical Digest Series Volume 5* (Optical Society of America), 99 (1992)

Chapter 3

Intensity Noise Characteristics of a Single-Frequency Fiber Laser

This chapter investigates the intensity noise characteristics of the single-frequency fiber laser discussed in this thesis. The spectral content of the laser noise is the focus of the investigation. The intensity noise spectrum consists of three distinct spectral regions. The first region is defined by the free spectral range of the laser cavity. This region extends from DC to one half the free spectral range of the laser cavity. The second and third regions are defined by the bandwidth of the NB FFP. The second region consisting of frequency span from the end of the first region to roughly twice the NB FFP bandwidth, followed by the third region.

In the third region the intensity noise is very low. In order to accurately measure it a balanced homodyne system is employed. This system allows one to make a calibrated measurement of the intensity noise relative to the shot noise limit. It is shown that by proper configuration of the laser cavity, it is possible to reduce the excess noise in this region to the shot noise limit.

Each of these regions is discussed in detail in terms of accurate measurement of the noise power per unit frequency. The measurement systems used to determine the noise

power are also discussed. A brief discussion of the expected noise spectra is included to provide perspective.

3.1 Low and Intermediate Frequency Intensity Noise Spectra

As mentioned above the intensity noise spectra can be broken down into three distinct spectral regions. The first of these is the region from DC to one-half the free spectral range of the laser cavity. For the laser discussed in this thesis, this is DC to 2 MHz. At these low frequencies, one expects the primary source of intensity noise to be shot noise driven relaxation oscillations.

Relaxation oscillations in a laser occur due to interaction between the lasing field and the inversion in the optical gain medium [1]. To see how this works, consider the consequences of a small fluctuation in the intensity of the laser field in the cavity. For example, if there is a small decrease in the lasing field, fewer emissions are stimulated from the optical gain media. Assuming a constant pumping rate, this results in an increase in the inversion, which leads to an increase in the optical gain. The increase in the optical gain results in an increase in the optical field intensity.

Thus gain saturation acts as a restoring force for laser field fluctuations. It can be shown by a small signal analysis of the laser rate equations that the interaction between the optical gain and the laser field has the mathematical form of a damped driven simple harmonic oscillator [1]. The driving force for the system is spontaneous emission from the gain medium. The characteristic times of the interaction are the photon lifetime in the passive cavity and the spontaneous lifetime of the gain media.

The interaction has a natural resonance frequency known as the relaxation oscillation resonance frequency, ω_R. This frequency is given by the formula [1],

$$\omega_R = \sqrt{\frac{(r-1)}{t_c \tau} - \left(\frac{r}{2\tau}\right)^2} \approx \sqrt{\frac{(r-1)}{t_c \tau}} \qquad (3.1)$$

where t_c is the photon lifetime in the cavity, τ is the spontaneous lifetime of the gain medium and r is the ratio of the pump power to the threshold pump power. The approximation in 3.1 is justified in this case since the photon lifetime of the fiber laser is approximately 0.25 μs, the spontaneous lifetime of the gain medium is 12 ms, and $r \approx 5$ at maximum power. Equation 3.1 yields an expected relaxation oscillation frequency of 36.5 kHz for these values. Further from equation 3.1, it is expected that the relaxation oscillation frequency will increase as the square root of the optical power (which is proportional to $r - 1$).

In measuring the intensity noise spectra in the low frequency regime, a direct detection system in combination with an RF spectrum analyzer was used. The noise power is characterized in terms of the relative intensity noise. For a directly detected field, the relative intensity noise (RIN) is defined as the ratio of the mean square power per unit bandwidth of the fluctuating photocurrent to the average photocurrent power. It is possible to show [2] that for the case of spontaneous emission driven relaxation oscillation noise, the RIN as a function of frequency, Ω, is given by

$$RIN = \frac{\frac{1}{\tau_R^2} + \Omega^2}{(\omega_R^2 - \Omega^2)^2 + \frac{\Omega^2}{\tau_R^2}} \Delta\omega_{ST} \qquad (3.2)$$

where τ_R is the stimulated lifetime of the gain medium and $\Delta\omega_{ST}$ is the Schawlow-Townes linewidth.

If the dominant noise source in the system is relaxation oscillation noise, the measured RIN should have a frequency dependence similar to that described by equation 3.2. For typical parameter values, equation 3.2 has a peak, which is located approximately at ω_R. For $\Omega << \omega_R, 1/\tau_R$ the RIN is relatively flat as a function of frequency. For $\Omega >> \omega_R, 1/\tau_R$ the RIN rolls off as $1/\Omega^2$.

To measure the relative intensity noise, the direct detection system shown in figure 3.1 was employed. The output of the fiber laser is collimated using a fiber input-output coupler, then focused onto a photodiode. The photodiode used was a BT+D model PDH0004 made of InGaAs/InP with a 50 micron diameter active region. It has a responsivity of 1.0 A/W at 1550 nm and a bandwidth of 2.4 GHz. The photodiode is connected to a bias T and reverse biased to 10 V. A current meter is connected in series with the DC bias to monitor the average photocurrent. In addition an electrical RC low pass filter with a 1 kHz corner frequency was connected to the DC port of the bias T to eliminate low frequency electrical noise from the power supply line.

The bias T is a Picosecond Pulse Labs device model 5575A with a 32 ps rise time, a 10 kHz low frequency cutoff (which set the low frequency cutoff for the measurement), and a 0.6 dB insertion loss. The AC port of the bias T is connected to a Trontech RF amplifier model W500K in series with another RF amplifier (same model) and then to a Tektronics RF spectrum analyzer model 2782. Each of the RF amplifiers has a gain bandwidth from 1 kHz to 500 MHz, a gain of 30 dB, and a noise figure of 2.2 dB.

Calibration of the system was accomplished by using an HP model 8640B signal generator. The output power of the signal generator was adjusted so that the amplifier system had the same thermal noise floor during the calibration as it had during the measurement. At high frequencies (>300 MHz) the laser intensity noise power sunk below the thermal noise floor of the measurement system. Verifying that the thermal noise floor of the measurement system was the same during the measurement and calibration in these frequencies permitted gain saturation of the amplifier to be removed as a source of

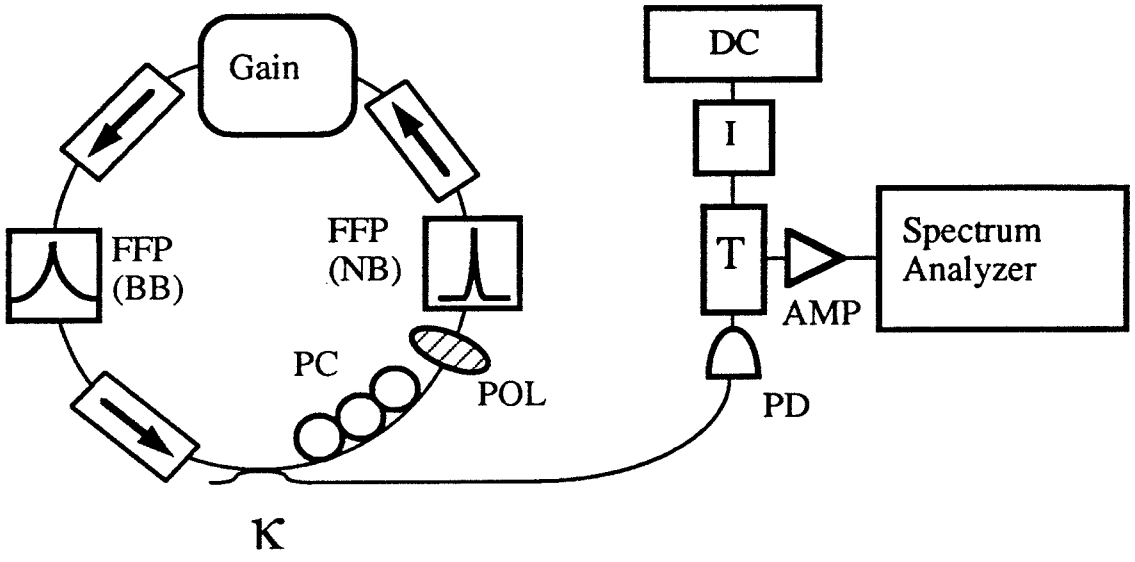

Figure 3.1: Experimental set-up for measuring the low frequency intensity noise spectra. PC: polarization controller, POL: polarizer, DC: power supply, I: current meter, T: bias T, AMP: RF amplifier, PD: photo-diode, κ: output coupling coefficient.

systematic error in the measurement. The oscillator frequency was varied over the measurement range and the system gain was calibrated as a function of frequency. The tandem amplifiers were found to have a gain of 48 dB by this technique. The gain variation over the frequency range from 10 kHz to 500 MHz is a maximum of +/- 1.0 dB. As these frequencies are much lower than the photodiode bandwidth, the frequency response of the photodiode was assumed to be flat over this range.

During the measurement the RF spectrum analyzer is used to average 10 consecutive spectrum analyzer traces in order to provide a more accurate reading of the noise power. The data is then read into a 486 DX personal computer using software from Tektronix. It is possible, using the computer, to divide out the average photocurrent power and the resolution bandwidth, converting the data to RIN. In addition the calibration data is used to correct the RIN for the net system gain between the output of the laser and the RF spectrum analyzer. The resulting calibrated data is printed out for detailed study.

A typical RIN spectrum in the frequency region from 10 kHz to 1 MHz is plotted in figure 3.2. The resolution bandwidth of the spectrum analyzer for this trace was 10 kHz and the output power of the laser was 813 μW. This output power corresponds to r = 4.6 for this configuration of the laser. In figure 3.2 the RIN of the laser is observed to increase steadily from about 20 kHz to a peak of -105 dBc/Hz at 32 kHz (confirmed by decreasing the span and resolution bandwidth of the spectrum analyzer to zoom in on the peak) and then roll off at 20 dB/decade above 100 kHz. The expected relaxation oscillation frequency from equation 3.1 is 35 kHz in good agreement with the measured value.

In order to positively identify the RIN spectra as shot noise driven relaxation oscillations, equation 3.2 was used to fit the data in figure 3.3. The measured value of ω_R was used as well as the theoretical value of $\Delta\omega_{ST}$, 0.003 Hz. τ_R was used as the fitting parameter and was determined from the fit to be 0.1 ms. In figure 3.3, it can be seen that the measured data at low frequency does not agree well with the theoretical fit. It is suspected that a source other than spontaneous emission is driving the system at low

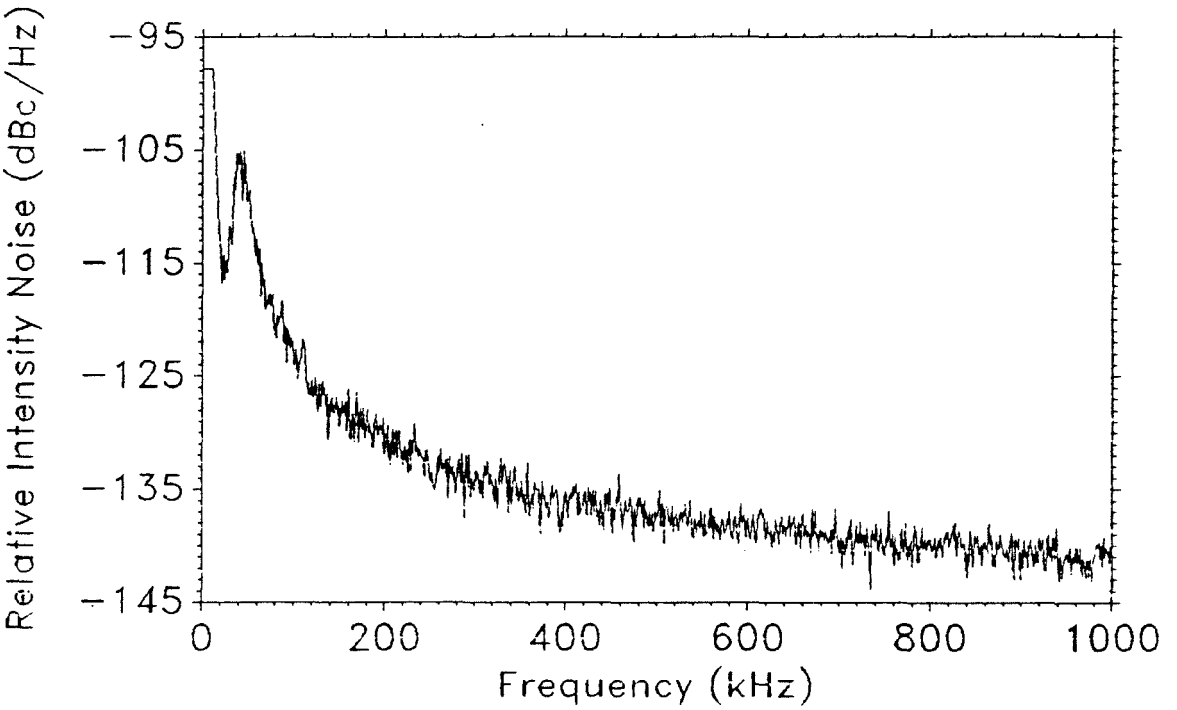

Figure 3.2: Relative intensity noise spectrum of the fiber laser from 10 kHz to 1 MHz.

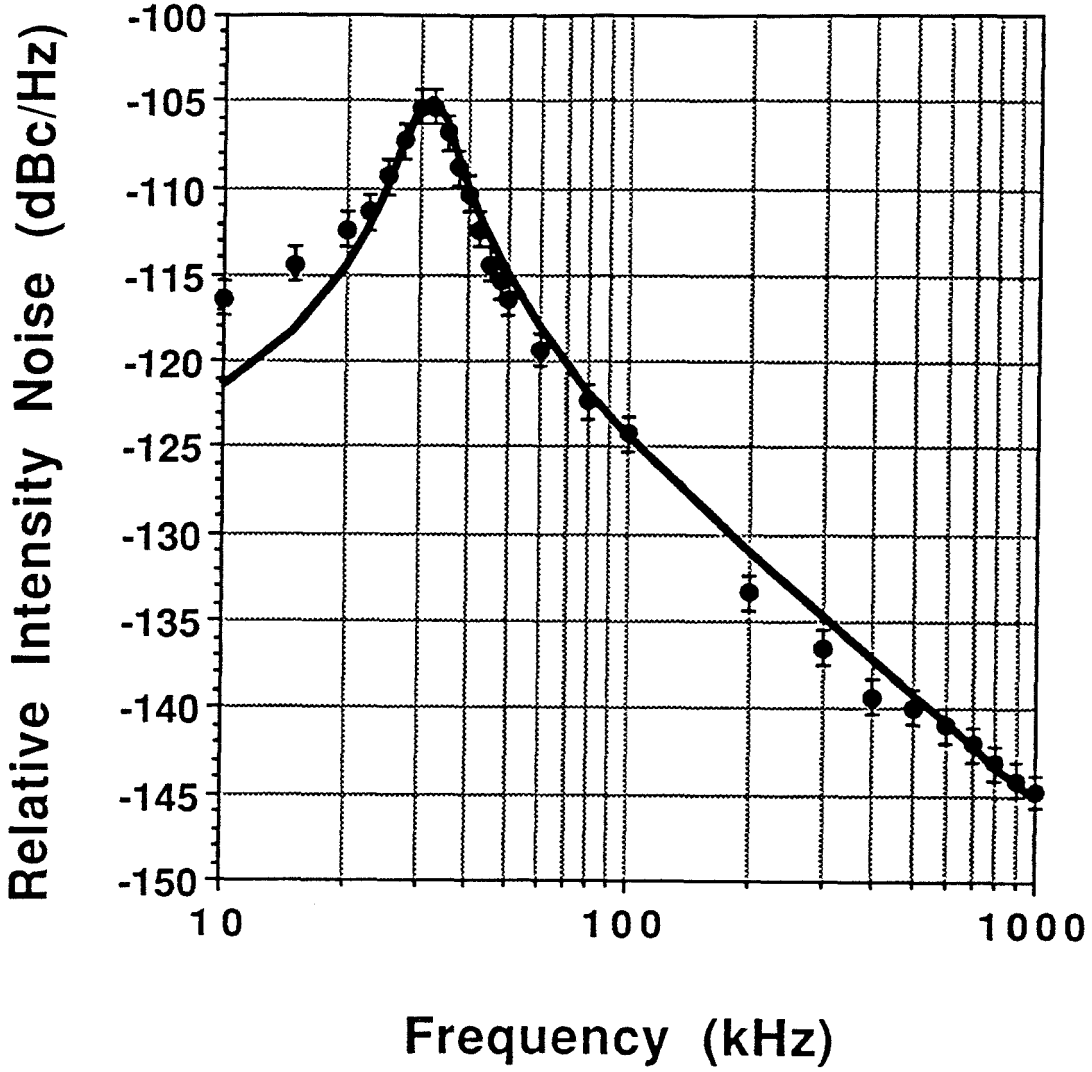

Figure 3.3: Theoretical fit of figure 3.2 data to equation 3.2. The discrepancy at low frequency is probably due to a noise source other than spontaneous emission driving the relaxation oscillation.

frequency. One possibility is room microphonics interacting with the long cavity length to create length fluctuations or time dependent birefringence.

As a final check that the source of the low frequency noise is indeed relaxation oscillation noise, the relaxation oscillation frequency is plotted as a function of the laser output power in figure 3.4. The value of the pumping parameter r was determined from the output power vs. pump power curve. The theoretical line going through the data points in figure 3.4 was determined by plotting equation 3.1 as a function of power based on the measured relation between r and power and using a t_C of 0.25 μs and τ of 12 ms.

As described above, the intensity noise of the laser rolls off at 20 dB per decade of frequency from 100 kHz out to 2 MHz. At this point the intensity noise from the two sidemodes adjacent to the lasing mode begin to cause an increase in the laser intensity noise. This effect can be seen in figure 3.5. Figure 3.5 is a spectrum analyzer trace of the frequency range from 1 MHz to 20 MHz taken using the same experimental setup described above for measuring the relaxation oscillation noise in the frequency region below 1 MHz. The average laser power (813 μW) has been divided out, but the resolution bandwidth (30 kHz, increasing the resolution bandwidth did not change the peak heights) was not divided out of the relative noise power.

The dominant intensity noise source in this frequency regime is clearly the main lasing mode beating with amplified spontaneous emission in the adjacent longitudinal modes of the resonator. The adjacent longitudinal modes do not have sufficient gain to lase; however, the net loss for these modes is still quite small, hence their linewidths are quite narrow. Because of the narrow bandwidth peaks in the intensity noise spectrum, it is not possible to characterize the noise in this region as broadband noise, so units of dBc/Hz are not used. In this frequency region sidemode suppression (dBc) is the best indicator of the laser intensity noise. The theoretical factors governing sidemode suppression have been discussed in section 2.1.

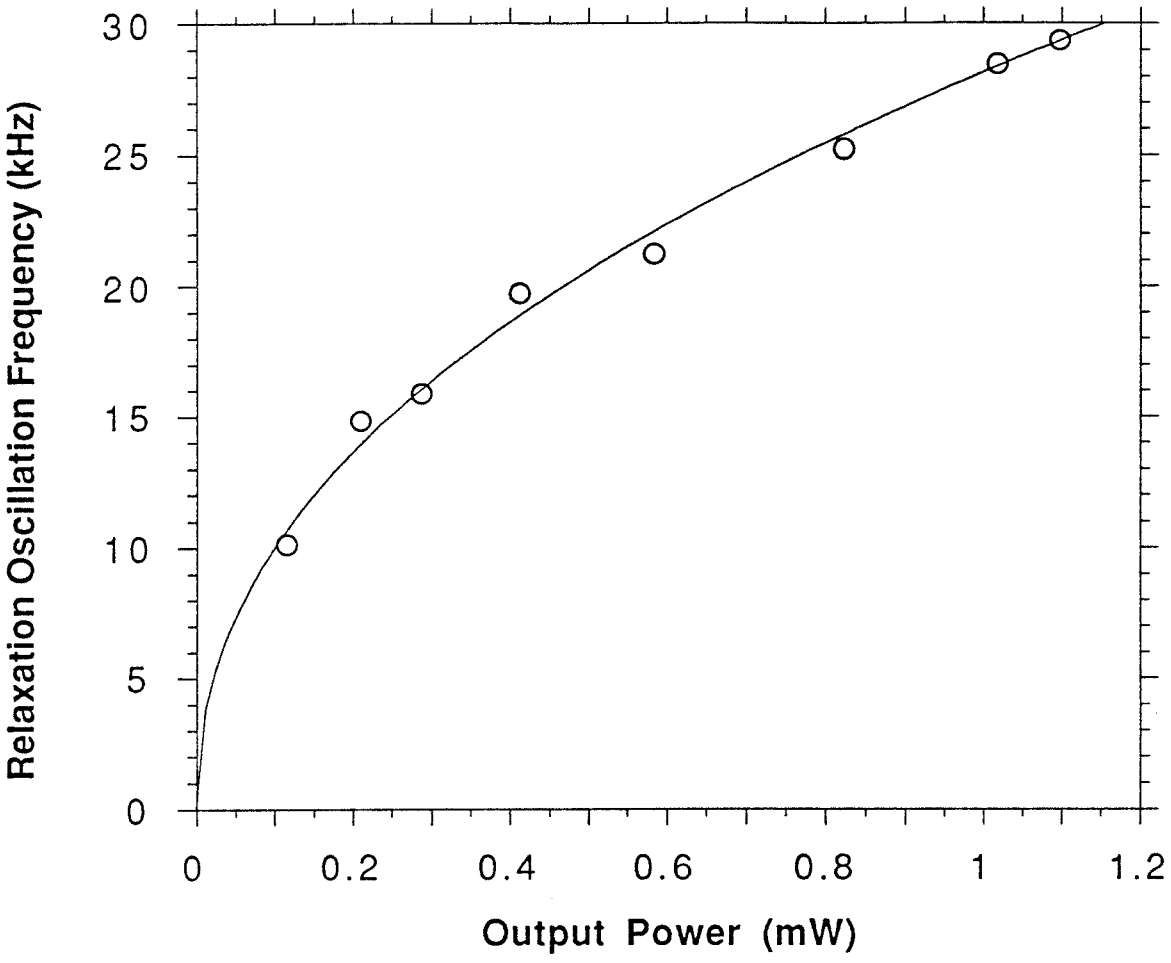

Figure 3.4: Relaxation oscillation frequency vs. fiber laser output power. The data has been fit to equation 3.1.

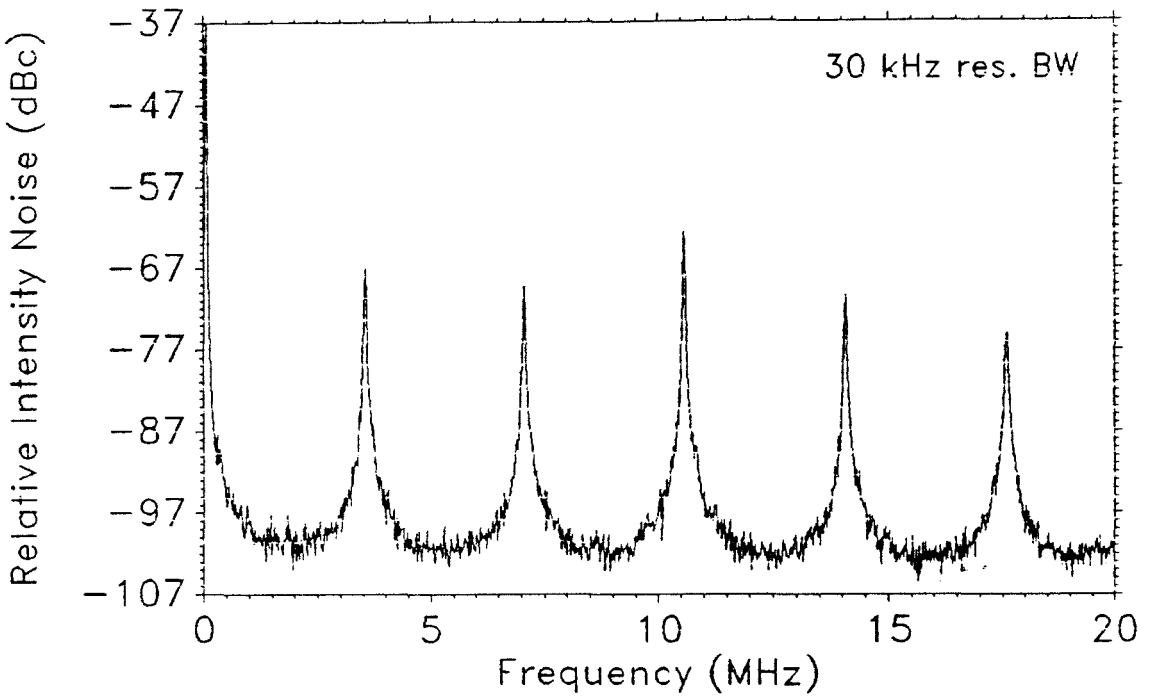

Figure 3.5: Intensity noise spectrum of the fiber laser from 1 MHz to 20 MHz. The sidemode suppression of the laser is at least 60 dB. The laser output power was 813 μW.

It can be seen in figure 3.5 that the third sidemode at 11 MHz is the largest. Its sidemode suppression relative to the main lasing mode is 62 dB. Figure 3.6 shows a spectrum analyzer trace at the same power level with a resolution bandwidth of 300 kHz only looking at the overall trend in the sidemode suppression from 1 MHz to 400 MHz. A pattern can be seen; approximately every third peak is larger than its nearby neighbors.

The frequency spacing of these peaks is approximately 11-12 MHz. If the amplified spontaneous emission spectra was to experience a frequency dependent loss or gain from, for example, a parasitic Fabry-Perot cavity, an 11-12 MHz trend would indicate a Fabry-Perot cavity about 9 m in length. A cavity of this length is most likely occurring between one of the high reflectivity dielectric mirrors in the BB FFP and a splice in the laser. Most probably the problem splice is at the interface between the polarization preserving fiber attached to the polarizer and the normal fiber that makes up the rest of the cavity. This problem could be eliminated in the future by adding another isolator to the cavity or by making the entire cavity out of polarization preserving fiber.

Figure 3.6 clearly shows the sidemode suppression rolling off as a function of frequency in the general trend expected based on equation 2.4. At around 100 MHz, it begins to become difficult to distinguish the individual longitudinal modes. At around twice the NB FFP filter bandwidth or about 250 to 300 MHz, the peaks disappear almost completely. As shown below beyond these frequencies, it is again possible to characterize the intensity noise spectra as broadband noise. However, for these frequencies the noise level is quite close to the thermal noise floor of the measurement system. In order to accurately characterize the intensity noise in this higher frequency, lower noise regime, a better measurement system must be constructed. This is discussed in detail in the next section.

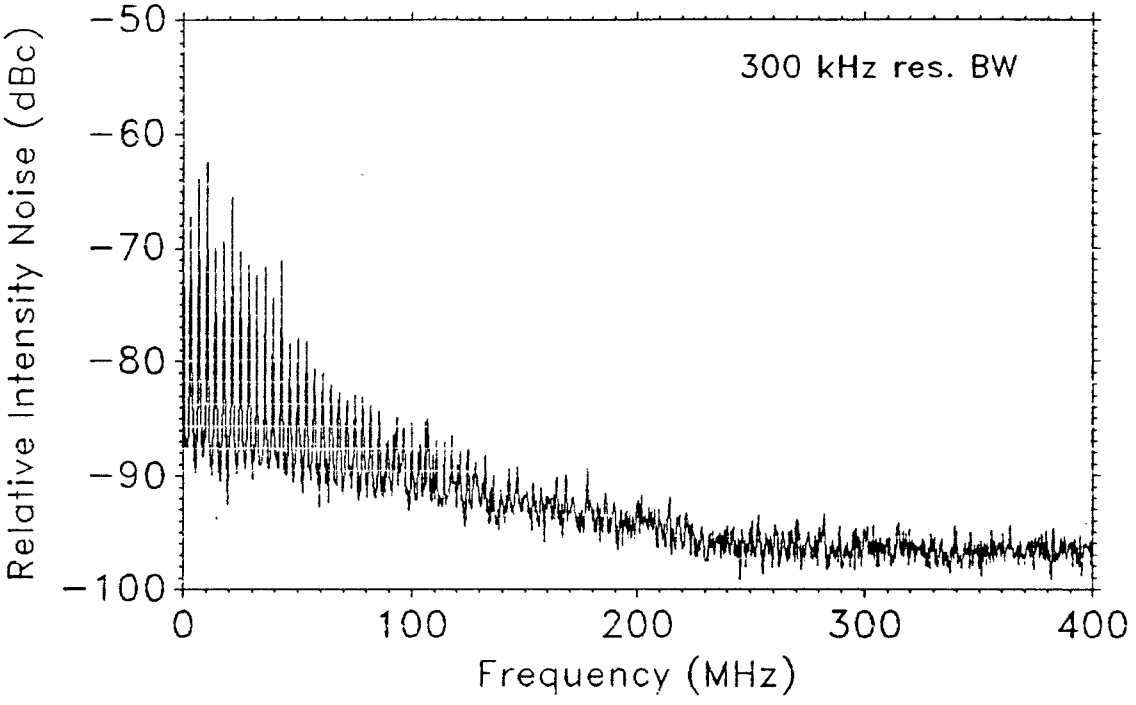

Figure 3.6: Intensity noise spectrum of the fiber laser from 1 MHz to 400 MHz. The laser output power was 813 μW.

3.2 Measurement of the High Frequency Intensity Noise Spectra Using the Balanced Homodyne Technique

The intensity noise of a laser at a given frequency is shot noise limited if the noise power at that frequency is due to random arrival of photons at the input of the detection system. This random arrival is governed by Poissonian statistics and has a power spectral density of 2eI, where e is the charge of an electron and I is the average photocurrent at the photodetector.

Uncertainty relations (between photon number and phase, for example) guarantee that any physical system has a minimum amount of noise. When the uncertainty in a system is solely due to the uncertainty relation and this uncertainty is equally divided between the two observables of the relation, the system is said to be in a minimum uncertainty state [3]. In a minimum uncertainty state the uncertainty of each of the two observables is said to be at the standard quantum limit (SQL). If the intensity noise of a laser is shot noise limited, the intensity noise is at the SQL for the system.

This is very interesting because it implies the system is approaching a fundamental operating limit. (Uncertainty in the observable can be reduced below the SQL but only at the expense of an increase in the uncertainty in the conjugate observable [4, 5, 6].) Measurement of the phase noise would be required in order to claim the system was in a minimum uncertainty state. However, intensity noise at the standard quantum limit in combination with single frequency laser operation is an excellent start towards this goal. Furthermore, the low intensity noise properties of such a laser would have many applications in measurements where low laser intensity noise is an important parameter, such as some fiber optic sensor systems.

The standard technique for measuring the intensity noise of a laser was discussed in section 3.1. However, this technique does not permit accurate determination of the

standard quantum limit. The balanced homodyne system [7] (figure 3.7) was developed to allow accurate measurement of the SQL. The balanced homodyne system measures the SQL when the two amplified photocurrents from detectors D1 and D2 are coherently subtracted and the laser noise power when the two photocurrents are coherently summed in a hybrid junction.

The two detectors D1 and D2 are the same model as the detector used earlier. The amplifiers are Avantek amplifiers model ACT10-213-1, frequency range 10-1000 MHz, gain 52 dB (+/- 1.5 dB) and a noise figure of 3.7 dB. The RF spectrum analyzer (same as above) is operated in the zero span mode. In this mode the noise power within one resolution bandwidth of the set frequency is continuously measured. The chopper and lock-in amplifier (EG&G, model 5208) distinguish the laser noise power from the thermal noise of the measurement system, thus increasing the sensitivity of the measurement. The chopper modulates the signal beam at around 200 Hz which will not affect measurement of the noise power at several hundred MHz. The microwave mixer is used to add or subtract the photocurrents.

The path lengths between the beamsplitter and the mixer must be carefully balanced so that in the subtract mode the mixer eliminates all of the excess noise from the laser. Balancing is performed by injecting light from a 1.5 μm distributed feedback semiconductor laser into the unused port of the fiber laser output coupler and modulating the light at the frequency at which one wishes to measure the intensity noise. The optical intensities reaching the two detectors are adjusted by rotating a half-wave plate before a polarization sensitive beamsplitter, and the path lengths of the two arms are adjusted to give a common-mode rejection of > 50 dB. A polarizer before the balanced homodyne system maintains the intensity balance when the fiber laser output is measured and an external polarization controller is optimized before each measurement to ensure that maximum power is transmitted to the measurement system. The shot noise floor is confirmed by retracing it with the laser output power fixed and externally attenuated.

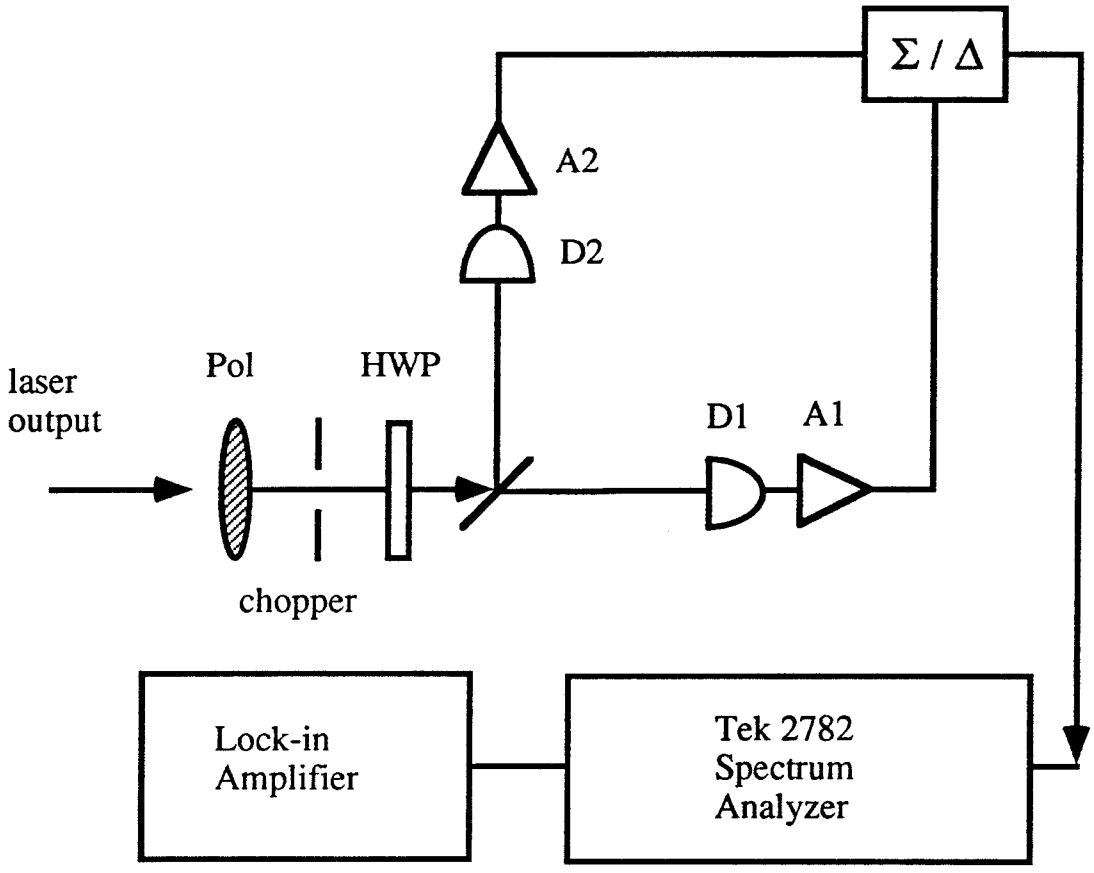

Figure 3.7 Balanced homodyne detection system to determine laser noise power relative to the SQL (shot noise floor). The SQL is measured when the photocurrents are differenced; the laser noise is measured when the photocurrents are summed. (HWP: half-wave plate; D1 and D2: photo-detectors; A1 and A2: RF amplifiers).

A correction for losses of 56% between the output of the laser ring and the detectors is given by:

$$W_{obs} = \eta W + 1 - \eta \tag{3.3}$$

where W_{obs} is the observed noise power normalized to the SQL; η is the overall efficiency, and W is the actual noise power normalized to the SQL. As actual calibration of the noise power throughout the entire measurement system is difficult and probably not that accurate, the noise power data will be presented in either arbitrary units or normalized to the SQL.

The noise power versus laser power at a fixed wavelength is shown in figure 3.8, along with the shot noise limit. The laser configuration is shown in figure 3.1 (later this configuration will be altered). The noise power varies linearly with the output power. Because of the linear dependence of noise power on laser output power, the noise can be characterized in terms of noise power relative to the SQL by the ratio of the slopes of the two lines. Figure 3.9 shows the noise power relative to the SQL as a function of RF spectrum analyzer frequency. A series of resonances with a 4 MHz period are observed, which are clearly very weak sidemodes of the laser. The combination of the still visible sidemodes and the linear increase in noise power with laser power indicates that the measured noise arises from beating between the lasing mode and amplified spontaneous emission in the strongly suppressed sidemodes. The amplified spontaneous emission power is independent of the amount of power in the lasing mode because the inversion of the EDFA is clamped at the threshold inversion. Thus as observed, the beat noise between the lasing mode and the amplified spontaneous emission will increase linearly with the power in the lasing mode.

The noise power data in figure 3.9 were taken at around 300 MHz in frequency. If the dominant noise source is beating noise between the amplified spontaneous emission in

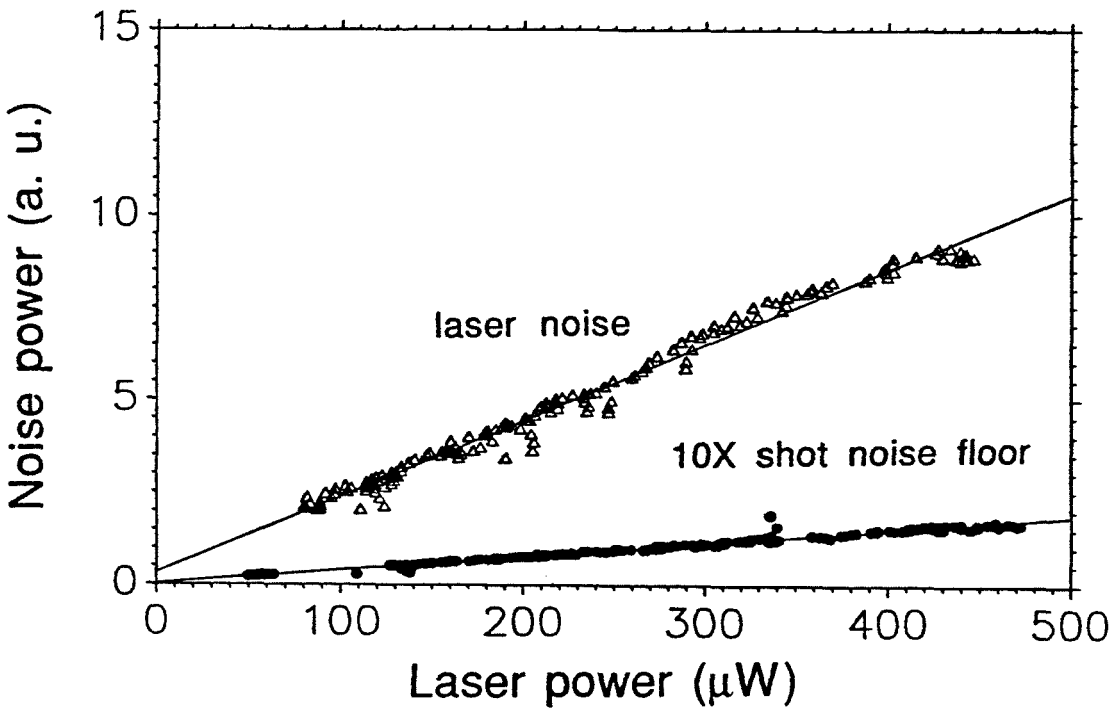

Figure 3.8: Noise power (arbitrary units) vs. laser power. 50% output coupling, 300 kHz resolution bandwidth. Top line: balanced homodyne in sum mode; Bottom line: balanced homodyne in difference mode.

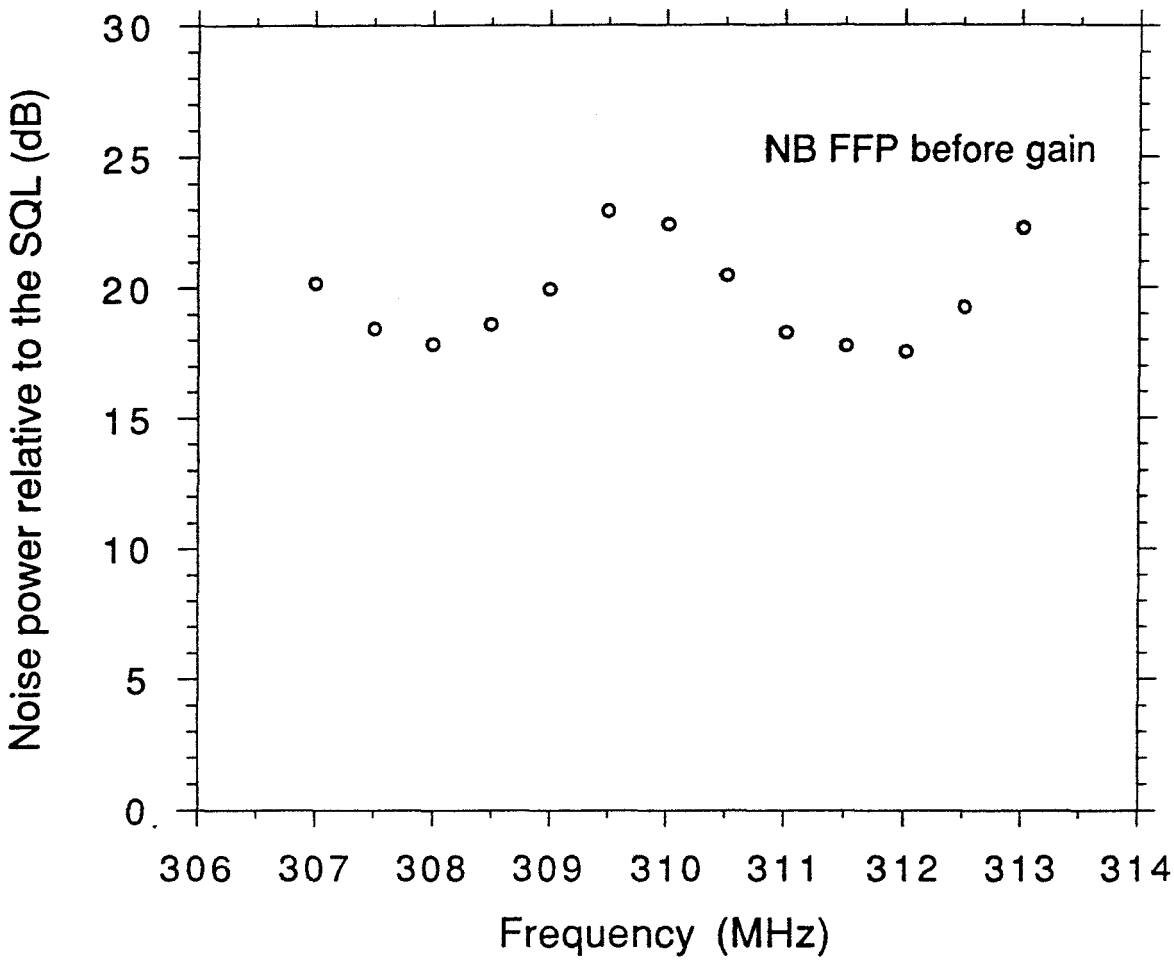

Figure 3.9: Noise power relative to the SQL as a function of spectrum analyzer frequency. 50% output coupling, 300 kHz resolution bandwidth.

the sidemodes and the lasing mode it should be possible to reduce this noise by using the NB FFP filter, which has a bandwidth of 125 MHz, to selectively attenuate the sidemodes and not the lasing mode. The data in figure 3.9 were taken with the NB FFP filter before the gain and the BB FFP filter after the gain. The BB FFP has a bandwidth of 33 GHz resulting in virtually no attenuation of the sidemodes at 300 MHz. The NB FFP filter has an attenuation of 17 dB at 300 MHz away from its transmission peak. Therefore, if the position within the cavity of the NB FFP and BB FFP are exchanged, there should be a 17 dB reduction in the intensity noise of the laser at this frequency.

Figure 3.10 shows the noise power relative to the SQL for the case of the NB FFP filter after the gain as in figure 2.5 and for the case of the NB FFP filter before the gain as in figure 3.1. A reduction of the intensity noise by 15 dB is apparent. Further, the noise power relative to the SQL is now < 5 dB, which is quite close to optimal performance. To further decrease the noise power relative to the SQL, the effect of the output coupler on the noise characteristics was investigated.

The transmission of the output coupler affects the intensity noise in two ways. First, shot noise is directly proportional to the laser output power. Because of the large loss in this laser, the output power increases roughly as the transmission of the output coupler increases, until the gain is no longer fully saturated (see section 2.1, 2.2). Thus the SQL will increase linearly with the output coupler transmission. The amount of amplified spontaneous emission from the gain medium coupled out of the laser will also increase linearly with increasing output coupling. Therefore, the noise power due to beat noise at the photodetector will increase as the square of the output coupler transmission while the SQL increases linearly with the output coupler transmission. If the output coupling decreases, then the ratio of the noise power relative to the SQL will decrease linearly with it.

Furthermore, decreasing the output coupler transmission coefficient will decrease the amount of gain required to achieve oscillation, which will decrease the amount of

spontaneous emission from the laser. The amplified spontaneous emission power has a spectral density given by, $n_{sp}(G-1)h\nu$, where G is the power gain of the amplifier, n is the optical frequency and n_{sp} is the integrated spontaneous emission factor given in Ref. 8 by

$$\overline{n_{sp}} = \frac{G}{G-1}\int_0^l dz\ g(z)\ n_{sp}(z)\, e^{-\int_0^z g(z')dz'} \tag{3.4}$$

where $g(z) = \sigma_e N_2(z) - \sigma_a N_1(z)$ and $n_{sp} = \sigma_e N_2(z)/g(z)$; σ_e and σ_a are the emission and absorption cross sections, respectively, N_1 and N_2 are the upper and lower state population densities, respectively, and l is the total amplifier length. (When n_{sp} is independent of z, $\overline{n_{sp}} = n_{sp}$.) Clearly, the dependence of the spectral density of the amplified spontaneous emission power on the gain is not linear when the spontaneous emission factor is a function of position in the amplifier. However, there is still a general trend of decrease in amplified spontaneous emission for a decrease in gain.

Three output couplers were available for testing this concept. The output couplings available from these couplers were 10%, 50% and 90% transmission. The 90% output coupler resulted in decreased tuning range over the 50% output coupler because it increased the gain necessary to achieve oscillation. The data from the 50% output coupler has already been presented in figure 3.10. The data from the 90% coupler is presented in figure 3.11 and the data from the 10% output coupler is presented in figure 3.12.

Again the placement of the NB FFP filter is seen to have a dramatic effect on the noise power relative to the SQL. The transmission of the 90% output coupler is 2.55 dB higher than that of the 50% output coupler. Comparison of figures 3.10 and 3.11 show the relative noise power increased by about 5 dB, 2.55 dB from the increased output coupling and the rest from an increase in amplified spontaneous emission due to the increased gain

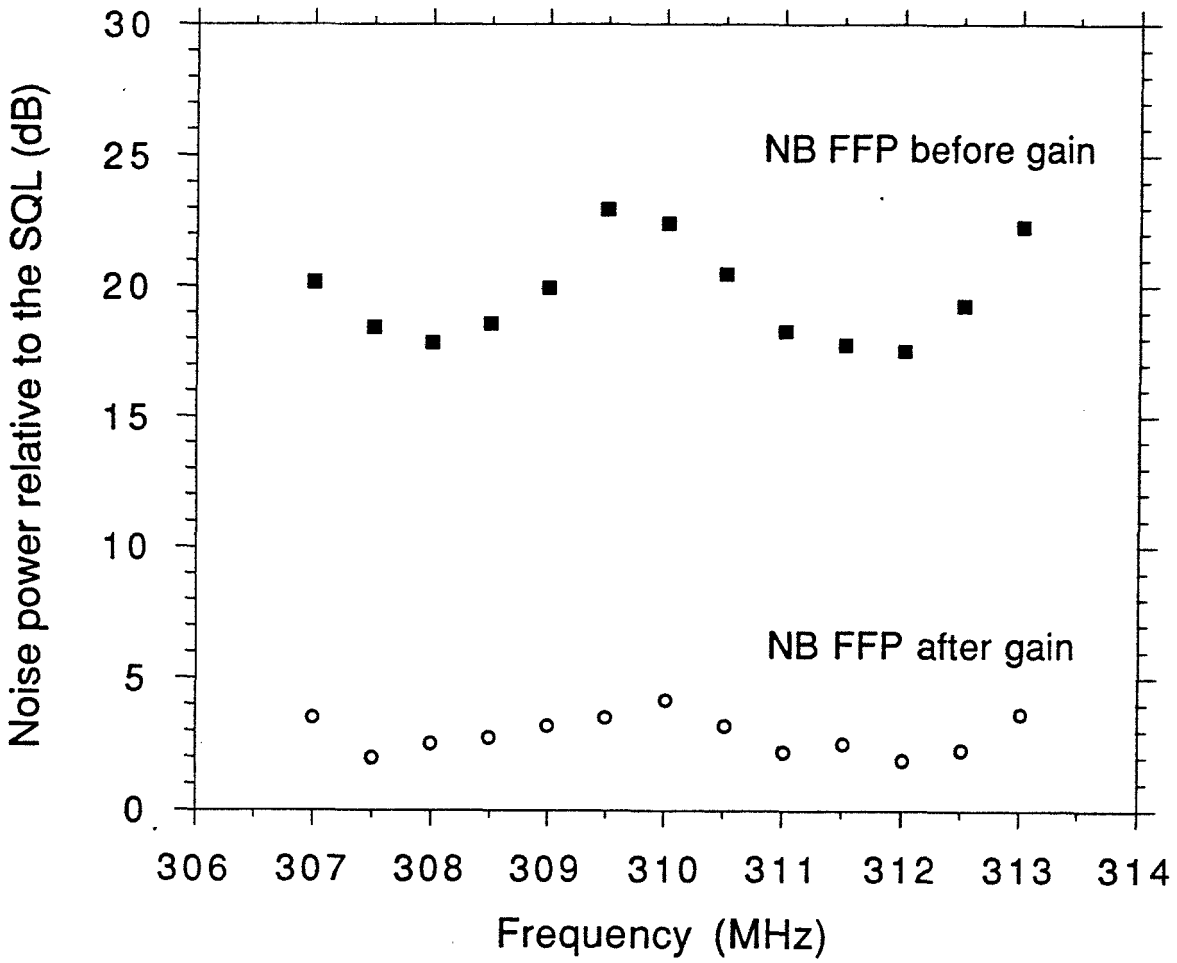

Figure 3.10: Noise power relative to the SQL as a function of spectrum analyzer frequency. 50% output coupling, 300 kHz resolution bandwidth.

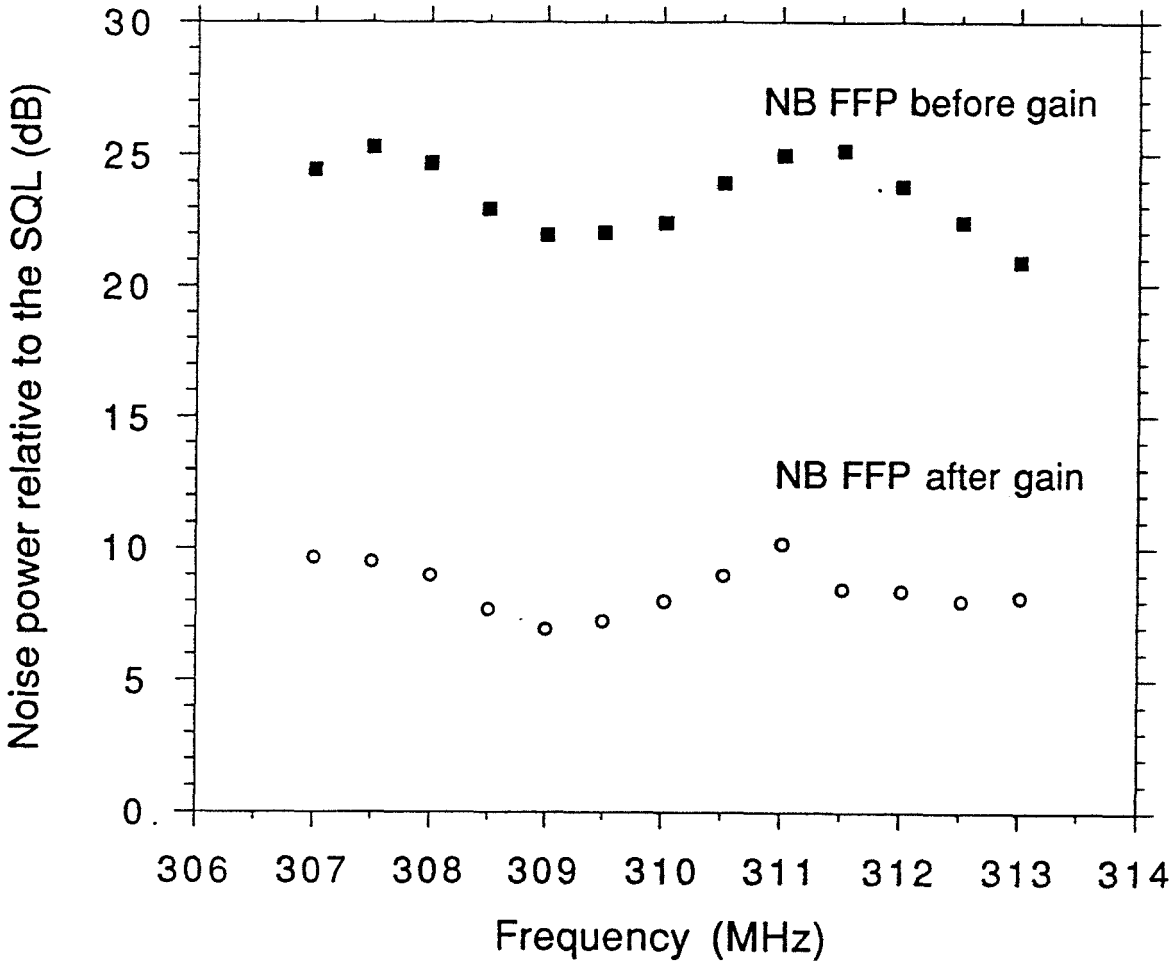

Figure 3.11: Noise power relative to the SQL as a function of spectrum analyzer frequency. 90% output coupling, 300 kHz resolution bandwidth.

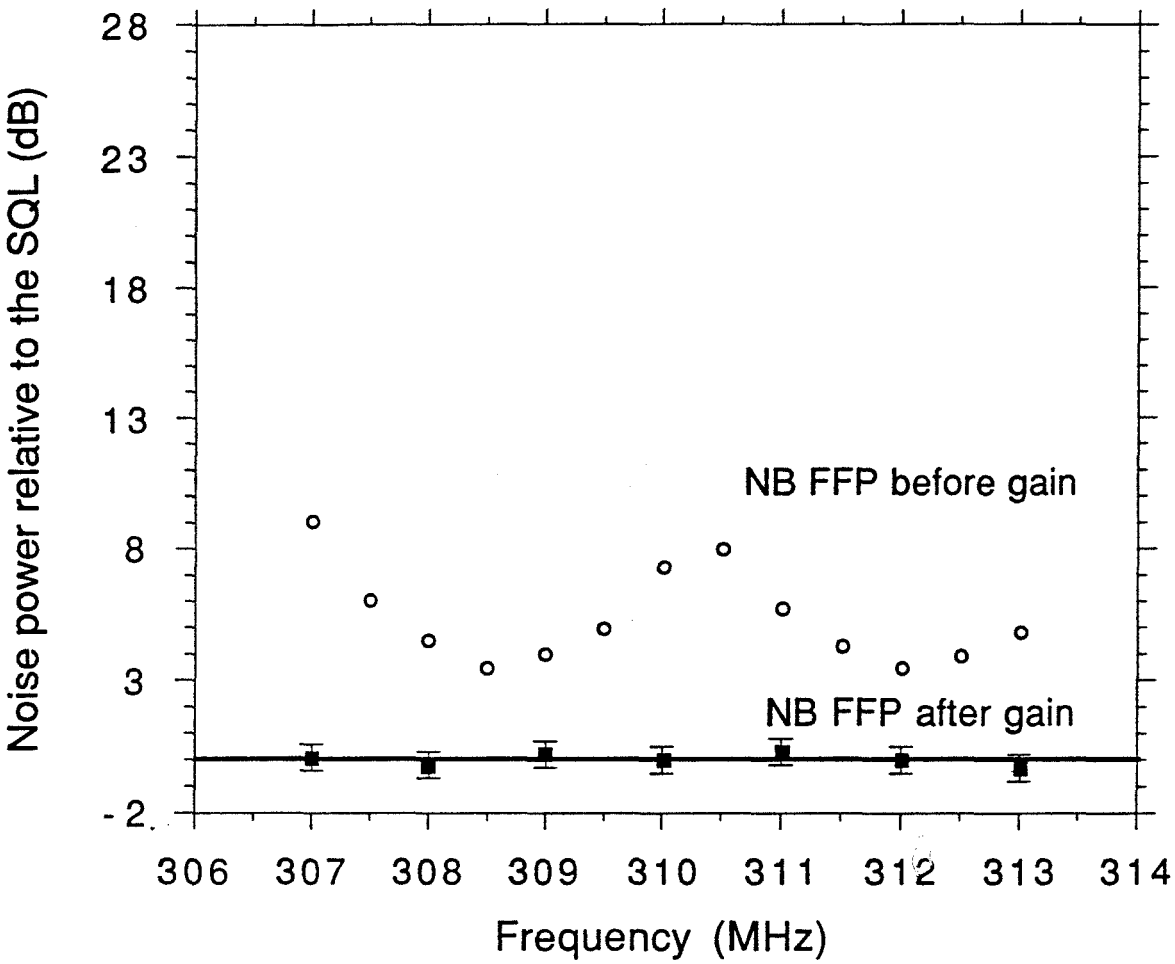

Figure 3.12: Noise power relative to the SQL as a function of spectrum analyzer frequency. 10% output coupling, 300 kHz resolution bandwidth.

required to oscillate. The transmission of the 10% output coupler is 6.99 dB less than the 50% output coupler. Comparison of figures 3.10 and 3.12, for the case of the NB FFP filter before the gain, show the relative noise power decreased by around 12 dB. Again, the decreased EDFA gain required to oscillate resulted in lower amplified spontaneous emission. For the case of the NB FFP filter after the gain and 10% output coupling, the noise power relative to the SQL is within the experimental uncertainty of the SQL. The laser output power with the intensity noise at the SQL was 200 mW.

In this chapter the intensity noise spectra of the fiber laser has been studied in detail. At frequencies less than one-half of the free spectral range of the resonator, the dominant intensity noise source is relaxation oscillation noise. This noise had a peak value of -105 dBc/Hz at the relaxation oscillation frequency which varies from 10 kHz to 35 kHz as the output power varies from 0.1 mW to 1.0 mW. This noise rolls off at 20 dB/decade away from this peak. At around 2 MHz the 20 dB/decade roll-off in the relaxation oscillation noise begins to experience a noise floor due to beating noise between the lasing mode and the strongly suppressed sidemodes.

At full power all sidemodes are suppressed by at least 60 dB. The sidemode suppression increases rapidly for modes spaced farther from the lasing mode. At twice the NB FFP bandwidth, the sidemodes have lost their strongly peaked nature and while still visible are essentially broadband noise again. If the NB FFP is not placed before the EDFA and the 50% output coupler, this broadband noise is around 20 dB above the shot noise floor as measured with a balanced homodyne. If the NB FFP is between the EDFA and the output coupler, the amplified spontaneous emission power can be reduced by 15 dB, relative to the SQL at a cost of a 3 dB reduction in laser output power, bringing the measured noise to within 5 dB of the SQL for 50% output coupling.

The intensity noise due to beat noise can be further reduced by lowering the output transmission coefficient. Lowering the output coupling decreases the intensity noise power relative to the SQL by the same amount. An additional decrease is obtained due to the

decrease in the amplified spontaneous emission noise when the gain is decreased due to the lower output coupling. However, the precise dependence of the noise power decrease due to the gain decrease is complicated. For an output coupling of 10% and the NB FFP between the EDFA and the output coupler, the intensity noise was reduced to the SQL for frequencies greater than twice the NB FFP bandwidth.

References

[1] Amnon Yariv, *Introduction to Optical Electronics, Third Ed.* (Holt, Rinehart and Winston, New York, 1985) p. 188

[2] Kerry J. Vahala, *Dynamic and Spectral Features of Semiconductor Lasers*, Ph.D. dissertation, California Instit. Technol., Pasadena, CA (1985)

[3] D. Stoler, *Phys. Rev. D* **1**, 3217 (1970)

[4] L. Wu., H. J. Kimble, J. L. Hall, H. Wu, *Phys. Rev. Lett.* **57**, 2520 (1986)

[5] R. E. Slusher, L. W. Hollberg, B. Yurke, J. C. Mertz, J. F. Valley, *Phys. Rev. Lett.* **55**, 2409 (1985)

[6] G. J. Milburn, M. D. Levenson, R. M. Shelby, S. H. Perlmutter, R. G. DeVoe, D. F. Walls, *J. Opt. Soc. Am. B* **4**, 1476 (1987)

[7] B. L. Schumaker, *Optics Letters* **9**, 189 (1984)

[8] E. Desurvire, IEEE Photon. Technol. Lett. 2, 208 (1990)

Chapter 4

Linewidth and Frequency Jitter Measurements Using an Improved Delayed Self-Heterodyne Interferometer

This chapter investigates the linewidth and frequency jitter of the single-frequency fiber laser discussed in this thesis. A loss-compensated recirculating delayed self-heterodyne interferometer (RDSHI) was conceived and demonstrated to permit accurate measurement of the narrow laser linewidth with reasonable amounts of fiber delay. The RDSHI will be described in detail. The linewidth of the fiber laser is then investigated using the RDSHI. One of the advantages of the RDSHI is that it allows one to measure the laser linewidth as a function of delay time. Based on this feature the fiber laser is shown to have a linewidth dominated by frequency jitter. The timescale of this frequency jitter was determined to be on the order of a millisecond.

4.1 An Improved Delayed Self-Heterodyne Interferometer for Linewidth Measurements

The classic method for determining the linewidth of a laser is to construct two lasers, stabilize them to an external reference cavity to remove long term drifts in relative frequency, tune them close together and observe their inter-frequency beat note with a fast photo-diode. This technique has two major drawbacks; the need for two independent, tunable lasers and the need for frequency stabilization systems for both lasers. The delayed self-heterodyne interferometer (DSHI) has been an important tool for the measurement of laser linewidths since its conception [1], because it permits measurement of a laser's linewidth without the drawbacks of the classic technique.

The conventional experimental set-up for a DSHI linewidth measurement is shown in figure 4.1. The output of a laser is split by an acousto-optic modulator into a component that has been frequency shifted by ω_A and a component that is essentially unaffected by passage through the AOM except for attenuation. The frequency shifted component of the light is coupled into an optical fiber and undergoes a large time delay τ_D and is then sent to a beamsplitter. At the beamsplitter, the time delayed, frequency shifted light recombines with the unaffected beam. The two signals form a beatnote at ω_A on the photodiode. The beat note can then be observed using an RF spectrum analyzer.

The basic idea in this experiment is that if the delay time of the long optical fiber is longer than the coherence time of the laser, which is inversely proportional to the laser's linewidth, then the time delayed signal will no longer have any phase relation to the undelayed signal. Thus it acts as an independent laser source and the two signals will not interfere coherently. With no relation between the phases, the beat note measured on the spectrum analyzer is twice the laser linewidth in the case of a Lorentzian linewidth and 1.414 times the linewidth in the case of a Gaussian linewidth. If there were no delay and

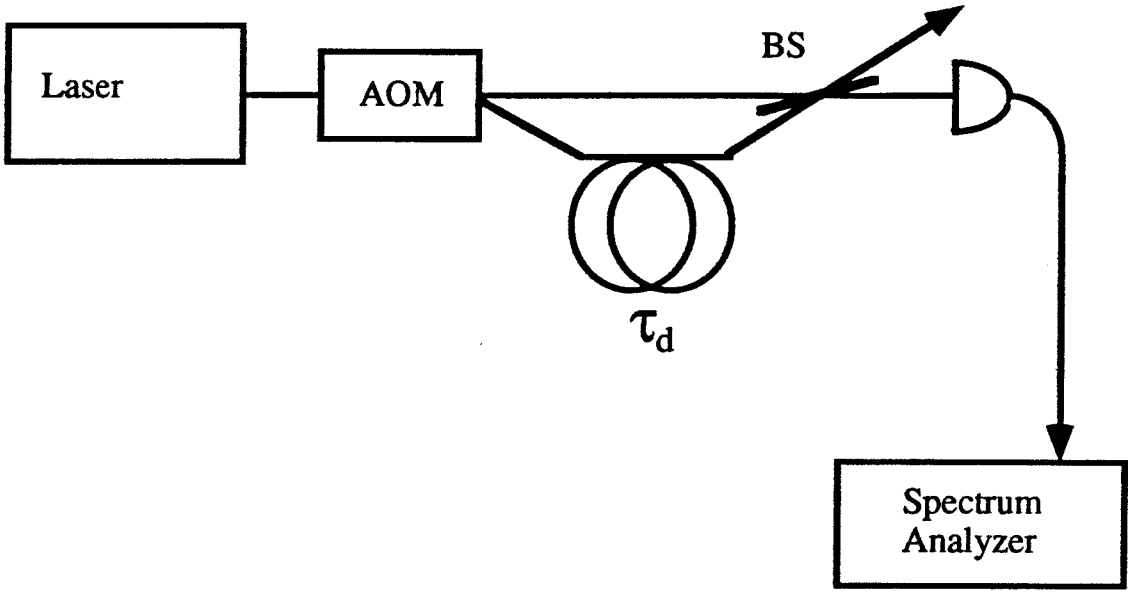

Figure 4.1: The conventional delayed self-heterodyne interferometer. AOM: acousto-optic modulator, τ_d: fiber delay line, PD: photodiode.

the signals were coherent, information concerning the laser linewidth would be difficult or impossible to determine. The AOM serves mainly to move the beat note away from the large noise floor inherent in any spectrum analyzer near DC. (Side note: This system uses long lengths to measure narrow spectral profiles. At the other extreme, it is possible to very accurately (10 μm) measure distances using a source with a broad spectral profile. This is known as optical coherence domain reflectometry [2].)

As the resolution of the DSHI is inversely proportional to the length of the delay line, the DSHI trades off the drawback of two independent, frequency stabilized lasers for a very long piece of fiber. For state-of-the-art semiconductor lasers, which typically have linewidths on the order of hundreds of kHz to several MHz, this trade off is very reasonable as a 5 km fiber delay yields a DHSI resolution of 40 kHz. However, for fiber lasers, which have much narrower linewidths, the tradeoff is not so reasonable. In a recent experiment a 72 km fiber delay was used to measure the linewidth of a fiber laser to be less than 1.4 kHz [3] and the measurement was still limited by the length of the delay line. A 72 km, 1.5 μm fiber delay line at current market prices would cost $12,600 and have a net loss of 14.4 dB. Increasing the resolution of the DSHI, another order of magnitude would cost $126,000 and the delay line would have a net loss of 144 dB. Clearly, the trade-off with the classic technique is beginning to favor two lasers.

Tsuchida [4] reported on an improvement to the DSHI method which uses a recirculating delay, allowing the same fiber delay to be used multiple times. Placement of the acousto-optic modulator in the delay arm of the recirculating DSHI (RDSHI) permitted multiple delays to be determined by counting frequency shifts. However, due to large losses, Tsuchida was only able to measure up to three passes through the fiber delay.

A significant improvement to the RDSHI may be obtained by including in the delay arm an erbium-doped fiber amplifier. By partially compensating the large loss of the delay arm with gain from the fiber amplifier, beat notes from light that has passed through the delay as many as 30 times are easily discerned. An 11 km fiber delay line yields a

resolution limit of 18.2 kHz with a conventional DSHI. The loss-compensated RDSHI yielded a resolution limit of 606 Hz for the same fiber length. If the 72 km delay line used in the experiment mentioned above were inserted into this improved system, a resolution of 92 Hz would be obtainable.

The experimental setup for the loss-compensated RDSHI is shown in figure 4.2. Components include an acousto-optic modulator (AOM), which provided a frequency shift of 140 MHz with a conversion efficiency of 10% at 1550 nm; two fiber input/output couplers to collimate the light out of the fiber for transmission through the AOM and then to refocus it back into the fiber at the AOM output; a delay line consisting of an 11 km length of optical fiber having a net loss of 0.2 dB/km in the wavelength range of interest; and a fused fiber-optic coupler with a 90/10 coupling ratio. 90% of the light per pass was returned to the recirculator and 10% was sent to the photodiode. It is estimated that the total loss per pass through the recirculator was 18 dB. Light was detected with an Ortel photodiode (model 2515B) having a frequency response up to 15 GHz. This created the potential to see light that had been delayed by as many as 100 passes through the fiber delay line. The output of the photodiode was observed on a Tektronics spectrum analyzer (model 2782) with a maximum bandwidth of 33 GHz.

In addition to these components which are standard in a conventional RDSHI, an erbium-doped fiber amplifier (G) with two fiber-optic isolators having a reverse isolation of 35 dB each was added to the recirculator. Two commercially available amplifier units were tested. One was a germanium-only codoped gain module capable of providing 40 dB of small-signal gain at 1537 nm and a maximum saturation output power of 8.43 dBm. It could provide sufficient gain to compensate the loss in the RDSHI delay arm over a bandwidth of 6 nm about 1537 nm. The other module was an aluminium-germanium codoped gain module capable of providing 37.2 dB of small signal gain at 1532 nm and a maximum saturation output power of 10.3 dBm. It could provide sufficient gain to

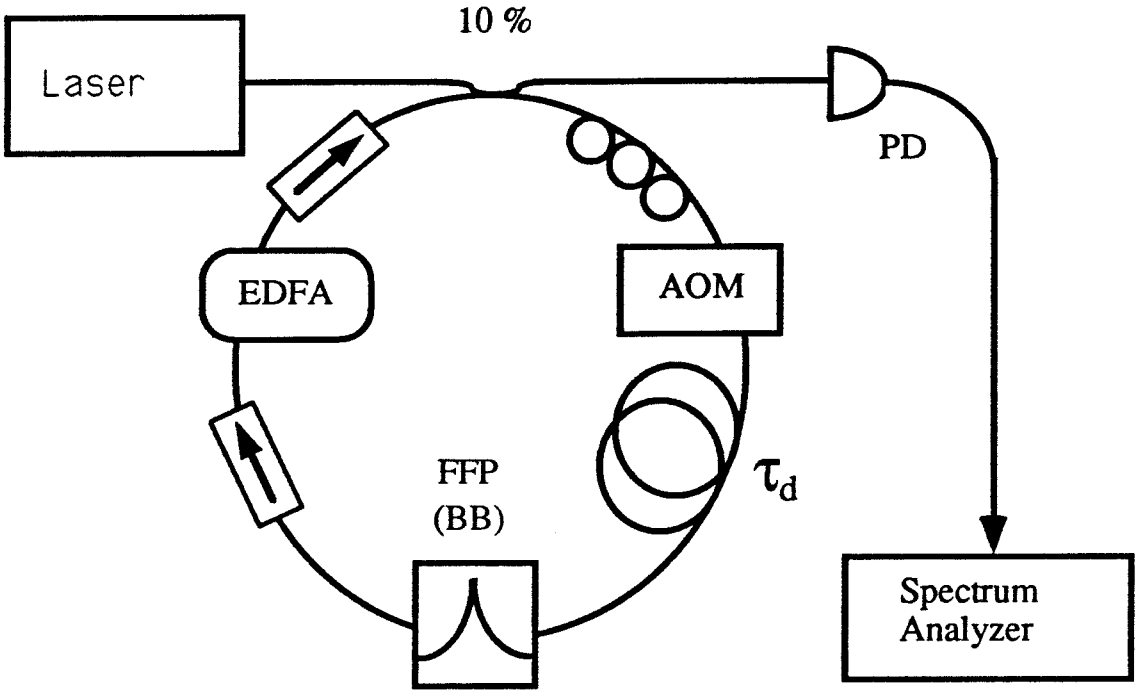

Figure 4.2: The loss-compensated recirculating delayed self-heterodyne interferometer. EDFA: erbium doped fiber amplifier, AOM: acousto-optic modulator, τ_d: fiber delay line, FFP (BB): fiber Fabry-Perot filter, PD: photodiode.

compensate the loss in the RDSHI delay arm over a bandwidth of 30 nm from 1528 nm to 1558 nm.

The light beam diffracted by the AOM closes the recirculating loop. Thus with no RF drive power to the AOM, the loop is open. With zero signal input to the RDSHI and the AOM on, strong beat notes (>30 dB above the noise floor) spaced 18.2 kHz apart (the free-spectral-range of the delay arm) were seen on the spectrum analyzer. This indicated the recirculator was oscillating. This was obviously undesirable as it might interfere with the measurement.

Two steps were taken to prevent the system from oscillating. First, a fiber Fabry-Perot (FFP) filter was included in the delay arm. The FFP filter had a free-spectral-range of 32 nm and a 3 dB bandwidth of 40.2 GHz. This inhibited broadband oscillation, restricting it to the immediate spectral region surrounding the FFP filter transmission peak, which was adjusted to transmit the signal wavelength. Second, the pump power to the amplifier was adjusted downward until the signal input power was sufficient to saturate the gain to a point below the oscillation threshold. This prevented oscillation while still greatly reducing the net system loss. Taking these steps, spectrum analyzer beat notes now occurred only at the expected 140 MHz spacing, with none observable at the 18.2 kHz spacing indicative of oscillation.

It was observed that loud acoustic noises were capable of broadening the measured linewidths (by a factor of about 2-5). To test whether this acoustic broadening was from the measurement system or from the test laser, the entire 11 km fiber delay line was placed in a styrofoam box to isolate it from these acoustic noises. There was no observed decrease in the laser linewidth due to this system change. However, placing the test laser in a similar box did produce a narrowing of the linewidth. Furthermore, after 22 passes through the recirculator, the linewidth was observed to saturate at 4 kHz and did not keep increasing as would be expected if the RDSHI was the cause of the broadening. It was concluded that the measured broadening was due to the test laser.

In reference 4 the case of a RDSHI in which the net system loss is greater than 6 dB is considered theoretically. This is clearly not the case for the loss-compensated system. For high recirculator loss the main contribution to the power of the kth-order beat note is from the undelayed signal field beating with the signal field that has passed through the recirculator delay k-times. For the case of a loss-compensated recirculating delay it is necessary to consider multiple contributions to the kth-order beat note. (For the purposes of discussion, the case of the laser coherence time less than k times the recirculator round-trip time will be considered.) In particular, the signal field that has been delayed by n + k passes (n = 0, 1, 2...) can beat with a signal field that has been delayed by n passes to generate a contribution to the kth-order beat-note intensity. It is therefore necessary to sum over n, which in this case can be as large as 100. Provided that $k\tau_D$ is greater than the laser coherence time, each of these contributions will have the same lineshape. The kth beat-note under these conditions will therefore have a lineshape equivalent to a normal DSHI with the same equivalent delay time.

Figures 4.3 and 4.4 show the photocurrent power spectra for various conditions. In figure 4.3 the amplifier has been removed from the recirculator. Only a few AOM beat-note peaks are seen. In figure 4.4 the amplifier has been inserted and many more AOM beat-note peaks are visible. It is estimated that loss per pass has decreased from 18 dB in the uncompensated case to approximately 0.2 dB per pass with compensation.

Figure 4.5 shows the measured FWHM linewidth of the laser as a function of order. The RDSHI resolution as a function of order is also plotted. The spectrum analyzer was used to average the linewidth over several seconds. The measured linewidth is observed to increase with increasing order and ultimately saturate at 4 kHz around the 22nd order. This behavior is characteristic of a laser with both a short term and long term frequency stability and is discussed below.

However, before this increase could be attributed to the fiber laser, it was necessary to eliminate the possibility of spectral broadening due to the erbium amplifier.

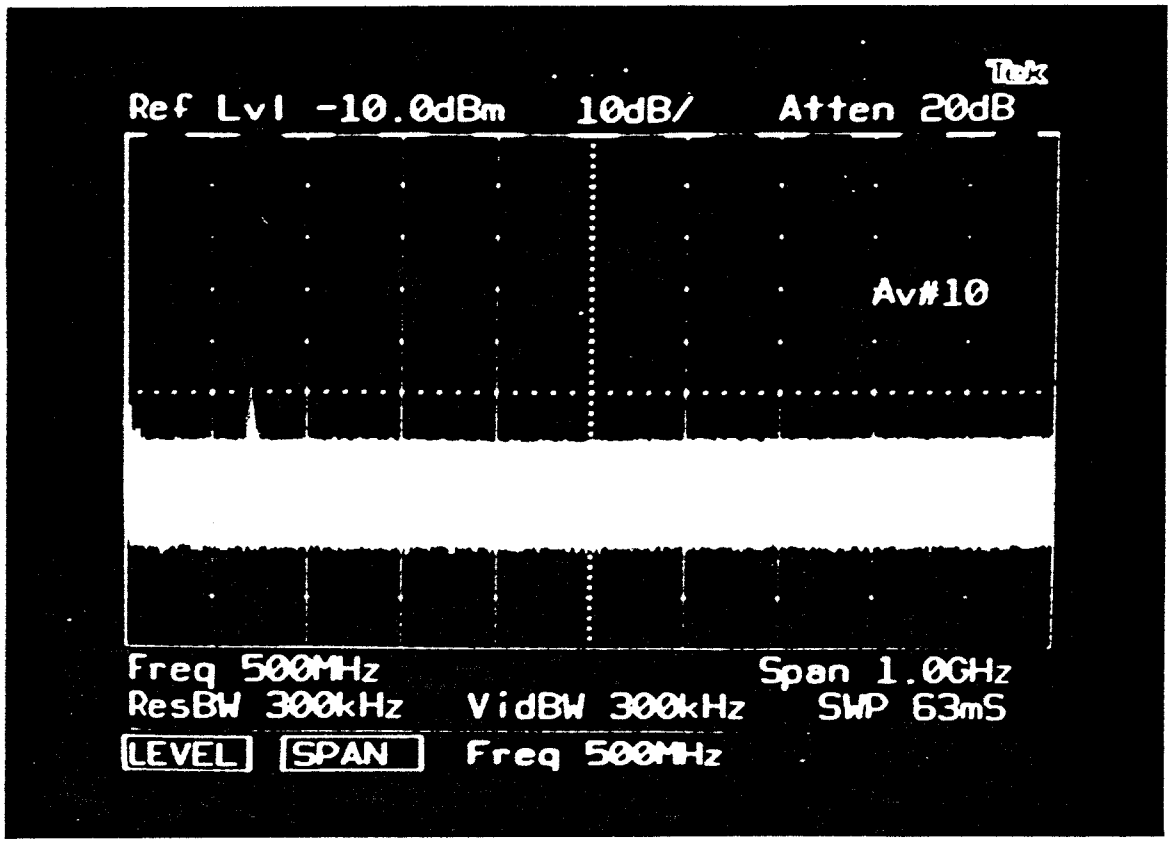

Figure 4.3: Photocurrent power spectra of the recirculator output in the case of no EDFA in the recirculator. Only one beat note is clearly visible, although three beat notes are present.

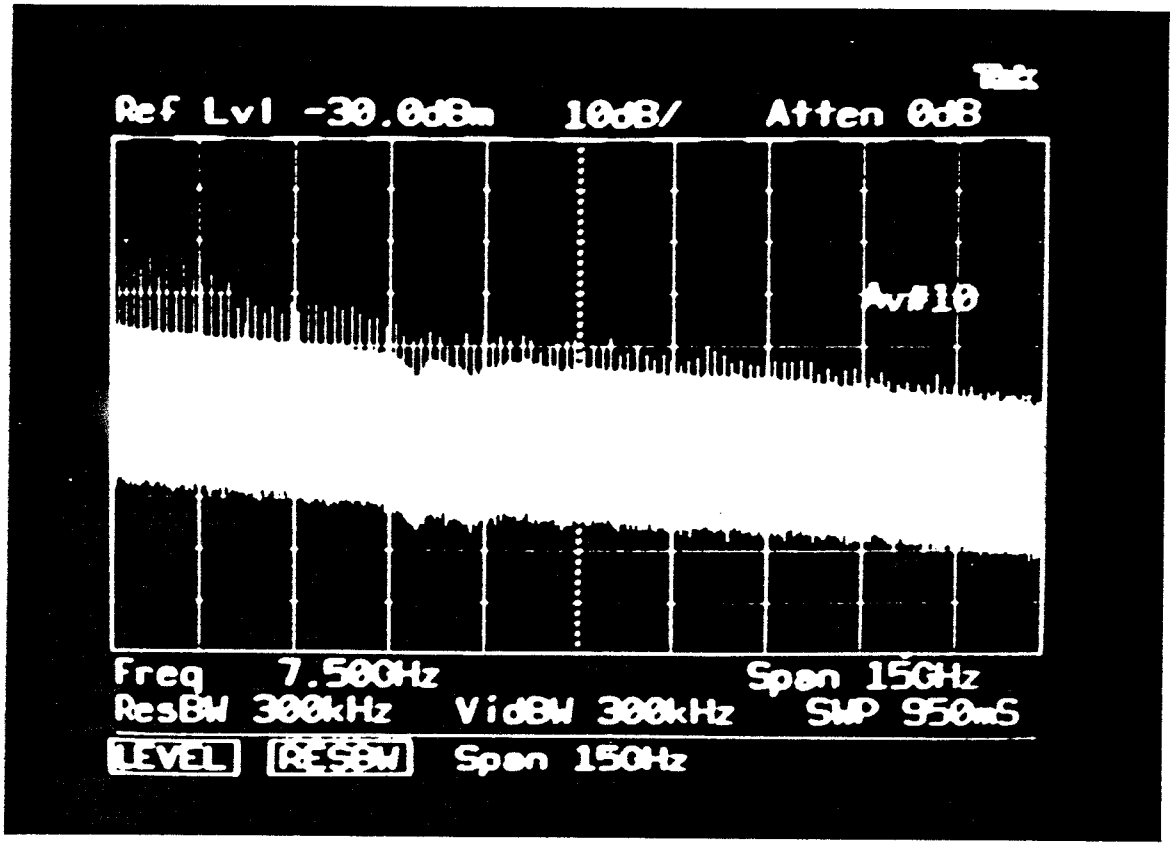

Figure 4.4: Photocurrent power spectra of the recirculator output in the case of an EDFA in the recirculator. Many beatnotes are visible.

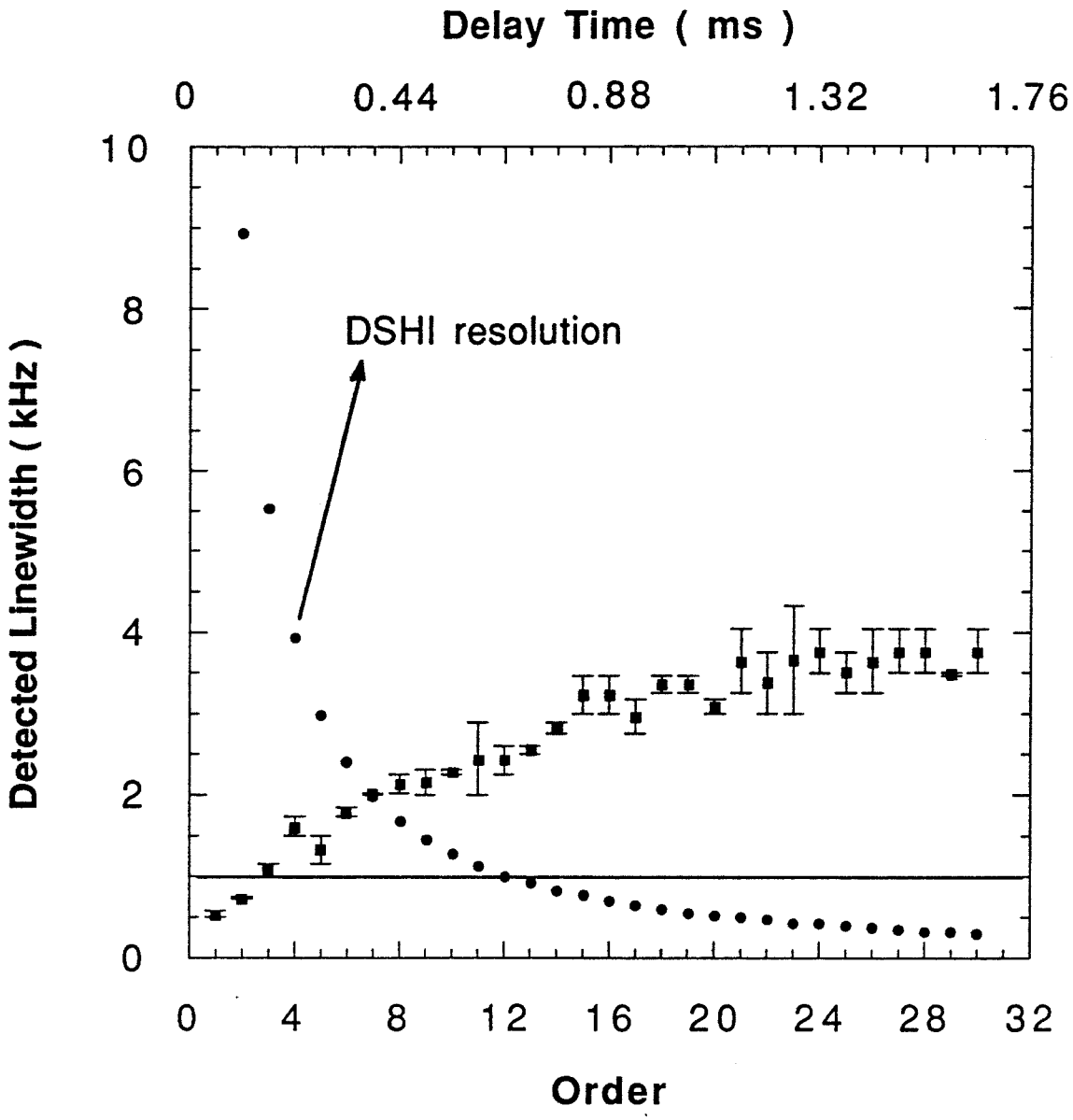

Figure 4.5: Measured linewidth of the fiber laser as a function of order (lower axis). The RDSHI resolution as a function of order is also plotted. Total delay time of the signal may be read from the upper axis.

There is apparent disagreement in the literature [3, 5] as to whether erbium-doped fiber amplifiers broaden the linewidth of a coherent source. To investigate further we removed the 11 km delay line from the RDSHI in order to make k τ_D much less than the laser coherence time [5]. The results are shown in figure 4.6. Figure 4.6 shows, from top to bottom, the linewidth at 1st, 20th and 30th orders, respectively. The maximum observed FWHM linewidth is less than 400 Hz indicating that spectral broadening from the amplifier should not interfere with our measurement (the resolution limit of which is 606 Hz at 30 orders with the 11 km delay line).

As a further check, figure 4.7 shows the measured linewidth in the case of the amplifier in the system (left column) and not in the system (right column). Only the first three orders could be observed in both systems (1st order in the upper row, 3rd order in the lowest row). The only discernable difference in the system with the amplifier and the system without the amplifier was a decrease in the beatnote power due to the large recirculator loss in the case with no amplifier.

The work described above was published in reference 6. A few months later Ishida considered a nearly identical system [7]. Ishida used two acousto-optic modulators in his system. One in the delay loop shifting the frequency by -200 MHz as above (except also used to couple light out of the recirculator, as opposed to using the 90% output coupler), and one before the recirculator shifting the frequency by -150 MHz. A 27 km dispersion shifted fiber delay line was used in the recirculator. Use of two AOMs allowed separation of the k-th beat note arising from the undelayed signal beating with the signal delayed k times occurring at (200 k + 150) MHz from the component of the beatnote due to the sum over n of the (n + k)-th delayed signal beating with the k-th delayed signal occurring at 200 k MHz. The former beat note was 15-20 dB bigger than the latter beat note. A third beat note occurring at (200 (k + 1) - 150) MHz was attributed by Ishida to beating between the undelayed, unshifted signal and signals due to four-wave mixing in the 27 km dispersion

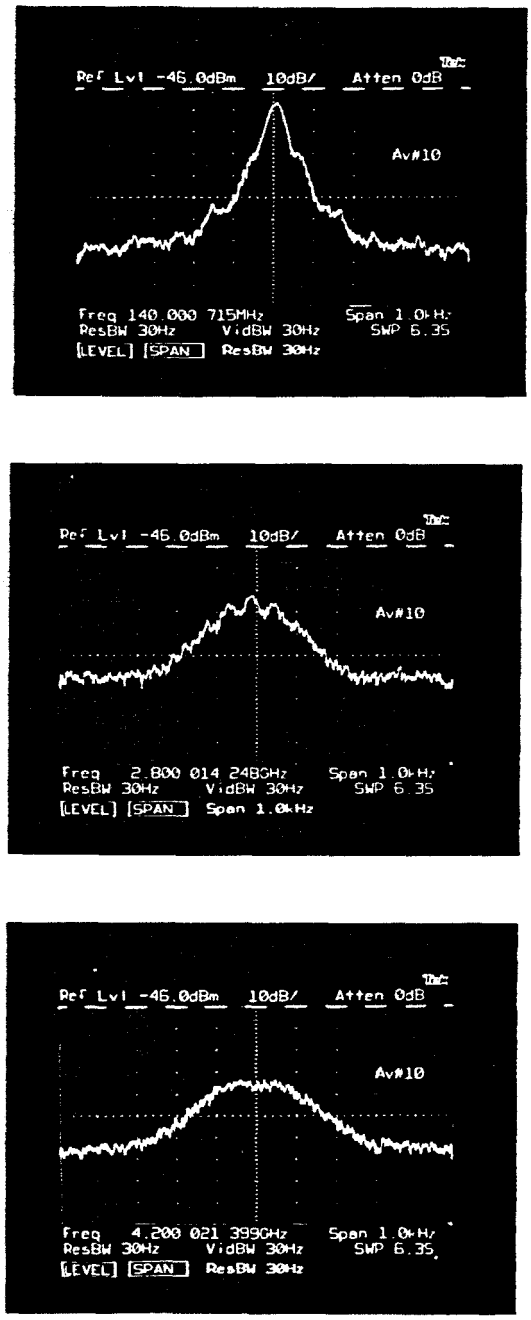

Figure 4.6: RDSHI output without the delay line. Top: 1st order; middle: 20th order; bottom: 30th order.

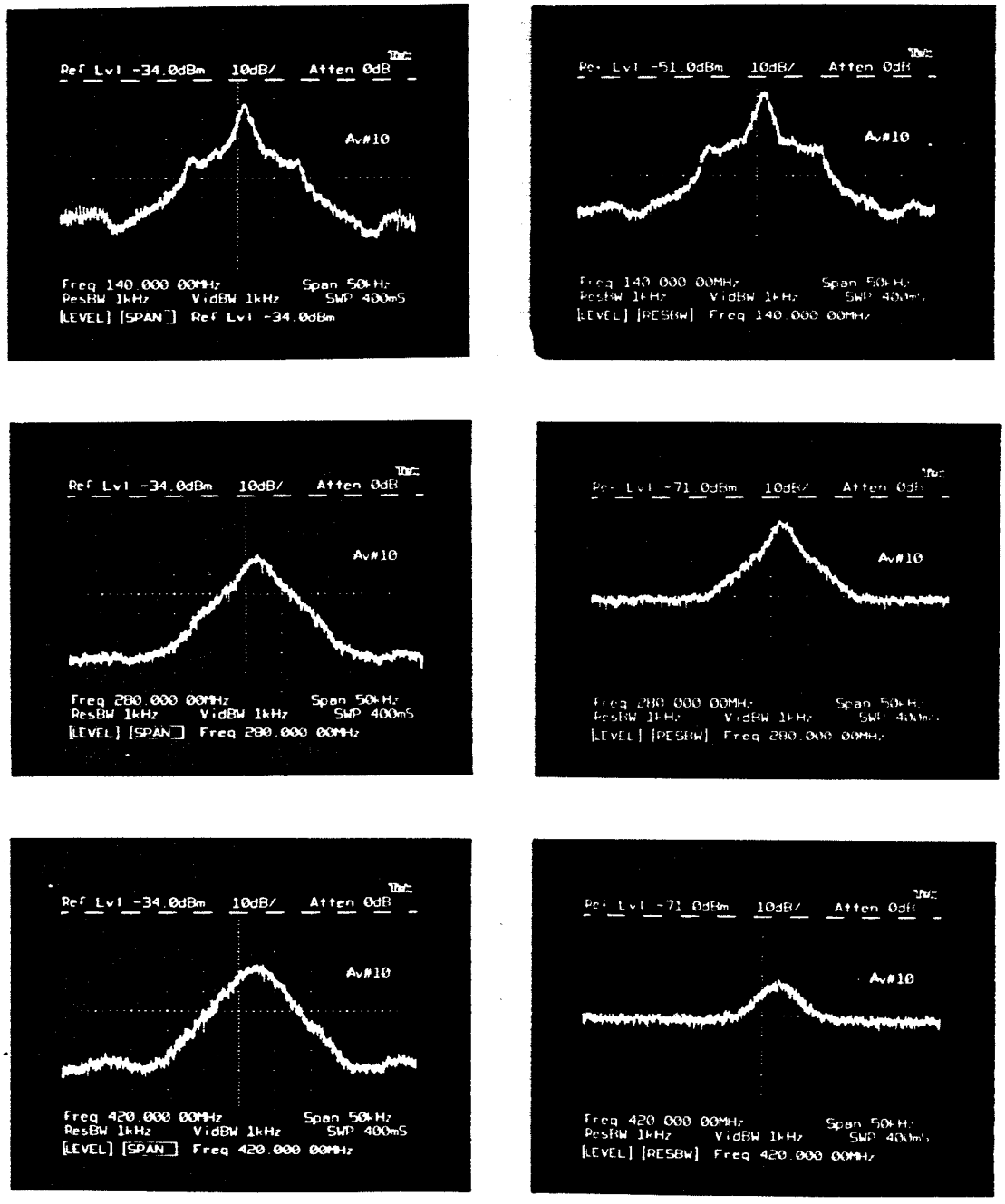

Figure 4.7: RDSHI output with the EDFA (left) and without the EDFA (right). Top row: 1st order, middle row: 2nd order; bottom row: 3rd order.

shifted fiber [], which generated new frequencies at (50 +/- 200 k) MHz. The four-wave mixing signals were 25-30 dB below the undelayed signal beating with the k-th beat note.

In the RDSHI used here to measure the fiber laser linewidth, the three beat notes seen by Ishida are degenerate in frequency. However, those not due to four-wave mixing have already been accounted for and would not generate an error in the linewidth measurement. Furthermore, Ishida's fiber delay was 2.45 times as long as the delay used here and the delay line was made from dispersion shifted fiber which has better four-wave phase matching characteristics than the fiber used here. Even with the greater likelihood of four-wave mixing in Ishida's experiment the four-wave mixing signal power was 30 dB below the measurement signal power. Thus in the present experiment, four-wave mixing should not introduce significant error in the measurement.

4.2 Linewidth and Frequency Jitter Measurement of a Single-Frequency Fiber Laser

The linewidth of the fiber laser was measured between the wavelengths of 1531 nm and 1538 nm, using the tenth order of the loss compensated RDSHI (corresponding to a resolution of 1.2 kHz). The beat spectrum (figure 4.8) was taken in the averaging mode of the spectrum analyzer over a period of several seconds with the resolution bandwidth setting at 1 kHz. The full width at half maximum was calculated from the 3 dB and 6 dB points of these spectra assuming a Lorentzian lineshape. An upper bound on the natural linewidth was 2 kHz as given by the intersection of interferometer resolution and linewidth data plotted in figure 4.5. There was no noticeable dependence on the laser wavelength (Figure 4.9), laser power, or co-dopant of the erbium fiber used in the EDFRL. This suggests that an extrinsic noise source is dominant over the linewidth of this laser. (The Schawlow-Townes linewidth, for example, has an inverse dependence on the laser power and gives a sub-Hertz value for the EDFRL at these power levels). Frequency jitter of the

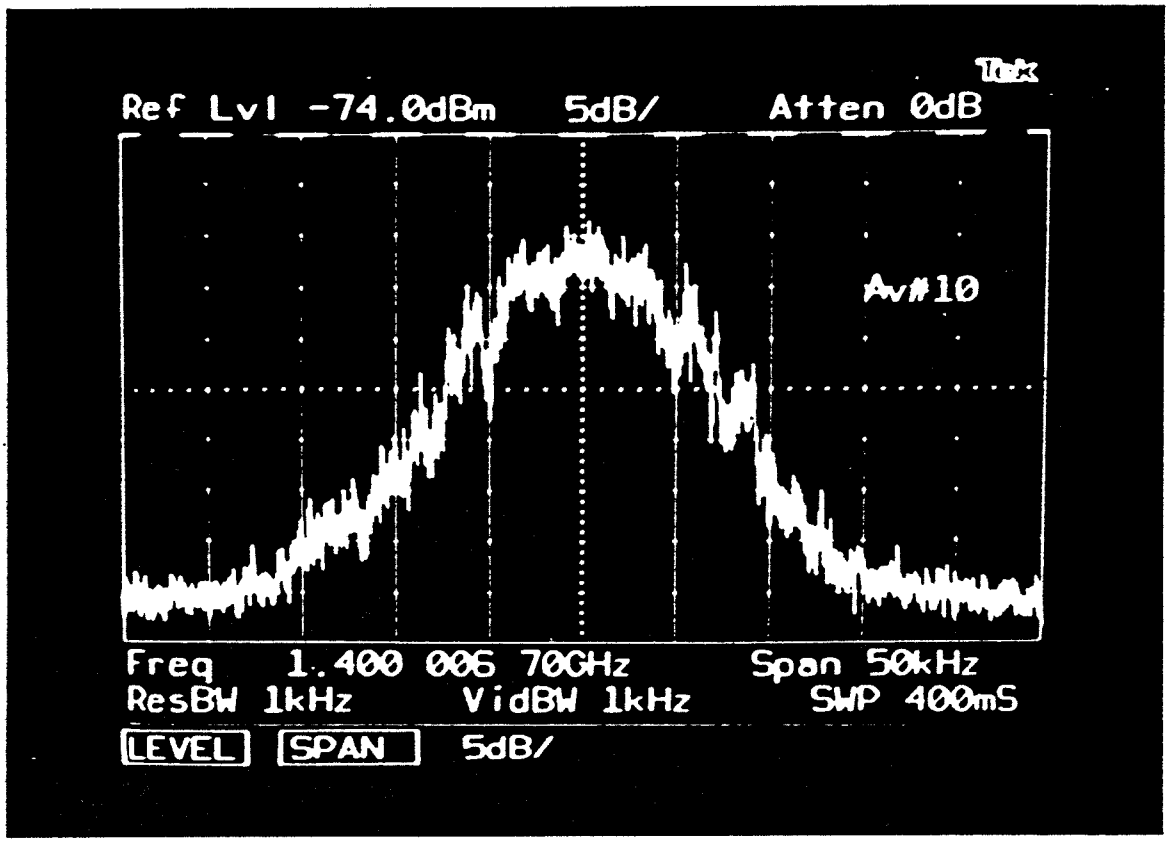

Figure 4.8: Typical spectrum of the RDSHI at the 10th order.

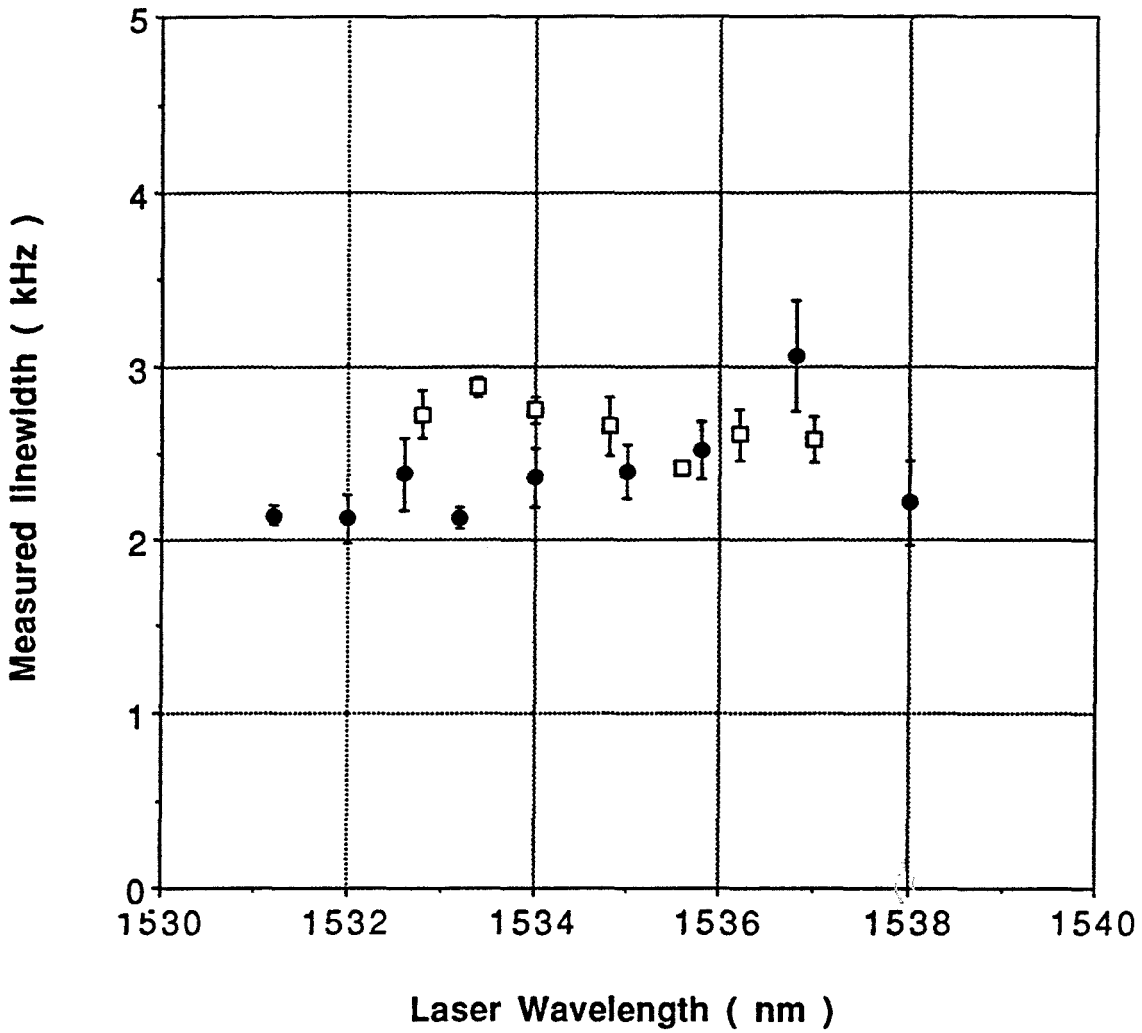

Figure 4.9: Measured linewidth of the fiber laser between the wavelengths of 1531 and 1538 nm. Circles, aluminum-codoped EDFA in the fiber laser; squares, germanium-codoped EDFA in the fiber laser.

detected beatnote induced mainly by acoustic or thermal cavity length fluctuations of the fiber laser is the most likely source.

A laser linewidth that is broadened by frequency jitter due to cavity length fluctuations may not obey the simple rule that the coherence time is inversely proportional to the laser linewidth. To see this more clearly, consider figure 4.10, where laser frequency is plotted as a function of time (in units of loop delay). In this figure the thickness of the line representing the frequency is equivalent to the laser linewidth one would expect from the Schawlow-Townes formula. If the dominant component of the laser linewidth is frequency jitter, a single delay will be enough to see only the frequency deviation corresponding to the average frequency jitter in one delay time. As this may be bigger than the reciprocal of the delay time, one may erroneously conclude the full rms laser linewidth has been measured. However, a truly independent laser has not been simulated until the frequency jitter timescale has been exceeded by the fiber delay.

Therefore, in order to ensure that the frequency jitter component of the laser linewidth can be measured, a delay line long enough to give time for the laser to exhibit its full root mean square (rms) frequency variation must be placed in the conventional DSHI. If the delay line is not long enough, then only a fraction of the full rms jitter will be measured. Using the loss compensated RDSHI, the beat spectrum can be measured at every order (up to 30th, see figure 4.5) to determine the dependence of the lineshape and linewidth on the delay line length. The FWHM was again measured and calculated from the 3 dB and 6 dB point of the beat spectrum, assuming a Lorentzian lineshape. At higher order a smooth transition from a Lorentzian lineshape to a Gaussian lineshape was observed, as expected for the case of a lineshape dominated by frequency jitter. So the linewidth at higher order was calculated based on the Gaussian lineshape. The laser linewidth saturated to a constant value of approximately 4 kHz after 22nd order, indicating that the frequency jitter timescale has been exceeded at this delay length.

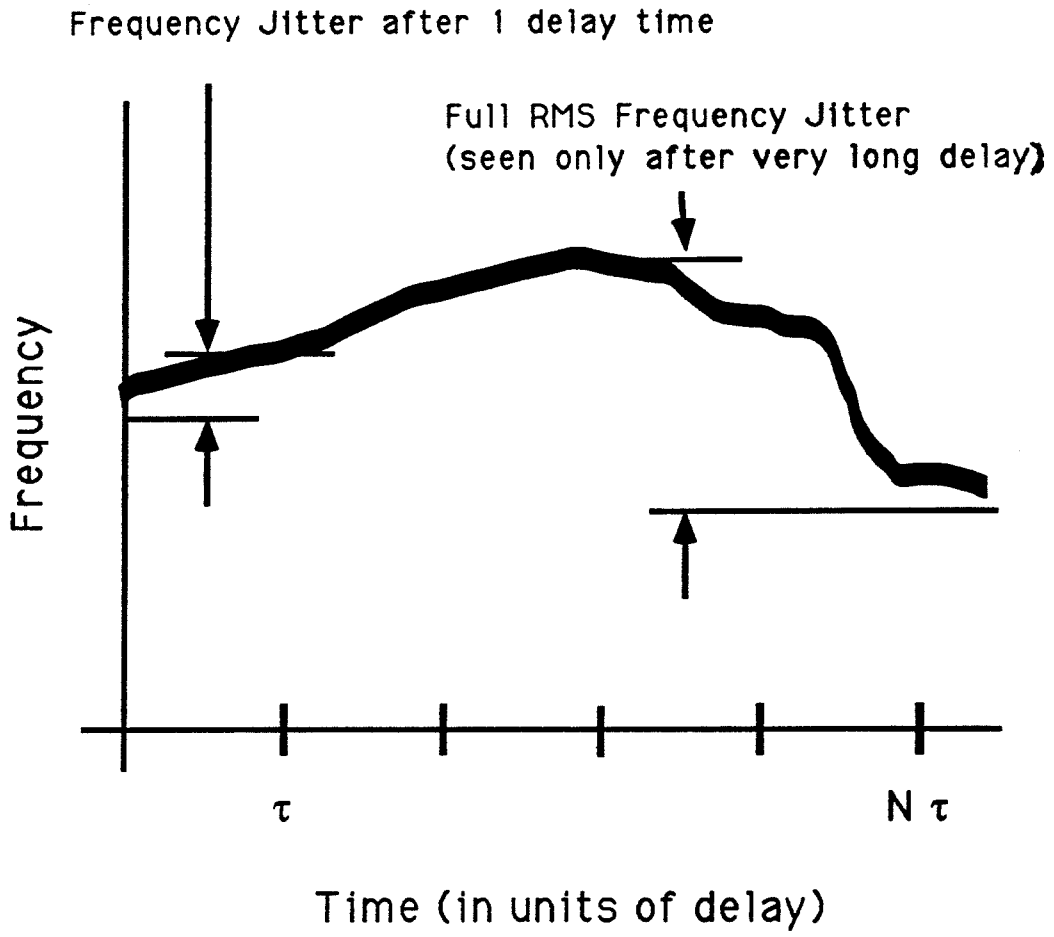

Figure 4.10: One possible case of laser frequency vs. time. Demonstrates RDSHI can be used to measure rms frequency jitter on timescales of a few milliseconds.

For convenience the total delay time has been used to scale the top of the plot in figure 4.5 and order number has been used to scale the bottom. From this plot it can be seen that the frequency jitter timescale of the fiber laser is 1 ms and the rms frequency jitter is 4 kHz. Furthermore, since the resolution of the measurement system to the natural component of the linewidth is exceeded at around 2 kHz resolution, it can be safely concluded that this component of the linewidth is less than 2 kHz. In order to measure this component of the linewidth, the frequency jitter must be removed from the laser and thus an active stabilization system must be employed. Active stabilization of the laser frequency will be considered in the next chapter.

References

[1] T. Okoshi, K. Kikuchi, A. Nakayama, *Electron. Lett.* **16**, 630 (1980)

[2] E. A. Swanson, D. Huang, M. R. Hee, J. G. Fujimoto, C. P. Lin, C. A. Puliafito, *Optics Letters* **17**, 151 (1992)

[3] H. Okamura, K. Iwatsuki, *Electron. Lett.* **26**, 1965 (1990)

[4] H. Tsuchida, *Optics Letters* **15**, 640 (1990)

[5] G. J. Cowle, P. R. Morkel, R. I. Laming, D. N. Payne, *Electron. Lett.* **26**, 424 (1990)

[6] J. W. Dawson, N. K. Park, K. J. Vahala, *IEEE Photon. Tech. Lett.* **4**, 1063 (1992)

[7] O. Ishida, *IEEE Photon. Tech. Lett.* **4**, 1304 (1992)

Chapter 5

Frequency Stabilization of a Single-Frequency Fiber Laser

This chapter discusses frequency locking of the single-frequency fiber laser to an external fiber Fabry-Perot filter using the Pound-Drever technique [1]. As discussed in the previous chapter, the linewidth of the fiber laser is dominated by frequency jitter. This frequency jitter is believed to be due to cavity length fluctuations from thermal and acoustic perturbations. These fluctuations cause the fiber laser linewidth to broaden to 4 kHz rms on a timescale of 1 ms. On much longer timescales the laser frequency may be observed (using the SuperCavity Fabry-Perot) to drift due to thermal length changes of the laser cavity. Over a period of 10 sec to 1 minute, the laser frequency drifts about 2 MHz which is sufficient to induce a mode hop.

It is desired to stabilize the laser frequency at least to within the 4 kHz measured linewidth and to eliminate mode hopping due to thermal drift of the cavity. In this chapter, the Pound-Drever technique will be reviewed, changes to the fiber laser cavity necessary to implement this system will be presented, and, finally, possible improvements to the stabilization technique will be considered.

5.1 Frequency Stabilization

Frequency stabilization of lasers has been a subject of active research since the early 1960's [2]. Many different methods have been proposed. Locking of the laser frequency to an atomic absorption line is very popular as it allows absolute stabilization of the frequency providing the temperature and pressure of the atomic cell is kept reasonably constant [3, 4, 5]. While an atomic line provides an absolute reference, it may be desirable to stabilize the laser frequency at a point that is some distance away from any convenient atomic standard, especially in the case of a laser source that is continuously tunable over a broad range.

Other stabilization methods, which provide greater flexibility in establishing reference points, include locking the laser frequency to the side of an interferometer fringe such as a Michelson or Fabry-Perot interferometer [6] or, alternatively, to the transmission peak [1, 7]. To lock to the transmission peak of a Fabry-Perot filter, it is necessary to find a way to determine which way the frequency is drifting. One way to do this is to dither either the laser frequency or the Fabry-Perot transmission peak. Intentionally dithering the parameter one is trying to stabilize is clearly not desirable in terms of obtaining a very stable source. However, dithering the Fabry-Perot is often a reasonable way to proceed.

The Pound-Drever technique offers several advantages over simply dithering the Fabry-Perot transmission peak. First, it is relatively simple to lock multiple lasers to the same reference cavity using this technique [8]. Second, if a Fabry-Perot is dithered to provide an error signal, the decay time of the optical cavity will limit the bandwidth of the error signal. However, using the Pound-Drever technique, the Fabry-Perot acts as a frequency discriminator on timescales longer than the cavity decay time and a phase discriminator on timescales faster than the cavity decay time [1]. This makes it possible to

phase lock two lasers to a Fabry-Perot cavity and achieve inter-frequency linewidths as small as 3 Hz [9].

While feedback bandwidths to the fiber laser have not yet exceeded the external cavity bandwidth, it was considered that this may be a desirable goal for future experiments. Furthermore, locking multiple lasers to the same reference cavity is desirable for use in wavelength division multiplexed fiber sensor systems, communications systems or for high resolution spectroscopic applications.

The typical experimental set-up for obtaining a Pound-Drever error signal is shown in figure 5.1. The output of a single-frequency laser is sent through an isolator to a phase modulator. The phase modulator is driven by an RF oscillator at a frequency, ω_{PM}, greater than two or three times the bandwidth of the Fabry-Perot being used. The laser spectrum now consists of the lasing mode and two sidebands at +/- ω_{PM}. The phase modulated light is then sent through a beamsplitter to the Fabry-Perot. (A polarization selective beamsplitter in combination with a quarter wave plate or an optical circulator may be used here for improved system performance.) Under ideal conditions, if the laser frequency is tuned so that it coincides precisely with the transmission peak of the Fabry-Perot, the lasing mode is fully transmitted. No part of the lasing mode is seen in the reflected signal in this case. The phase modulated sidebands are outside the transmission bandwidth of the Fabry-Perot and thus are fully reflected. The reflected signal is diverted by the beamsplitter to a photodiode.

If the lasing mode is not tuned precisely to the transmission peak of the Fabry-Perot, a small amount of the field will be reflected. Thus the signal arriving at the photodiode consists of the phase modulated sidebands and a small portion of the lasing mode. The lasing mode, in this case however, has undergone a phase shift with respect to the phase sidebands due to being reflected from near the transmission peak of the Fabry-Perot. A beat note at ω_{PM} is formed between the modulated sidebands and the partially reflected, phase shifted lasing mode at the photodiode. Phase sensitive detection of this

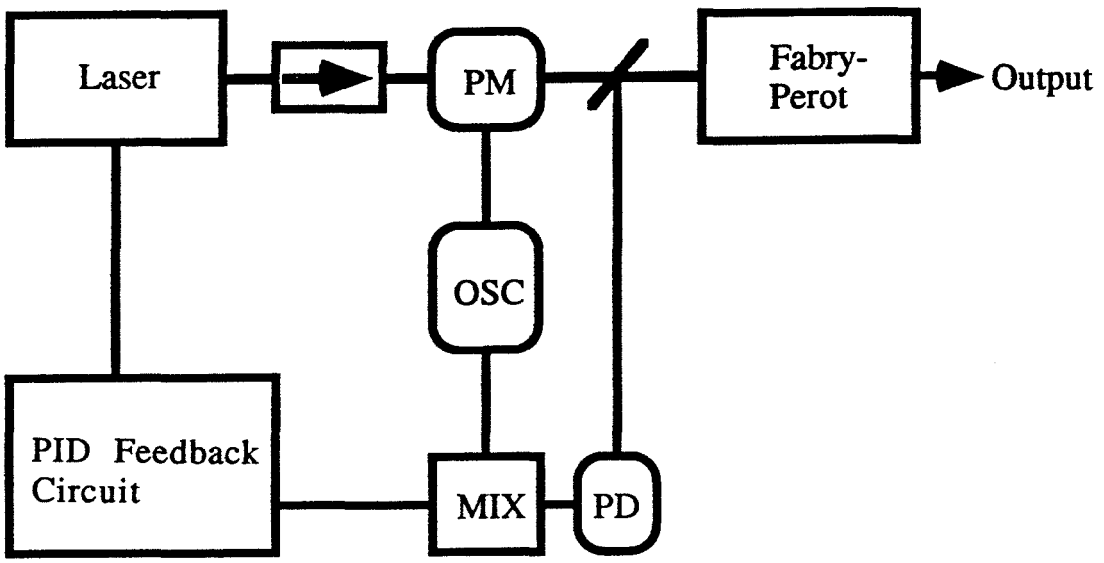

Figure 5.1: Pound-Drever technique for frequency locking a laser to an external Fabry-Perot cavity. PM: phase modulator; OSC: RF oscillator; MIX: RF mixer; PD: photodiode.

beat note via mixing with the original oscillator signal yields an error signal that is proportional in sign and amplitude to the deviation of the laser frequency from the transmission peak of the Fabry-Perot.

If the laser phase changes much faster than the decay time of the Fabry-Perot cavity, the signal reflected from the input mirror of the Fabry-Perot will not be in precise anti-phase with the field stored in the cavity. Therefore, a portion of the field stored in the cavity, which has a π phase shift with respect to the field reflected off the input to the Fabry-Perot, will arrive at the photodiode and beat with the sidemodes forming an error signal. This error signal is proportional in sign and amplitude to the laser's phase change. Thus, the system acts as a frequency discriminator on timescales slow in comparison to the cavity decay time and a phase discriminator on timescales faster than the cavity decay time. The transition between these two regimes has been shown to be smooth [1]. Thus, a servo system can operate properly with a response time far shorter than the cavity decay time when allowance is made in the feedback electronics for a $\pi/2$ phase change associated with the transition [1].

The error signal generated by the Pound-Drever technique is typically processed by proportional-integral-differential control electronics and fed back to the laser. Noise in the error signal system will limit the accuracy to which frequency deviations can be measured. In fact, noise in the error signal will be processed by the control electronics and impose frequency fluctuations on the laser. For a system limited only by the shot noise at the photodetector, the minimum achievable frequency jitter is given by [1],

$$\delta\nu(\tau) \geq \delta\nu_c \sqrt{\frac{hc}{P_0 T \eta \tau \lambda}} \qquad (5.1)$$

where $\delta\nu_c$ is the bandwidth of the Fabry-Perot, P_0 is the laser input power, T the Fabry-Perot transmission efficiency at the transmission peak, η is the quantum efficiency of the detector, $B=1/2\pi\tau$ is the measurement bandwidth, and $\tau>1/2\pi\delta\nu_c$.

5.2 Application of the Pound-Drever Technique to a Single-Frequency Fiber Laser

Consider the problem of frequency stabilization of the fiber laser. For the fiber laser's frequency to be capable of remaining locked to an external Fabry-Perot, the transmission peak of the internal NB FFP filter, which acts as the lasing mode selector, must also track the external Fabry-Perot transmission peak. Figure 5.2 illustrates this problem.

To solve this problem, two error signals and control circuits are required, one for the lasing mode and one for the internal mode selector. The Pound-Drever technique can be applied in both cases. By placing the phase modulator in the laser cavity prior to the output coupler and the NB FFP (see figure 5.3), an error signal may be obtained. This error signal is proportional to the frequency difference between the lasing mode and the transmission peak of the internal mode selector. Feedback to the internal mode selector permits tracking of the lasing mode thus eliminating mode hopping completely. If the lasing mode is then locked to an external cavity, the internal mode selector will be locked to the lasing mode and thus also will be locked to the external cavity.

The lasing spectrum emitted from the laser in this case already contains the phase modulated sidebands necessary for Pound-Drever locking of the lasing mode to an external cavity. The only further components required are an external Fabry-Perot, a 50/50 fused fiber coupler, another photodiode and a duplicate set of electronics. Controlling the lasing mode requires control of the cavity length. In bulk solid state, dye or gas lasers this is typically accomplished using a PZT. However, in the fiber laser, which has a much longer

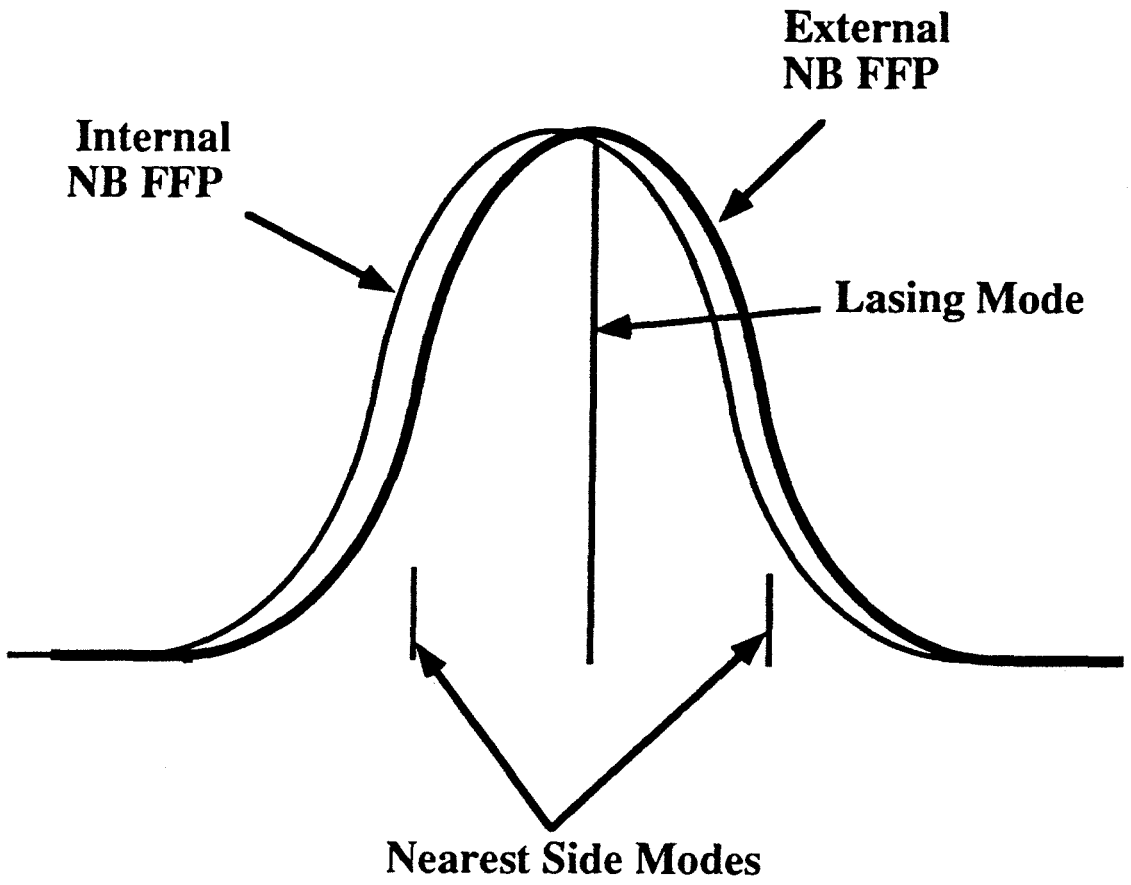

Figure 5.2: An internal tracking filter is required to achieve active locking to an external reference.

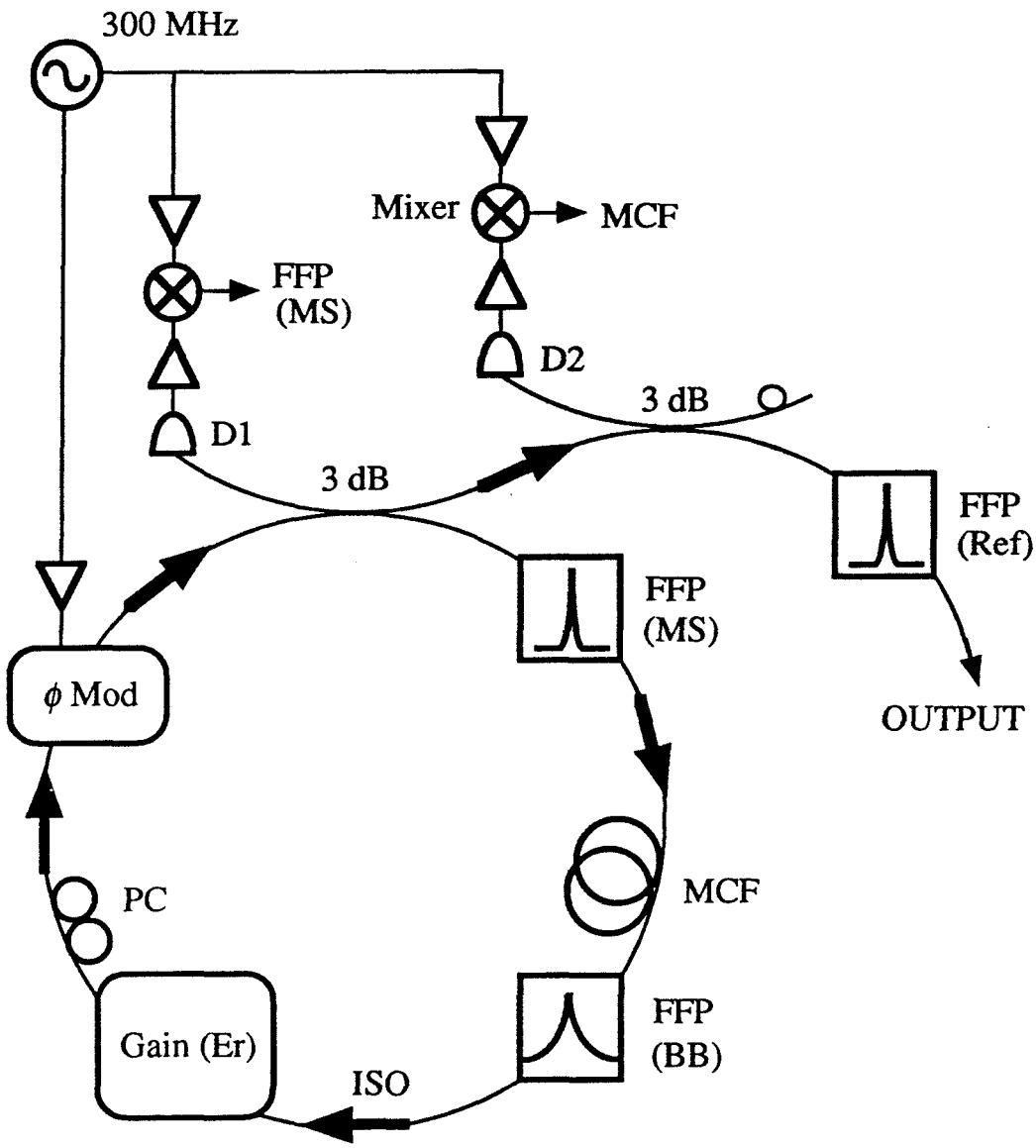

Figure 5.3: Experimental set-up for active stabilization of the fiber laser frequency. FFP(MS): the internal NB FFP(mode selector); D1, D2: photodetectors; ISO: isolators; MCF: metal clad fiber; ϕ Mod: phase modulator; PC: polarization controller; FFP (ref): external NB FFP(reference cavity).

cavity length, a PZT does not provide sufficient excursion to compensate for thermal expansion and contraction of the cavity due to room temperature changes of several degrees. To provide sufficient excursion for the feedback process, changes to the cavity length are accomplished via resistive heating of a metal clad fiber.

Again, figure 5.3 shows the experimental configuration used to implement the Pound-Drever system in all fiber form and lock the lasing mode to an external reference. The lithium niobate phase modulator placed prior to the output coupler was a United Technologies model APE PM - 1.5 - 1.0 - XX - 01. It was pigtailed with polarization preserving fiber, had a half-wave voltage of 6.6 V, and an insertion loss of 4.1 dB. It also acted as the polarizing element in the laser. The NB FFP filter located inside the resonator but after the output coupler acted as the mode selector for the laser. It had a free spectral range of 5.92 GHz, a finesse of 133, a bandwidth of 45 MHz and was tunable across one free spectral range by applying 16 VDC. The 3 dB output coupler acted as the beamsplitter between these two devices. The reflected signal containing the difference frequency information between the lasing mode and the NB FFP transmission peak was incident on detector D1. This signal was amplified with a 50 dB RF amplifier, sent through a high pass filter and mixed with part of the 300 MHz signal driving the phase modulator. BNC cables of varying lengths were introduced between the high pass filter and the mixer in order to achieve maximum phase matching between the signal and the local oscillator. A proportional integral differential control circuit was constructed from op-amps to process the error signal output from the mixer and feed it back to the internal NB FFP. This circuit had a bandwidth of 10 kHz.

The output of the fiber laser was sent through an optical isolator to another 3 dB fused fiber coupler. One output port of the coupler was sent to a fiber Fabry-Perot filter closely matched in free spectral range and finesse to the internal mode selector. This was done so that the laser could be tuned by the BB FFP filter and the new lasing frequency could easily acquire a lock to the external reference. It was also tunable, allowing the

lasing frequency to be fine tuned via tuning the external reference. The other output port of the 3 dB coupler was carefully terminated by tying a knot in it to produce large bending loss and dipping the end in an index matching gel. This prevented stray reflections from creating a Michelson interferometer effect and interfering with the error signal. The reflected signal from the reference FFP was incident on photodiode D2. The control circuit electronics were similar to those described above.

Again a proportional-differential-integral control circuit was constructed, only in this case, the voltage output was connected to a voltage controlled current source. This current source was capable of supplying 0.5 amps of current to the metal clad fiber. The metal clad fiber inserted in the cavity was a standard single mode fiber only coated with aluminium. It had a length of one meter, a resistance of about 2 Ω and an insertion loss of 3 dB. With the metal clad fiber inserted in the cavity, 0.5 amps of current applied, and with the NB FFP tracking circuit active, the lasing mode was observed to move about 200 MHz in one second. This indicated that the metal clad fiber could compensate for cavity length excursions as large as 50 μm and had a response time on the order of 5 ms/MHz.

Based on the frequency jitter timescale measured in the last chapter, this is sufficient to stabilize the laser frequency to within its frequency jitter linewidth. From equation 5.1, for operation at 1550 nm, a measurement bandwidth of 10 kHz, an optical power of 1 mW, a transmission efficiency of 50%, a cavity bandwidth of 45 MHz and an overall quantum efficiency in the system of approximately 20% due to losses in the system, the minimum frequency fluctuation obtainable is 160 Hz. However, since the laser is not in the configuration for shot noise limited operation, the actual noise *current* at the photodetector may be as much as 15 dB larger giving a minimum theoretical frequency fluctuation that is closer to 5 kHz. Possible ways to improve this limit will be discussed below.

The stabilization system was implemented. The error signal from mixer 1 is shown in figure 5.4; the upper curve is for the control loop closed and the lower curve is for the control loop open. Without feedback the error signal shows frequent modehops with

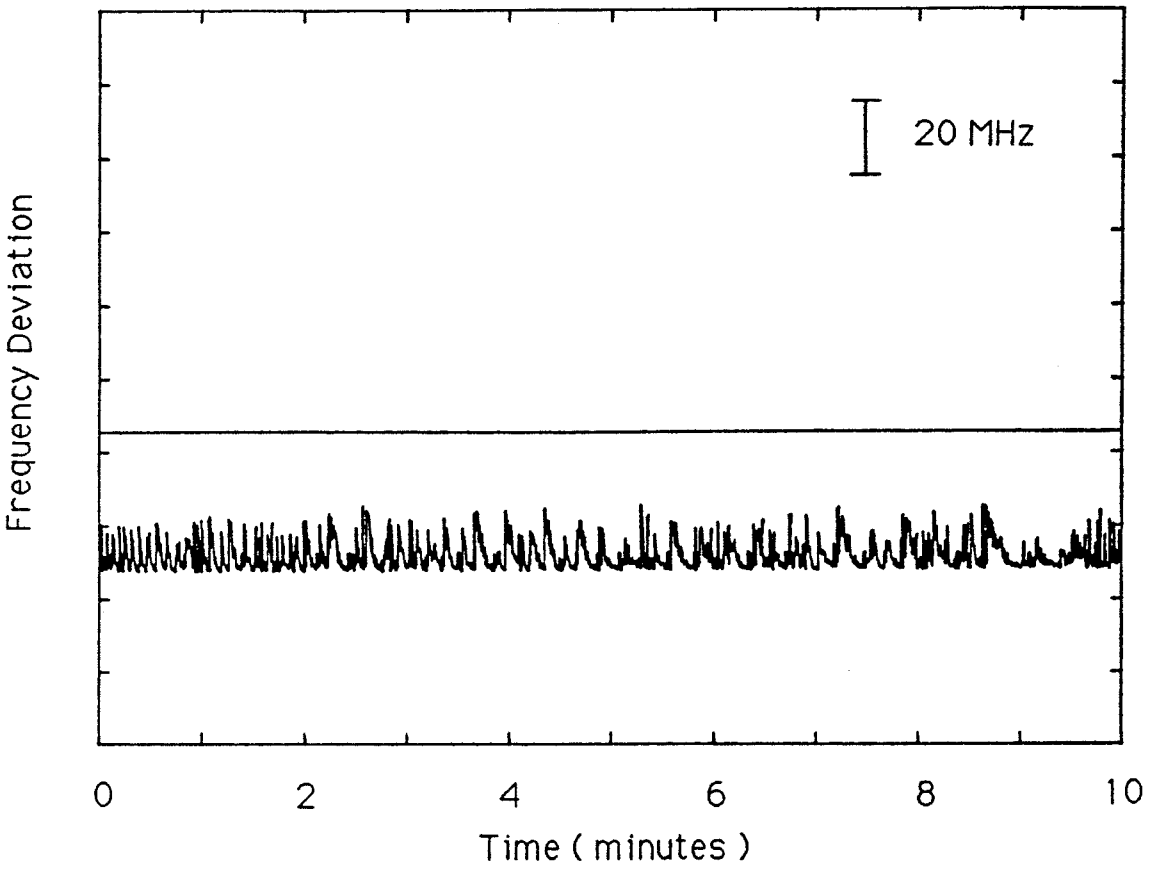

Figure 5.4: Error signal from the internal NB FFP. No feedback (lower curve); with feedback (upper curve).

frequency deviations from the transmission peak of the mode selector as large as +/- 5 MHz. This deviation is somewhat larger than expected (+/- 2 MHz) and is attributed to another weak Fabry Perot being formed between splices, as discussed in Chapter 3. With feedback, however, modehops are completely eliminated. This was confirmed by the chart recording shown in figure 5.4, observation of the lasing mode with the SuperCavity and observation of the error signal on shorter timescales with an oscilloscope. The oscilloscope provided resolution of the error signal to 1 mV, which corresponds to 100 kHz of frequency deviation. In addition, perturbing the system by varying the current to the metal clad fiber and banging on the optical table to induce strong acoustic perturbations confirmed that this loop of the stabilization system was quite robust.

The error signal from the external fiber Fabry-Perot is shown in figure 5.5, the upper curve is for the control loop closed and the lower curve is for the control loop open. Without feedback to the metal clad fiber, but with the first control circuit operating, the deviation between the lasing frequency and the transmission peak of the external Fabry-Perot is approximately +/- 15 MHz over a time period of 10 minutes. With feedback, this deviation is greatly reduced. Again, this was confirmed by observation of the lasing mode with the SuperCavity and observation of the error signal on shorter timescales with an oscilloscope. The oscilloscope resolution was 1 mV, which corresponded to 200 kHz of frequency deviation from the transmission peak of the external Fabry-Perot (the optical power is lower outside the cavity, thus the error signal is smaller). The external Fabry-Perot was tuned and mode hop free tracking of the transmission peak was observed with the SuperCavity over the 200 MHz range of the metal clad fiber. Again, banging on the optical table to induce strong acoustic perturbations showed this loop of the stabilization system was also quite robust. While it has been shown using the error signal that the frequency fluctuations of the laser have been reduced below 200 kHz, actual measurement of the stability must wait until components for two completely stabilized lasers may be obtained. The experimental set-up for this experiment is shown in figure 5.6.

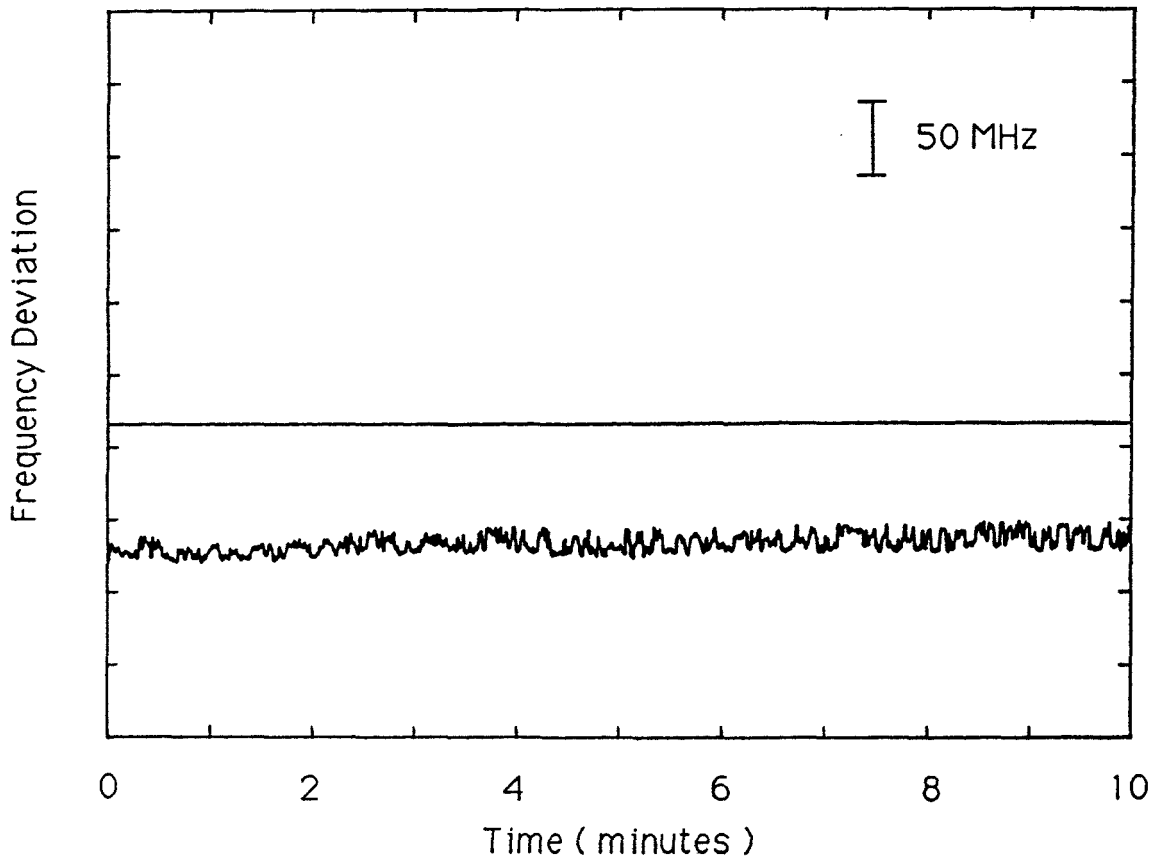

Figure 5.5: Error signal from the external refernce NB FFP. No feedback to MCF, but with feedback to internal NB FFP (lower curve); with feedback to both (upper curve).

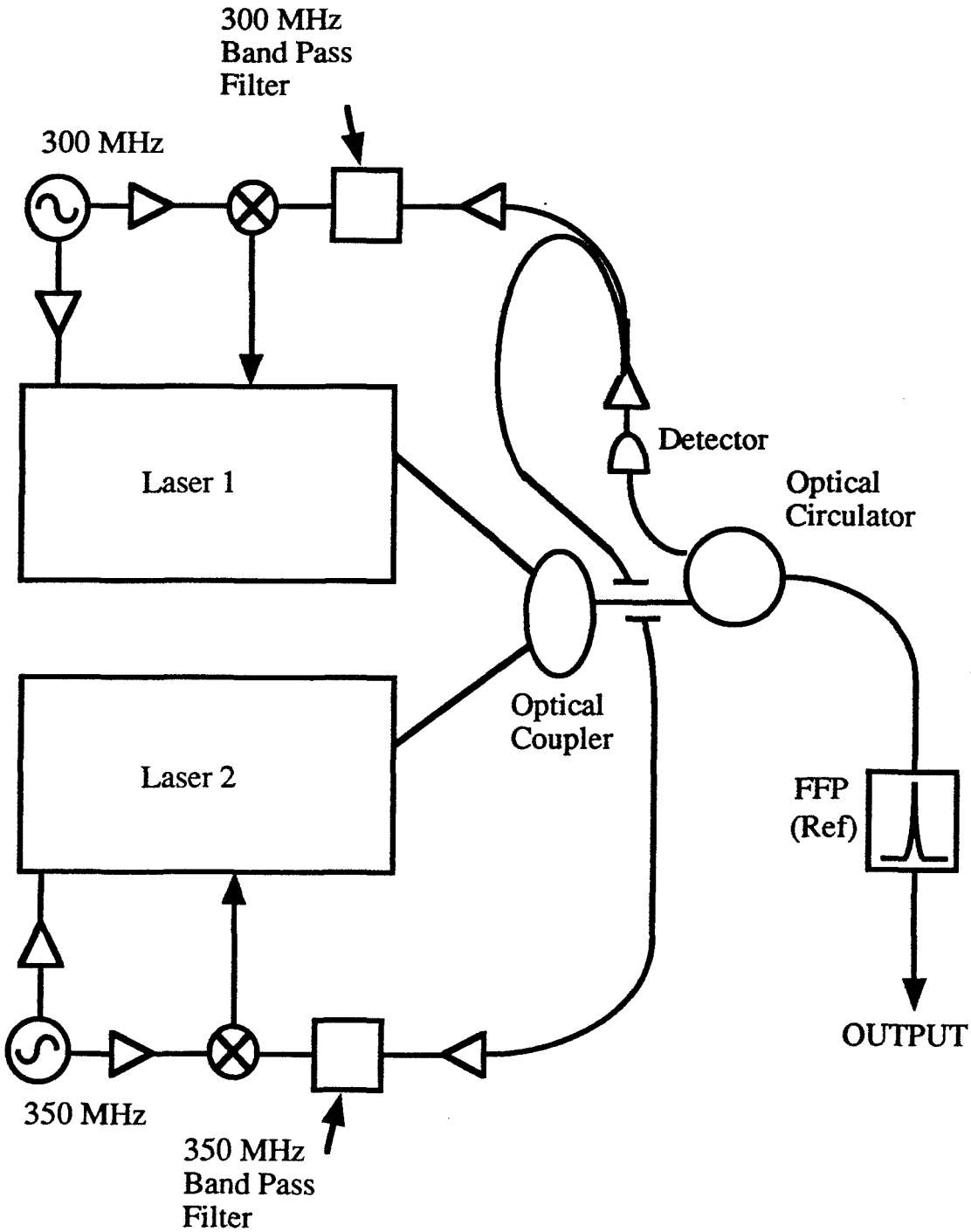

Figure 5.6: Experimental set-up to stabilize two fiber lasers to the same reference FFP (FFP (Ref)).

This experiment has demonstrated the feasibility of active stabilization of the fiber laser frequency. There are many improvements that could be made to future systems. For example, shortening the cavity length by cutting the pigtails on the equipment and using a shorter, more highly doped erbium fiber gain medium would increase the ease of achieving stabilization and increase the continuous tuning range of the laser. While finite excursion of the metal clad fiber will limit the continuous tuning range, it is anticipated that the quasi-continuous tuning or seamless tuning with stitching will be possible. The metal clad fiber used in this experiment changes the cavity length by 50 free spectral ranges. With a cavity length 10 times shorter, the continuous tuning range would be 10 times as large.

Tracking of the lasing mode with the NB FFP could also be accomplished by dithering the NB FFP to create an error signal. This would allow the phase modulator to be removed from the cavity and the NB FFP to again be placed prior to the output coupler, lowering the noise in the system to within 5 dB of the shot noise limit. Alternatively, or in conjunction with that method, a higher finesse Fabry-Perot, such as the SuperCavity, could be used to reduce the minimum frequency jitter by a large amount. It may be desirable to leave the phase modulator in the cavity since its large bandwidth would be useful to employ the phase discriminator aspects of the Pound-Drever technique.

From the results in this chapter and the previous three chapters, it is clear that the fiber laser has the potential to be a very stable, low noise, widely tunable source in the 1.5 μm wavelength region.

References

[1] R. W. P. Drever, J. L. Hall, F. V. Kowalski, J. Hough, G. M. Ford, A. J. Munley, H. Ward, *Appl. Phys. B* **31**, 97 (1983)

[2] A. D. White, *IEEE J. Quantum Elec.* **QE-1**, 349 (1965)

[3] S. L. Gilbert, *Optics Lett.* **16**, 150 (1991)

[4] M. Suzuki, S. Yamaguchi, *IEEE J. Quantum Elec.* **QE-24**, 2392 (1988)

[5] M. Arditi, T. R. Carvet, *Proc. IEEE* **51**, 190 (1963)

[6] E. A. Ballik, *Phys. Lett.* **4**, 173 (1963)

[7] A. D. White, *IEEE J. Quantum Elec.* **QE-1**, 322 (1965)

[8] B. Glance, et al., *Electron. Lett.* **23**, 750 (1987)

[9] T. Day, E. K. Gustafson, R. L. Byer, *Optics Lett.* **15**, 221 (1990)

Chapter 6

Multiple Wavelength Fiber Lasers

The previous five chapters have investigated single-frequency operation of an erbium doped fiber laser. Broad tunability, narrow linewidth, low intensity noise and active frequency stabilization have been demonstrated. Applications such as semiconductor four-wave mixing spectroscopy that take advantage of these properties are beginning to prove the laser's usefulness [1]. However, if the fiber laser were to be used in a wavelength division multiplexed telecommunications or sensor application, the cost would need to be greatly reduced in order to be competitive with commercial DFB lasers or even external cavity semiconductor lasers. The two major barriers here are the price of the pump diode and the price of the fiber Fabry-Perot and the optical isolators.

Commercial 980 nm pump diodes with output powers of 1 W are now available. A fiber laser can achieve a 1 mW output power (sufficient for many uses) over a broad tuning range with approximately 25 mW of pump power. This creates the possibility that 40 fiber lasers could be pumped with a single pump laser. Most of the cost would then be contained in components other than the gain media. So the question is how to reduce the cost of the components. Alternatively one might ask how to reduce the number of components. If the lasers can share the same location, they could conceivably share parts

of the same cavity, creating, in effect, one laser with multiple single-frequency outputs. This is the subject of this chapter.

Two means of creating multiple frequency lasers were investigated. In the first, carried out prior to the rapid drop in price of the 980 nm pump laser, the lasers share the same gain medium. Weak spectral hole burning in combination with careful matching of the loss to the gain at each wavelength allow multiple lasers to share the same gain medium. In the second, each laser has an independent gain medium and as many of the remaining cavity components as possible are shared.

The first section of this chapter investigates spectral hole burning in EDFAs. For most practical purposes the EDFA gain medium is homogeneously broadened and spectral hole burning can be safely ignored. However, a small amount of weak spectral hole burning is observable [2]. The second section investigates the case of the two-frequency fiber laser. The two-frequency fiber laser is studied both for the case of a shared gain medium and, two, independent gain media. The third section presents the results from a demonstration of a six-frequency, single gain medium fiber laser. The results of the second and third sections, in combination with the results of the previous four chapters are used to propose an N frequency, low intensity noise, narrow linewidth, frequency stabilized fiber laser based on state-of-the-art fiber optic technology.

6.1 Spectral Hole Burning in Erbium Doped Fiber Amplifiers

The gain spectrum of the erbium doped fiber amplifier has been extensively investigated [2, 3, 4, 5, 6, 7]. The broad gain bandwidth of the EDFA can be mainly attributed to the Stark splitting of the upper and lower levels of the 1550 nm transition (see figure 6.1), which creates a large number of transitions from 1470 nm to 1570 nm. The Stark splitting of the upper and lower energy levels results in a manifold of energy states at each level, which are populated in a Boltzmann distribution [5]. The Boltzmann

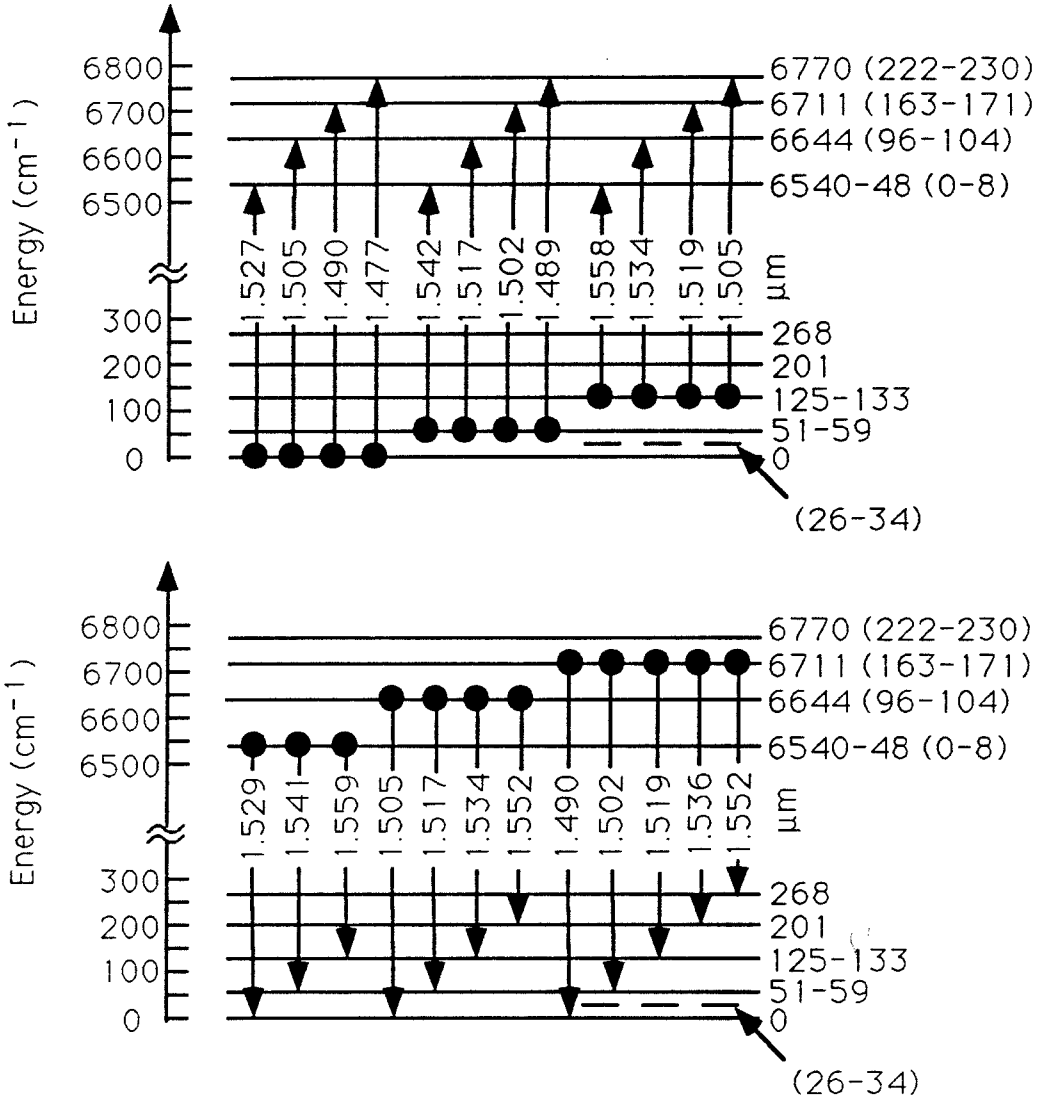

Figure 6.1: Energy level diagram showing Stark components of the upper and lower energy levels of the EDFA. Observed fluorescence transitions (lower); observed absorption transitions (upper). Source [5].

distribution of the energy levels results in absorption in the 1470-1520 nm range and fluorescence/gain in the 1520-1570 nm range when the amplifier is strongly pumped.

One might expect that due to the Stark split energy levels, strong spectral hole burning would be observed even at room temperature. However, the resulting energy levels are very closely spaced in energy (~50-100 cm^{-1}) and interaction with phonons in the glass causes a fast cross-relaxation between levels (which also results in a broad homogeneous linewidth for each level). As a result of this fast cross-relaxation, strong spectral holes are not observed at room temperature [3, 6]. However, at lower temperatures, the number and average energy of the phonons in the glass is greatly decreased and it becomes possible to observe spectral hole burning in EDFAs [3, 6]. As the temperature is increased from 7 K to 61 K, the observed spectral hole width increases from 0.21 nm to 1.3 nm. At room temperature the homogeneous linewidth of any transition between the upper and lower manifold is extrapolated to be on the order of 23 nm.

The cross relaxation process keeps the Boltzmann distribution of the electron populations in the Stark levels in rough equilibrium in the presence of strong saturating signals. As a result, gain cross saturation is observed; the gain at short wavelengths saturates more easily than the gain at longer wavelengths [2]. However, due to the finite rate of these processes, weak spectral holes at the saturating signal wavelengths are observed in the gain compression spectra [2]. These holes have a depth of about 1 dB and a width of about 1 nm.

To verify this result and investigate hole burning further, two single frequency fiber lasers were constructed and used to measure the small signal gain of the EDFA in the presence of a saturating signal of varying power and wavelength. The experimental set-up is shown in figure 6.2. Fiber laser #1 creates the saturating signal which is sent through a 50/50 fused fiber coupler to a Corning FiberGain module (EDFA), which is a germanium codoped amplifier with 37.1 dB of small signal gain at the gain peak (1537 nm) and a

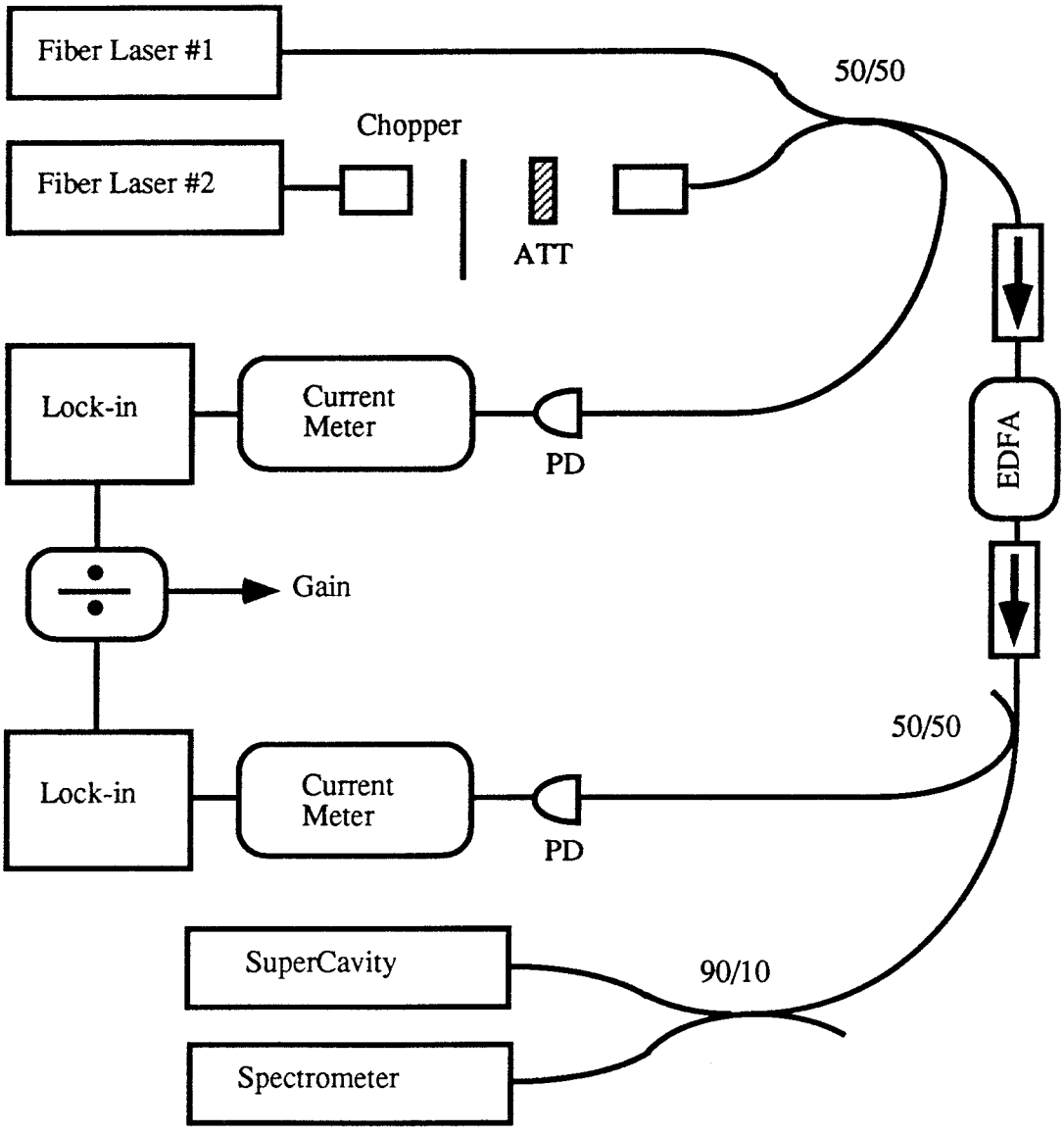

Figure 6.2: Experimental set-up for measuring gain cross-saturation and spectral hole burning. ATT: variable attenuator; PD: photo-diode.

saturation output power of +8.3 dBm. Fiber laser #2 acts as the probe to measure the small signal gain of the EDFA as a function of wavelength. The output of fiber laser #2 is collimated by a fiber input output coupler, attenuated to small signal power levels (~-35 to -40 dBm) and chopped to allow lock-in detection to distinguish the probe signal from the much stronger pump signal. The chopped, attenuated light is recoupled back into fiber by a second fiber input/output coupler and sent through the 50/50 coupler. One half goes to the EDFA and the other half is detected with a broad area Ge photodetector driving a lock-in amplifier.

The output signal from the EDFA is split by a 50/50 coupler. One-half goes to another Ge photodetector and a second lock-in measures the output probe power. The other half is sent to a 90/10 fused fiber coupler, 10% of this power is used to monitor stability of the two fiber lasers and 90% is sent to a spectrometer to monitor the wavelength. The signals from the two lock-in amplifiers are divided by an analog voltage divider and the gain (less a several dB correction factor accounting for coupling losses in the system) may be read directly from the output of this divider.

Figure 6.3 plots EDFA gain as a function of wavelength for the cases of no applied saturating signal, a -20 dBm saturating signal applied at 1536.6 nm and a -20 dBm saturating signal applied at 1537 nm. Gain cross saturation can be clearly observed. With the 1536.6 nm signal applied, the gain at 1538.6 is nearly unaffected, but with the signal applied at 1537, the gain at 1538.6 is down by 3 dB. At shorter wavelengths the gain is quite close to the same value in both cases. The amount of gain compression at shorter wavelengths is apparently decreasing as the probe is moved further from the saturating signal wavelength. Gain compression is ~5 dB at the saturating signal wavelength and decreased to around ~3 dB one nanometer to the blue side of the saturating signal.

Figure 6.4 shows the small signal gain spectrum as a function of saturating signal power applied at 1537.2 nm. As the saturating signal power is increased, the gain peak is steadily compressed. It can be seen that while the gain of the EDFA is essentially

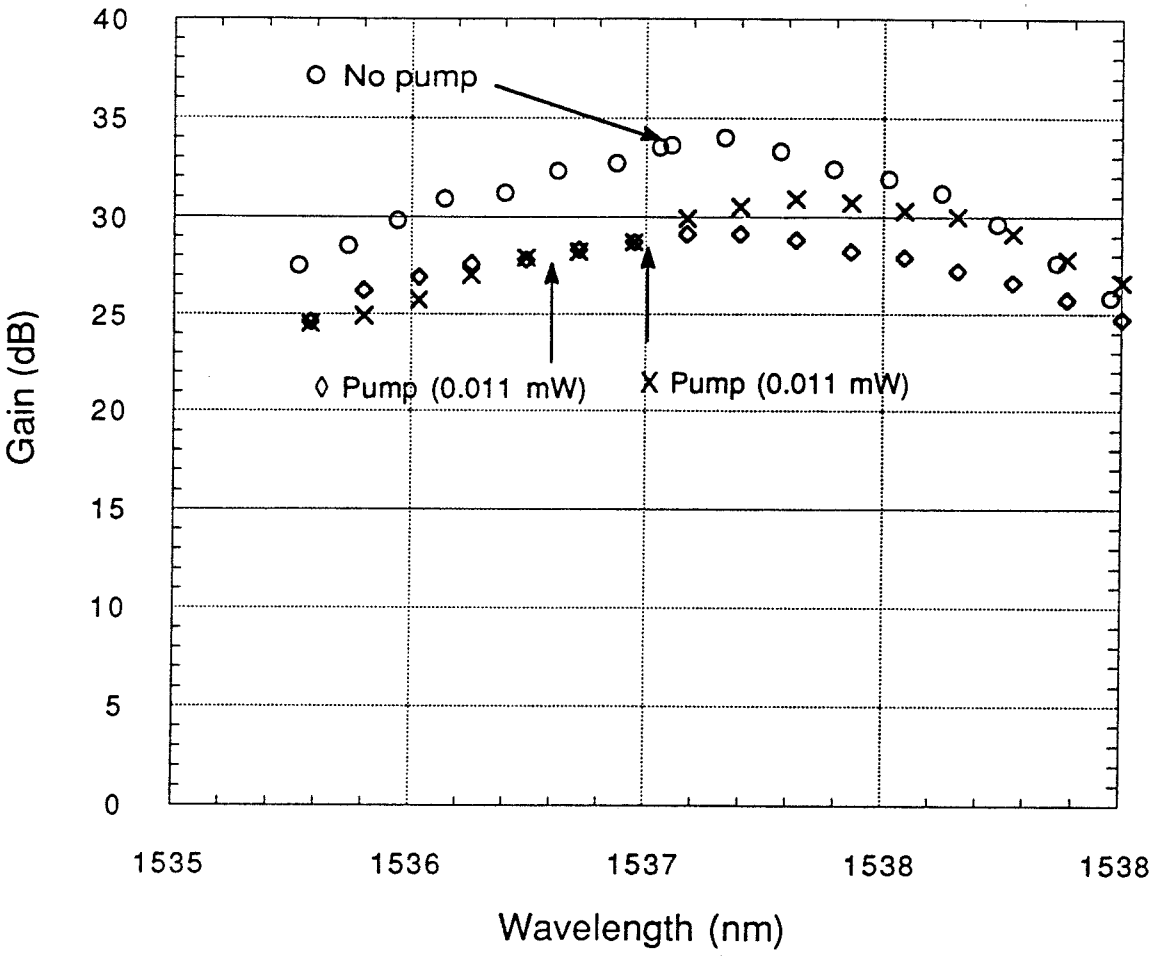

Figure 6.3: EDFA small signal gain vs. wavelength in the case of no other signal (circles); -20 dBm signal at 1536.6 nm (diamonds); -20 dBm signal at 1537 nm (X).

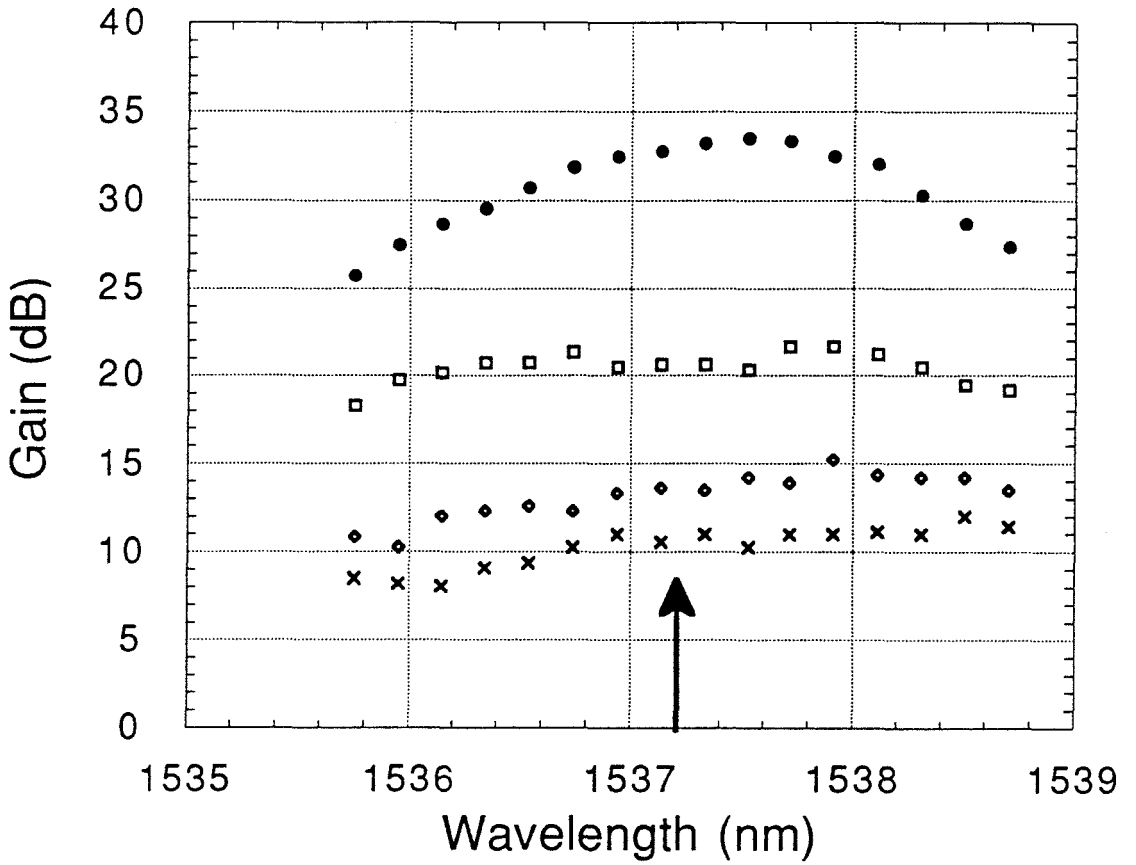

Figure 6.4: EDFA small signal gain vs. wavelength in the case of no other signal (circles); signal at 1537 nm at -11 dBm (squares); -5.3 dBm (diamonds); -1.1 dBm (X)

homogeneously broadened in that a saturating signal at one wavelength will saturate the amplifier across the entire gain spectrum, this saturation is not completely uniform. Multiple-wavelength operation of a laser would be difficult in an ideal homogeneously broadened gain medium. However, it is clear from the observation of gain cross-saturation that the EDFA is not an ideal homogeneously broadened gain medium.

6.2 Co-Lasing in an Electronically Tunable Fiber Laser

A dual-frequency, co-lasing, widely-tunable laser source has constructed from essentially the same components as the single-frequency source [8]. By using a single ring, however, a reduction in the number of components that would be needed to construct two separate, single-frequency sources is achieved.

Two experimental configurations for obtaining co-lasing operation were investigated. They are shown in figures 6.5a and 6.5b. In figure 6.5a we see the single gain module configuration. The gain module (G) is a commercial erbium doped fiber amplifier consisting of approximately 20 m of fiber. The index raising codopants included aluminum. The erbium doped fiber amplifier was pumped with a 980 nm laser diode and provided up to 37.2 dB of small signal gain and 10.3 dBm of maximum output power at 1532 nm. It was possible to achieve lasing over the entire region accessible with the tuning filters.

The two tuning filters were placed in the arms of a Mach-Zehnder interferometer created by two 3 dB fused fiber couplers. A calculation discussed below showed that the minimum frequency separation between the co-lasing frequencies was limited by the bandwidth of the tuning filters. The tuning filters were broadband Micron Optics Fiber Fabry-Perot filters (BB FFP). One had a free spectral range (FSR) of 4020 GHz, a bandwidth of 26.1 GHz, and an insertion loss of less than 3 dB. The other had a FSR of 4700 GHz, a bandwidth of 38.2 GHz and an insertion loss of less than 2 dB. It is

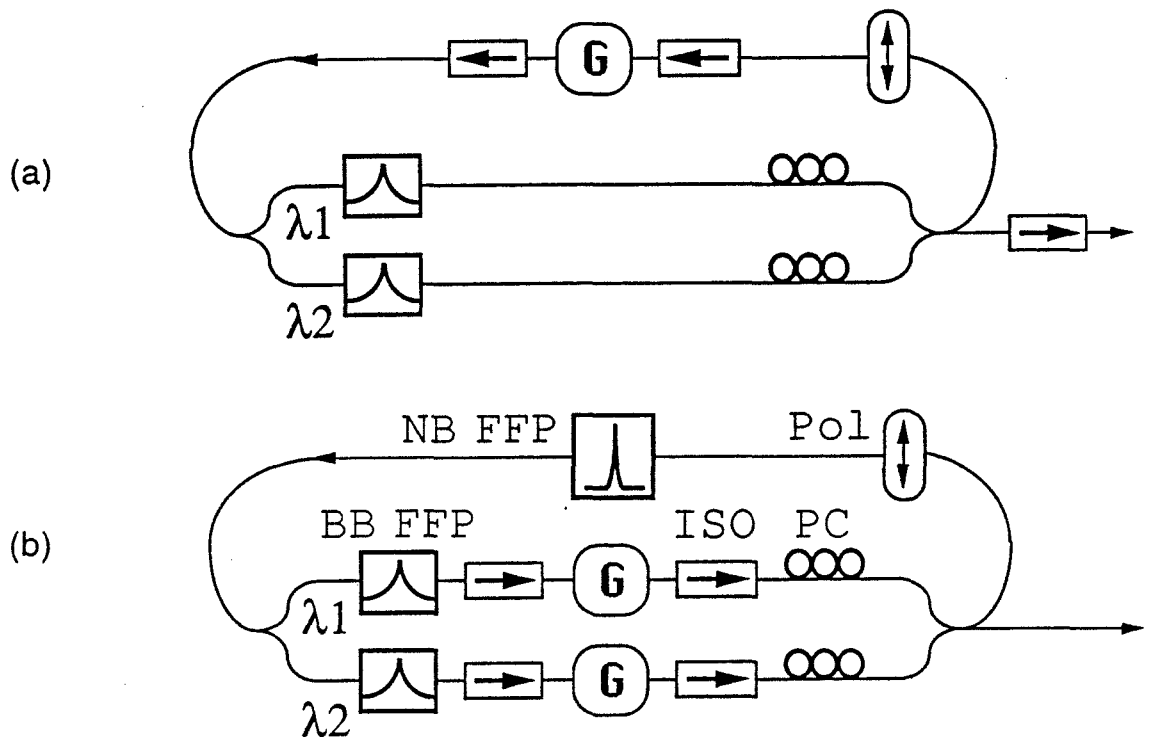

Figure 6.5: Dual-frequency fiber laser with one gain medium (a) and two independent gain media (b). G: EDFA; Pol: polarizer; PC: polarization controller; NB FFP: narrowband fiber Fabry-Perot; BB FFP: broadband FFP; ISO: isolator.

estimated that the total cavity length for either one of the two wavelengths was approximately 40 m corresponding to a mode spacing of 5 MHz. The total minimum loss seen by one wavelength was about 12 dB.

Co-lasing was achieved by tuning the BB FFP's to the desired wavelengths and then using the polarization controllers in combination with the polarizer to balance the losses with the amplifier gain. Output from the laser was split by a 3 dB coupler. Half the output was sent to a spectrometer and the other half to a scanning Fabry-Perot Interferometer (Newport Research Super-Cavity SR-170 FSR 6 GHz, resolution 1 MHz).

The Super-Cavity Fabry-Perot Interferometer showed that the configuration in figure 6.5a operated with only one longitudinal mode excited at each wavelength (see figure 6.6). The smaller peaks in the picture are transverse modes of the Super Cavity Fabry-Perot. Figure 6.7 shows a plot of the achievable tuning range for this configuration measured using the grating spectrometer. Each point on the graph represents one measured spectrum taken with FFP voltages fixed. Tuning was limited only by the free spectral range of the BB FFP's. Some difficulty in tuning was encountered around 1537 nm. It is believed that this is due to a system idiosyncrasy currently under investigation. When the filters were tuned into the same wavelength region and close enough in wavelength to create significant bandpass overlap (proximity tuning), a Mach-Zehnder effect occurred reducing apparent cavity loss to about 5 dB for a single mode. In this case the laser reverted to single-frequency operation.

Maximum output power per wavelength for co-lasing operation was approximately 200 μW. For proximity-tuning induced single wavelength operation, the power into the single lasing mode increased by more than a factor of two as compared to the power per mode measured for co-lasing operation. This increase was the result of the obvious increase (by an approximate factor of 2) in the quantum efficiency per mode and a decrease in lasing threshold caused by the apparent reduction in Mach-Zehnder loss mentioned above.

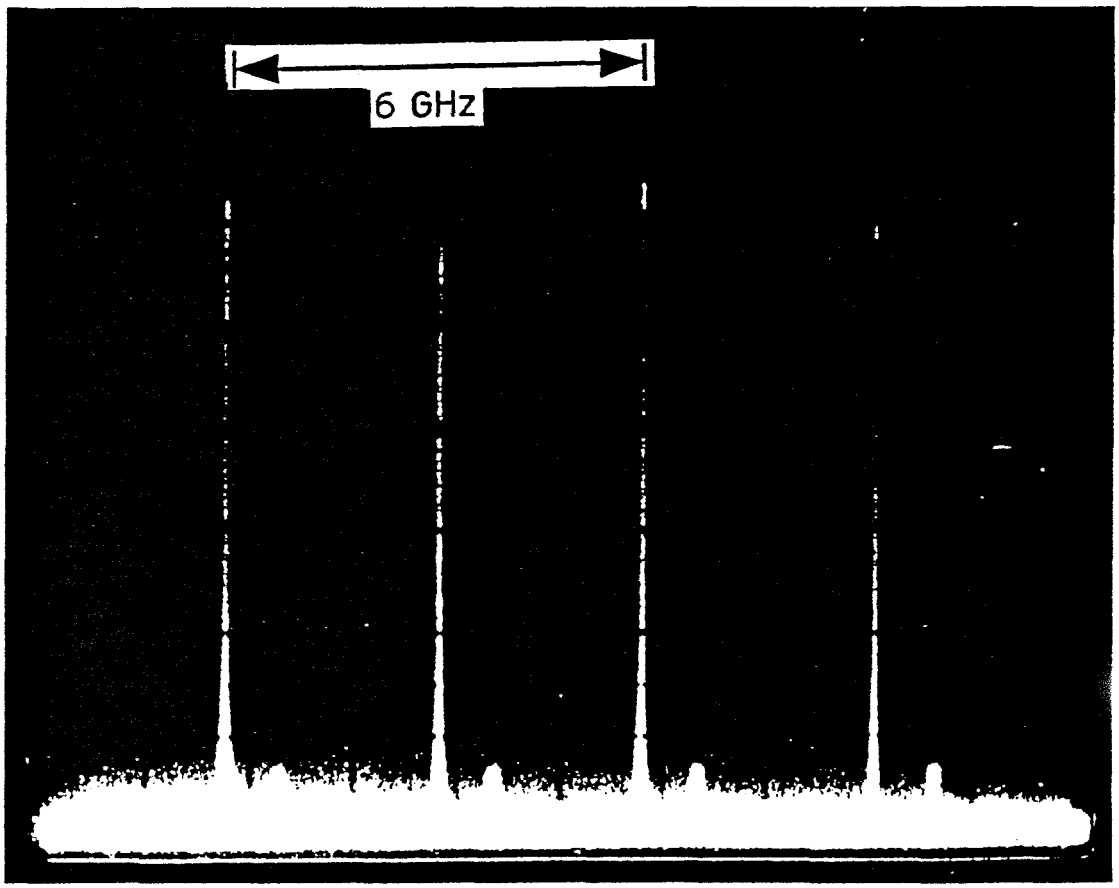

Figure 6.6: Typical output of the Newport Supercavity spectrum analyzer, showing two co-lasing modes separated by several nanometers in wavelength but folded over by the 6 GHz FSR of the Supercavity. The smaller peaks are the transverse modes of the Supercavity.

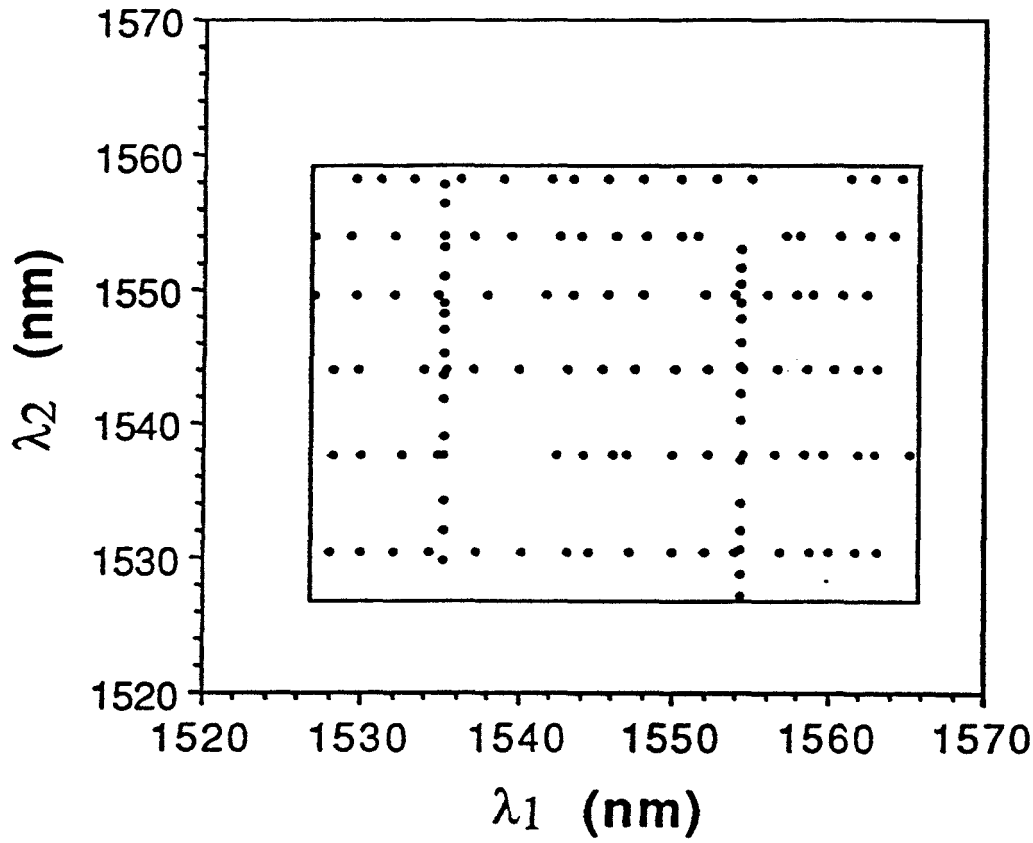

Figure 6.7: Experimental tuning data from configuration in figure 6.5a. Co-lasing was observed at each point on the graph.

Figure 6.5b shows the other configuration investigated. It contained two gain modules: the first being the module used above and the second gain module similar to the first, however, with a pure germanium index raising codopant (i.e., no aluminium). The second gain module had a small signal gain of 40.0 dB and a maximum output power of 8.43 dBm at 1536 nm. Tuning for this device was limited by the bandwidth of the second gain module. The configuration in figure 6.5b also contains a narrow band (NB) FFP filter. This device has a free spectral range of 10.4 GHz, a bandwidth of 130 MHz and an insertion loss of 4 dB. It also has some polarization dependence due to its long cavity length and high finesse, making the apparent fiber induced birefringence significant.

One of the advantages of the dual amplifier configuration is that there is no power sharing between modes. A further advantage of this configuration is that there is no need to adjust the polarization controllers to balance the gain and loss. The gain modules see only one narrow wavelength range and they dynamically adjust to balance the loss. With the NB FFP in place, the lasing modes have stability similar to the single frequency device. However, due to the narrower gain bandwidth associated with the germanium only codoped vs. the aluminium codoped gain module, the tuning area is reduced (See figure 6.8). It is apparent that the smaller gain bandwidth of the germanium codoped amplifier provided sufficient gain to achieve lasing only in the region 1533 nm to 1541 nm around the 1537 nm gain peak and in the region 1551 nm to 1555 nm around the 1555 nm gain peak. The tuning range could be improved by using two aluminium codoped gain modules. Another aluminium codoped gain module was not available at the time of this experiment. Lowering the cavity loss would also increase the tuning range.

Proximity tuning was again restricted by the finite bandwidth of the BB FFP. This phenomena has been investigated theoretically by considering transmission through a Mach-Zehnder interferometer with Fabry-Perot interferometers in its arms. Two cases are considered: nonoverlapping FFP filter resonances and overlapping FFP filter resonances. By using parameters characteristic of our fiber Fabry-Perot filters and assuming a 12 cm

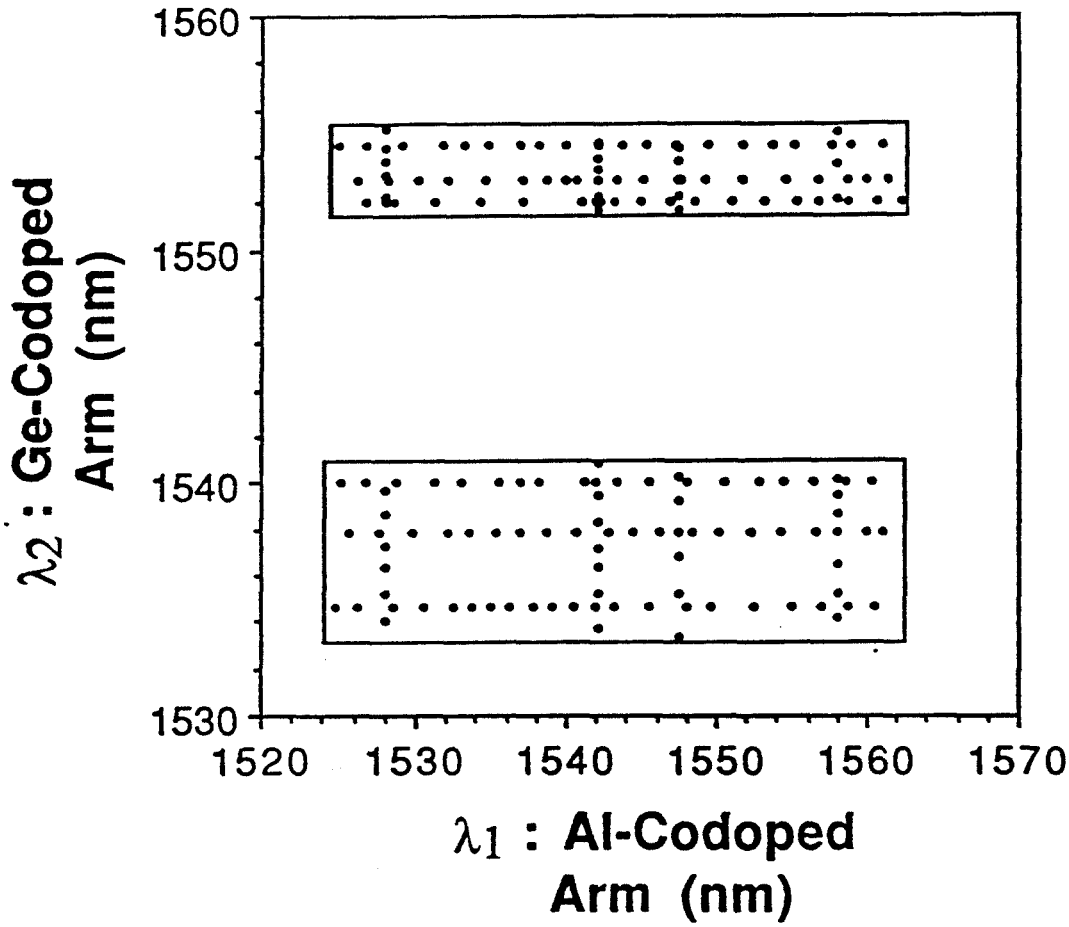

Figure 6.8: Experimental tuning data from configuration in figure 6.5b. Co-lasing was observed at each point on the graph.

path length difference for the Mach-Zehnder (the path length difference for the experimental case was not easy to determine with great accuracy but was close to this value), the transmission spectra shown in figure 6.9a and 6.9b were generated. Figure 6.9a is an example of non-proximity-tuning showing no serious deformation of the individual peaks. Co-lasing could be achieved in this regime. Figure 6.9b is an example of proximity-tuning and the resulting interference effects. Single mode operation would be favored in this case. In these plots, unity is full transmission through the interferometer. Insertion loss due to the BB FFP's was not included in this simple calculation.

6.3 N-Frequency Lasers

The dual-frequency laser has demonstrated the feasibility of multiwavelength laser operation. While the dual-frequency laser provides some cost reduction from sharing components between two lasers, true cost reduction will only be achievable in the case of a large number of frequencies. However, to scale up the number of frequencies, an approach, based on an FFP in each arm and an N-star coupler will quickly become unworkable in terms of total cavity loss and the number of FFP's required. To solve the loss problem and provide coarse frequency selection, wavelength division multiplexers were investigated [9].

Wavelength division multiplexers are presently a subject of active research due to the widespread interest in wavelength division multiplexing for telecommunications systems [10]. Two grating type wavelength division multiplexers were obtained from JDS Fitel at a cost of $6,000 each. These multiplexers had 8 channels, a channel spacing of 4.8 nm, a bandwidth of 0.8 nm and an insertion loss of 6 dB per channel. Multiplexers similar to these with up to 32 channels spaced 1 nm apart have also been constructed [10]. It is expected that better devices at lower cost will be obtainable as WDM communications systems become closer to realization.

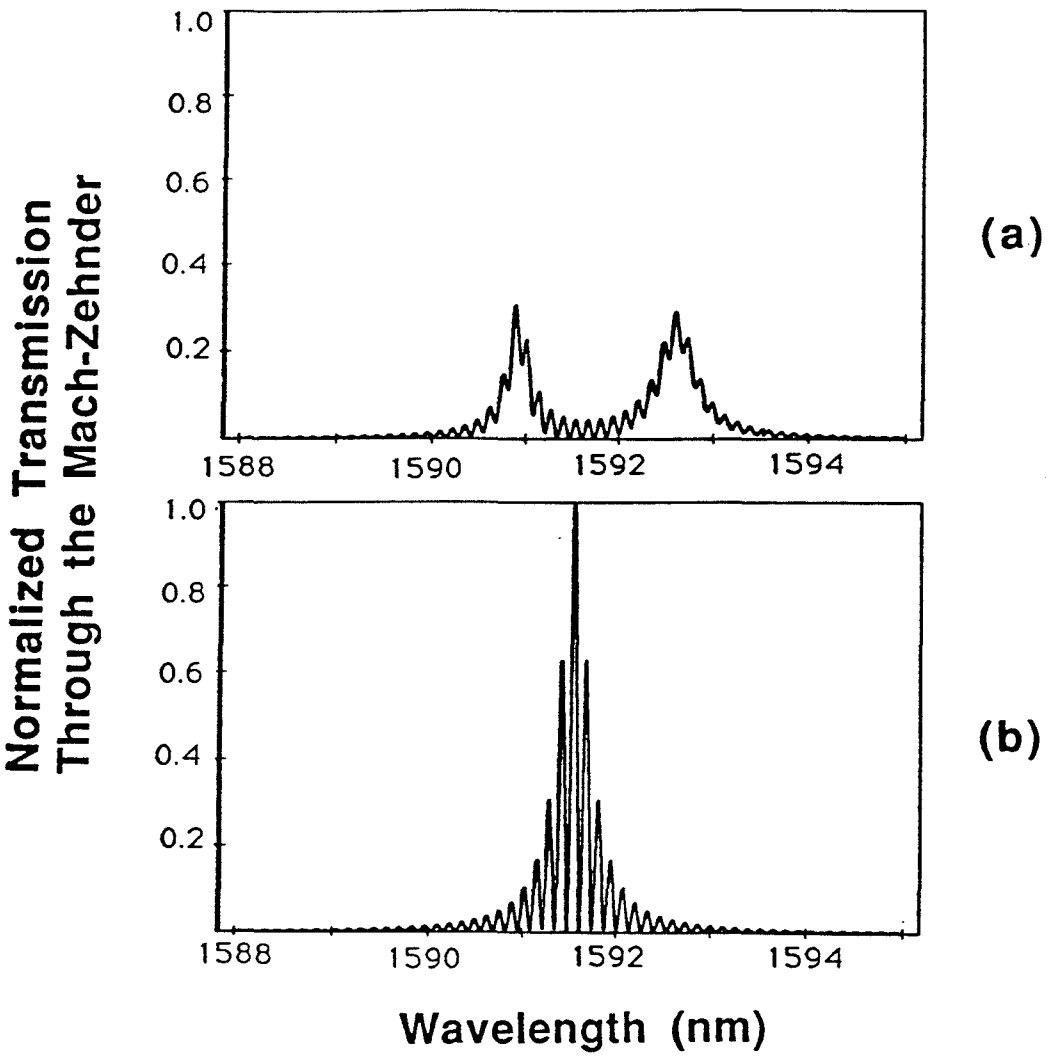

Figure 6.9: Theoretical calculations of Mach-Zender throughput. (a) Non-proximity tuning and (b) proximity tuning.

Figure 6.10 shows the simplest laser cavity configuration for a multichannel laser. The optical gain was provided by a Corning FiberGain module which has 20 meters of Aluminium codoped erbium-doped fiber pumped by a temperature-controlled 980 nm diode. With variable output couplers made from fiber loop mirrors (FLM) placed as shown in the figure, simultaneous lasing action was possible on all 8 channels by careful balancing of the output coupling loss and the gain for each channel. The output powers in this case ranged from 10 to 200 μW. However, a large power fluctuation was observed (about 3 dB variation) on a millisecond time scale when a single channel output was monitored using a photodiode and an oscilloscope. It is believed that this fluctuation results from modal instabilities due to spatial hole burning by the intensity standing-wave pattern of longitudinal modes well within the grating passband of each filter.

To test this hypothesis, and to eliminate the problem, a multichannel, traveling-wave, ring laser was constructed by employing a second WDM, wavelength matched to the first (figure 6.11). In this case, the variable cavity loss was provided by a polarization controller on each channel combined with an in-line polarizer (plasmon wave type, extinction ratio 24 dB). Due to the large losses and lack of spatial hole burning, lasing was simultaneously achieved on only 6 channels. The measured output power was about 50 to 150 μW for each channel and the total output power was approximately 1 mW. For this cavity configuration, the power fluctuation was greatly decreased, to the point where fluctuations were difficult to measure using the oscilloscope.

The spectrum shown in figure 6.12 was taken from the multiplexed output port of the laser, using a grating monochronometer. It clearly shows 6 channel operation from 1528 nm to 1557 nm, with channel separation of 4.8 nm. The output power for the highest peak (1537.8 nm) was about 150 μW at the demultiplexed output port. It was possible to balance the output powers of all channels at the demultiplexed output ports by adjusting the losses on each channel. Since it was also possible to achieve oscillation on the missing

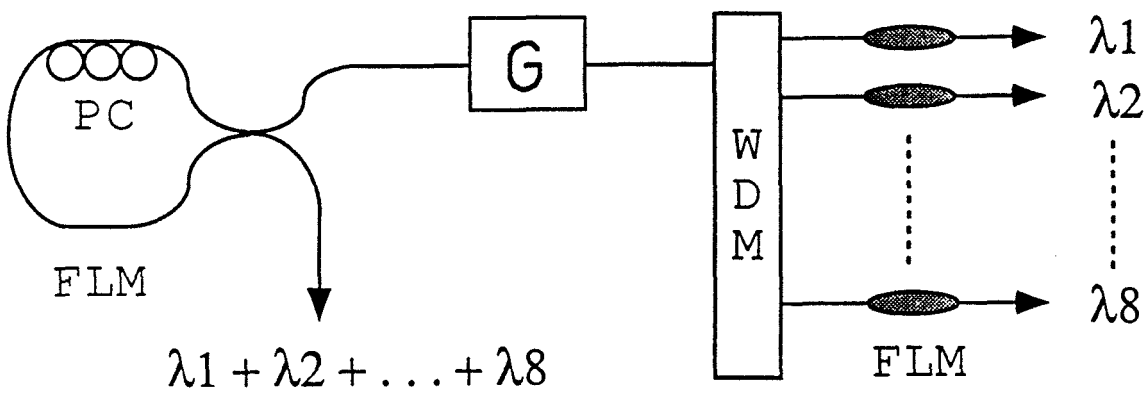

Figure 6.10: Eight-channel laser configuration based on a linear cavity. (FLM: fiber loop mirror; PC: polarization controller; WDM: wavelength division multiplexer; G: gain module.)

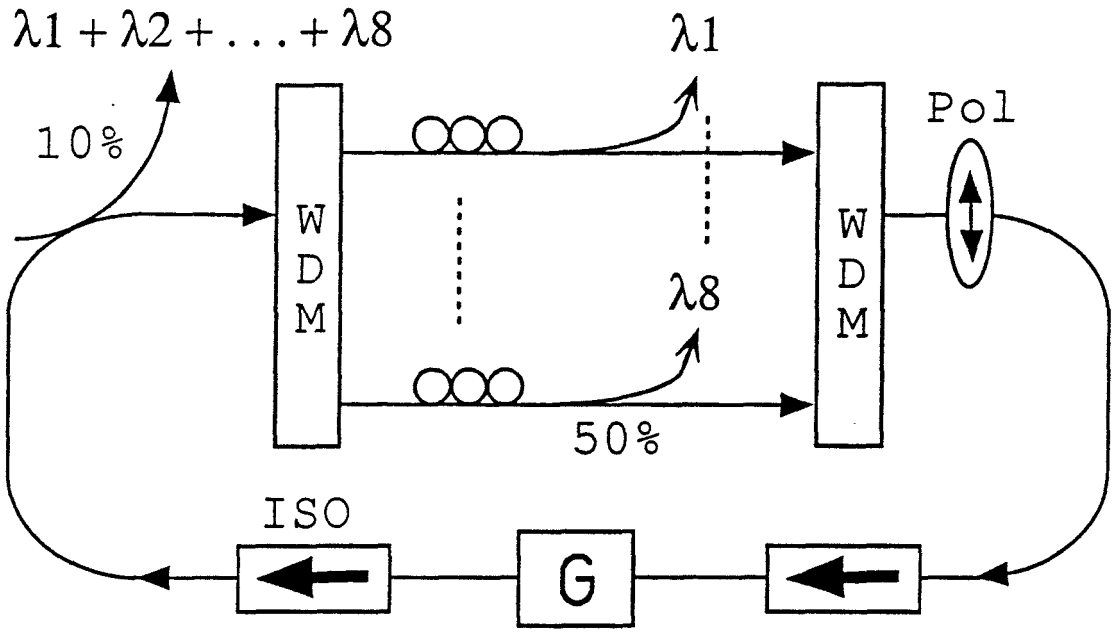

Figure 6.11: Eight-channel laser configuration based on a ring cavity. (WDM: wavelength division multiplexer; G: gain module; ISO: isolator; Pol: polarizer.)

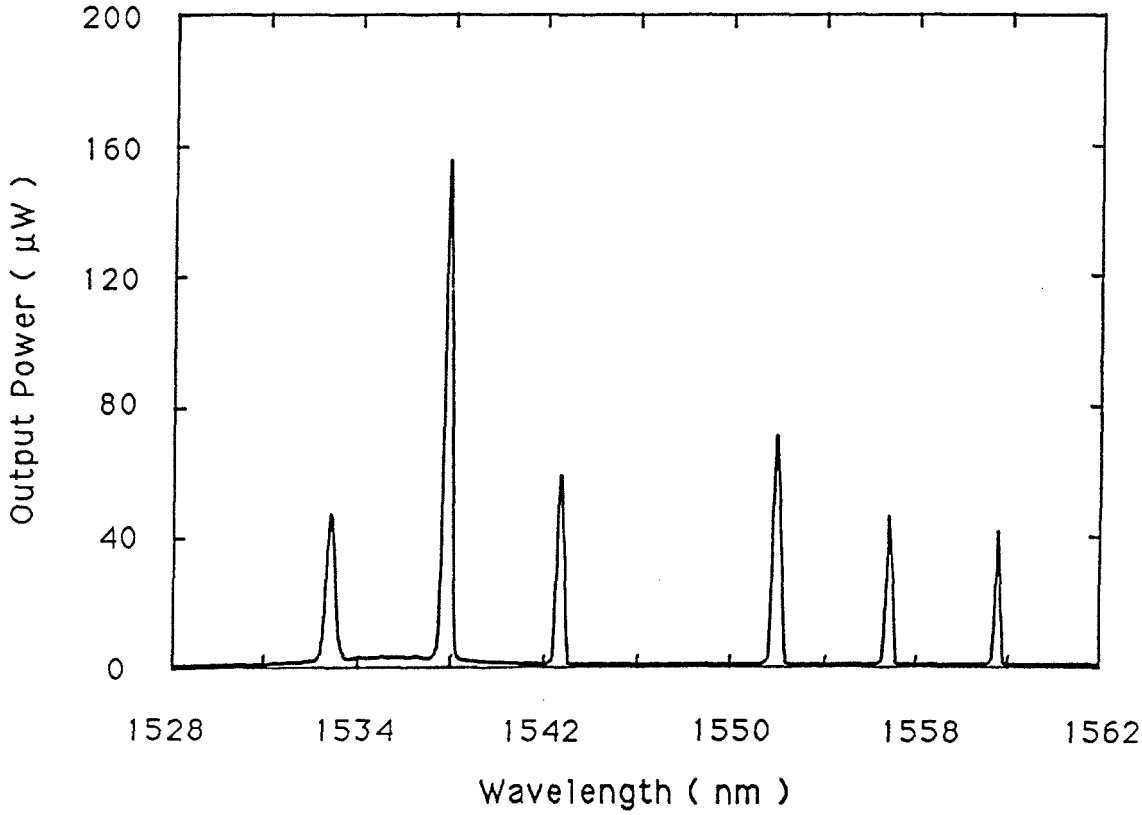

Figure 6.12: Spectrum from the multiplexed output port of a six-channel ring laser (figure 6.12). The output power for the highest peak at 1537.8 nm was about 150 μW at the demultiplexed output port.

channels in the spectrum (1542.7 nm, 1561.8 nm) in the other configuration, it should be possible to achieve 8 channel operation using independent gain media.

Based on the information learned in the dual frequency and multifrequency fiber laser experiments combined with information from Chapters 3, 4 and 5, an improved N-frequency fiber laser design is proposed in figure 6.13. This design offers actively stablized, low intensity noise single-frequency operation at N frequencies. Each frequency is locked to the NB FFP and the NB FFP is controlled by measuring the error signal obtained from an atomic source in combination with one of the frequencies located close to that source. The shared output coupler would provide a low intensity noise output for the N-frequencies. In this configuration all of the expensive components are shared by N lasers.

Each of the N lasers would ideally have its own highly doped, aluminum codoped EDFA, 2 fused fiber WDM couplers for combining the signal and pump, a metal clad fiber for independent length control of each cavity and the necessary electronics for the stabilization circuit. Total laser cost per channel would then depend on how densely the wavelengths could be packed in combination with how much the shared components cost.

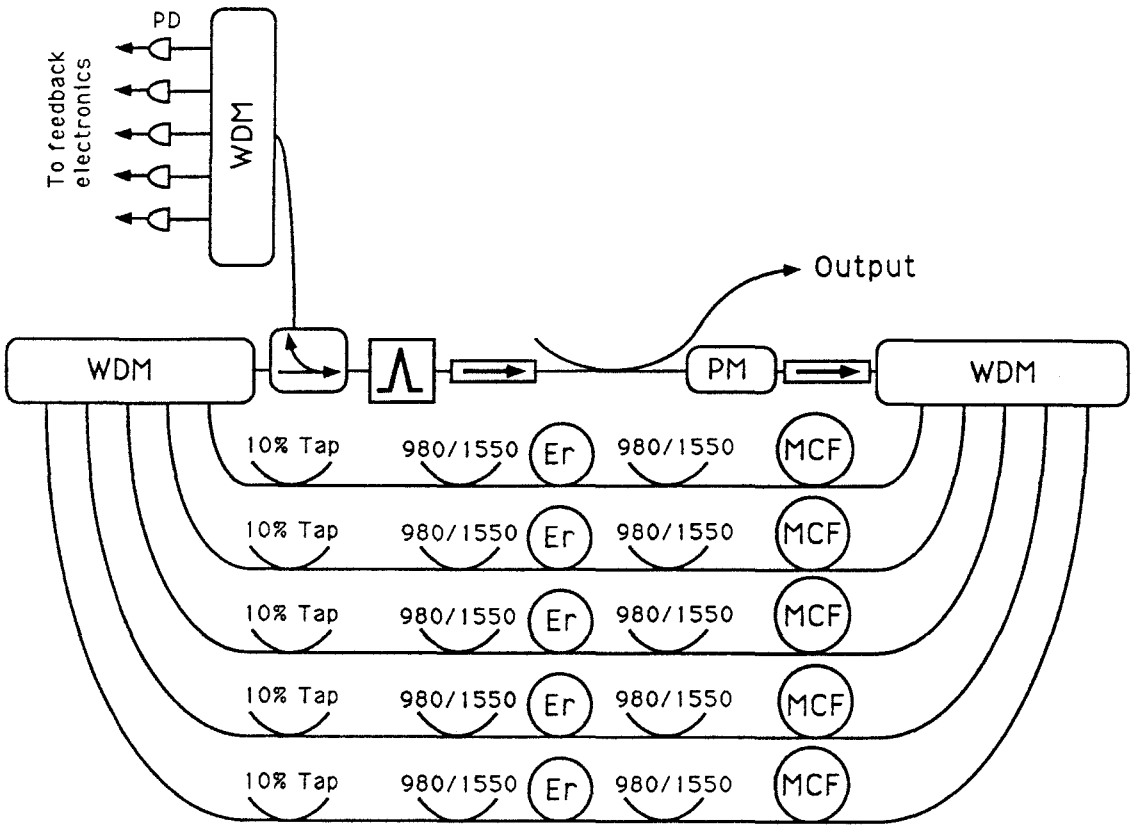

Figure 6.13: N-frequency fiber laser (proposed). WDM: wavelength division multiplexer; PD: photodiode; Er: erbium doped fiber; MCF: metal clad fiber; PM: phase modulator.

References

[1] J. Zhou, N. K. Park, J. W. Dawson, K. J. Vahala, et al., to be published *Appl. Phys. Lett.*

[2] M. Tachibana, R. I. Laming, P. R. Morkel, D. N. Payne, *Optics Lett.* **16**, 1499 (1991)

[3] E. Desurvire, J. L. Zyskind, J. R. Simpson, *IEEE Photon. Tech. Lett.* **2**, 246 (1990)

[4] C. R. Giles, D. DiGiovanni, *IEEE Photon. Tech. Lett.* **2**, 797 (1990)

[5] E. Desurvire, J. R. Simpson, *Optics Lett.* **15**, 547 (1990)

[6] J. L. Zyskind, E. Desurvire, J. W. Sulhoff, D. J. DiGiovanni, *IEEE Photon. Tech. Lett.* **2**, 869 (1990)

[7] N. Kagi, A. Oyobe, K. Nakamura, *J. Lightwave Tech.* **9**, 261 (1991)

[8] J. W. Dawson, N. K. Park, K. J. Vahala, *Appl. Phys. Lett.* **60**, 3090 (1992)

[9] N. K. Park, J. W. Dawson, K. J. Vahala, *IEEE Photon. Tech. Lett.* **4**, 540 (1992)

[10] D. R. Wisely, *Elec. Lett.* **27**, 521 (1991)